

MUTATIONS IN THE GDP-FUCOSE SYNTHESIS PATHWAY CAUSES VASCULAR
INSTABILITY, SWIMMING AND BALANCE DEFECTS IN ZEBRAFISH (*DANIO RERIO*)

by

Gerissa Fowler, B.Sc. (Hons)

A thesis submitted to the
School of Graduate Studies in partial fulfillment of the
requirements for the degree of
Master of Science in Medicine

Faculty of Medicine
Memorial University of Newfoundland
St. John's, Newfoundland

Date: October 2020

Abstract

The function of GDP-mannose 4,6-dehydratase (*gmds*) in cerebral vasculature, or general vascular development, of zebrafish has yet to be described. Mutations within the *gmds* gene can lead to a loss of fucosylation, which is important for a number of cellular functions. In this thesis, it was discovered that a mutation in *gmds*, resulted in a cerebral hemorrhage, curled tails and abnormal swimming behavior in homozygous mutant zebrafish, created using CRISPR-Cas9. Injections of GDP-fucose and high doses of fucose into *gmds* mutants rescued the cerebral hemorrhaging phenotype, but neither injection condition prevented the tails from curling. The mural cell marker, *foxc1b*, which is critical for vascular stability, was significantly downregulated in cerebral vasculature, which was confirmed with qPCR. Crossing the *gmds* mutants onto an *acta2:gfp* line revealed significant reduction of smooth muscle actin coverage in cerebral vasculature. A subset of *gmds* mutants showed a decrease in *slc17a8* expression, indicating a failure to orientate themselves in the water column may be attributed to a synaptic transduction defect in the lateral line neuromasts. In addition, *acta2:gfp* was not expressed in the swim bladder, potentially contributing to the inability to right themselves in the water column.

Acknowledgements

First and foremost, I would like to thank my supervisor, Dr. Curtis French, for the opportunity to complete my Master's degree in his laboratory, and for his endless patience, guidance, and kindness throughout my program. I would like to thank him for facilitating numerous conferences and publication opportunities that have opened up my academic network and allowed me to develop into a robust and confident researcher. I attribute a great deal of my success as a Masters student to his constant support and kind attitude, fostering a motivation to achieve.

I would like to show my gratitude to my supervisory committee, Dr. Michael Woods and Dr. Robert Gendron for their guidance, advice and support throughout my committee meetings and their editorial feedback of my Master's thesis.

I would also like to express my gratitude to Dr. Ann Dorward, who acted as a compassionate and constructive mentor to me throughout my Masters program, specifically in early years when I was struggling with the new responsibilities and transition to graduate school. I would also like to thank Danielle French who provided a considerable amount of training and guidance early in my Masters program, which significantly facilitated the learning process and gave me confidence in my research capabilities.

I offer my sincerest thanks to all financial organizations that have contributed to the success of my Masters through lessening the financial burden of my degree. I would like to thank Indspire, Terra Nova, and the NunatuKavut Community Council for their financial support.

Thank you to the Faculty of Medicine's Office of Research and Graduate Studies for offering support and guidance throughout my program as well as the thesis submission process.

Finally, I would like to pay special regard to my friends and family for their emotional support throughout my studies. I would like to extend my deepest and sincerest love to my parents, Lorraine Wheeler and Gerald Fowler, for their unwavering support. Their unyielding belief and confidence in me since I was a child is the reason I have made it so far and have equipped me with the determination to achieve my dreams. And of course, my dog - Summer, who has sat through countless practice presentations, giving me her undivided attention and emotional support.

TABLE OF CONTENTS

ABSTRACT	II
ACKNOWLEDGEMENTS	III
LIST OF TABLES	VII
LIST OF FIGURES	VIII
LIST OF VIDEOS	IX
LIST OF ABBREVIATIONS	X
1.INTRODUCTION	1
1.1 ZEBRAFISH AS A MODEL OF BLOOD VESSEL DEVELOPMENT.....	1
1.1.1 <i>Zebrafish as a Vascular Model</i>	1
1.1.2 <i>Vascular Development</i>	4
1.1.3 <i>Vascular Development in Zebrafish & Other Vertebrates</i>	12
1.2 ZEBRAFISH AND GENETIC MODIFICATION	15
1.3 GENETICS OF STROKE	21
1.3.1 <i>Ischemic Strokes</i>	24
1.3.2 <i>Hemorrhagic Strokes</i>	24
1.4 FUCOSYLATION AND GDP-MANNOSE 4,6 DEHYDRATASE (<i>GMDS</i>).....	26
1.5 DISEASES ASSOCIATED WITH <i>GMDS</i>	28
1.6 CEREBRAL SMALL VESSEL DISEASE GWAS	29
1.7 COMPARABLE <i>GMDS</i> MUTANTS.....	30
1.8 NEUROMASTS.....	32
2. RATIONALE, HYPOTHESIS AND RESEARCH OBJECTIVES	37
2.1 RATIONALE	37
2.2 HYPOTHESIS.....	37
2.3 RESEARCH OBJECTIVES	38
3. METHODS	39
3.1 FISH HUSBANDRY	39
3.2 BREEDING AND FIXATION	39
3.3 MICROINJECTIONS OF MORPHOLINOS, FUCOSE AND GDP-FUCOSE	40
3.4 CRISPR-CAS9 DESIGN.....	42
3.4.1 <i>Annealing of Oligonucleotides</i>	42
3.4.2 <i>Vector-Oligonucleotide Ligation</i>	42
3.4.3 <i>sgRNA</i>	47
3.5 MICROINJECTIONS OF CRISPR/CAS9	48
3.6 CHARACTERIZATION OF GENOTYPE AND PHENOTYPE OF MUTANTS	50
3.7 SANGER SEQUENCING	53
3.8 PROBE GENERATION AND WHOLE MOUNT <i>IN SITU</i> HYBRIDIZATION	55
3.8.1 <i>Complementary DNA synthesis (cDNA)</i>	55
3.8.2 <i>Antisense mRNA Probe Synthesis</i>	60
3.8.3 <i>In Situ Hybridization Protocol</i>	61
3.9 SCREENING MUTANT GENERATIONS.....	66
3.10 FUCOSYLATION MEASUREMENT	66
3.11 SCANNING ELECTRON MICROSCOPY (SEM).....	67
3.12 CONFOCAL IMAGING OF TRANSGENIC LINE.....	68
3.13 RNA ISOLATION AND CDNA SYNTHESIS FOR QPCR.....	69
3.13.1 <i>RNA Isolation</i>	69
3.13.2 <i>cDNA Synthesis</i>	71
3.14 QUANTITATIVE POLYMERASE CHAIN REACTION (QPCR).....	72
4. RESULTS	75
4.1 <i>GMDS</i> MUTANT CREATION.....	75

4.2	THE LOSS OF <i>GMD5</i> RESULTS IN CEREBRAL HEMORRHAGING AND CURLED TAILS	79
4.3	<i>GMD5</i> IS EXPRESSED IN THE PHARYNGEAL ARCHES AND LATERAL LINE NEUROMASTS.....	82
4.4	SALVAGE PATHWAY GENES CONTRIBUTE TO HEMORRHAGING PHENOTYPES	84
4.5	HEMORRHAGING PHENOTYPE CAN BE RESCUED WITH GDP-FUCOSE AND FUCOSE INJECTIONS.	86
4.6	<i>FOXC1A</i> AND <i>FOXC1B</i> EXPRESSION WAS REDUCED IN <i>GMD5</i> MUTANTS.....	88
4.7	GENERAL MURAL CELL MARKERS SHOW LOCALIZED GENE EXPRESSION CHANGES.....	91
4.8	ENDOTHELIAL CELL MARKERS EXHIBITED NO EXPRESSION CHANGES.....	93
4.9	<i>GMD5</i> MUTANTS HAVE LESS CEREBRAL SMOOTH MUSCLE CELL COVERAGE	95
4.10	LATERAL LINE NEUROMASTS LACK FUCOSYLATION AND SUBSET OF MUTANTS LACK <i>SLC17A8</i> EXPRESSION	98
5.	DISCUSSION	103
5.1	DISRUPTING <i>GMD5</i> FUNCTION RESULTS IN CEREBRAL HEMORRHAGING	103
5.2	HEMORRHAGING PHENOTYPE IS CAUSED BY LACK OF GDP-FUCOSE SYNTHESIS	104
5.3	FUCOSYLATION PATHWAY GENES ARE EXPRESSED IN AREAS IMPORTANT FOR VASCULAR DEVELOPMENT.....	106
5.4	THE LOSS OF <i>GMD5</i> RESULTS IN DOWNREGULATION OF MURAL CELL MARKERS: <i>FOXC1A</i> , <i>FOXC1B</i> , <i>TAGLN</i> AND <i>FBLN5</i>	108
5.5	<i>GMD5</i> MUTANTS EXHIBIT DECREASED SMOOTH MUSCLE ACTIN EXPRESSION OF CEREBRAL VASCULATURE	111
5.6	COMPARISON TO PREVIOUS <i>GMD5</i> MUTANTS	114
5.7	NOTCH SIGNALING CONTRIBUTIONS TO PHENOTYPES SEEN IN THE <i>GMD5</i> ^{<i>n1002</i>} , <i>SLYHERIN</i> AND <i>TOWHEAD</i> MUTANTS	115
5.8	IRREGULARITY OF INNER EAR AND NEUROMAST HAIR CELLS MARKERS MAY CONTRIBUTE TO ABNORMAL BALANCE AND SWIMMING BEHAVIOR IN <i>GMD5</i> MUTANTS.	117
5.9	STRENGTHS AND LIMITATIONS.....	121
6.	CONCLUSION	123
	SUPPLEMENTAL VIDEOS	124
	REFERENCES.....	125
	APPENDIX A	137
	APPENDIX B	143

List of Tables

Table 1. 1: Genes shown to be associated with ischemic stroke and hemorrhagic stroke found through linkage analysis, candidate gene association studies or GWA studies.....	22
Table 3. 1: Sequences of oligonucleotides used for microinjections.....	40
Table 3. 2: Annealing oligonucleotides reaction protocol.....	42
Table 3. 3: Ligation of Dr274 vector and oligonucleotide protocol.....	43
Table 3. 4: Reagents used for Dral digest.....	45
Table 3. 5: Reagents used to synthesize gRNA.....	47
Table 3. 6: <i>gmds</i> forward and reverse primers used to amplify the <i>gmds</i> region for PCR and Sanger sequencing.....	50
Table 3. 7: The PCR program used to amplify the <i>gmds</i> gene for genotyping.....	51
Table 3. 8: Sequencing reaction ingredients.....	53
Table 3. 9: Cycle sequencing program used to amplify the <i>gmds</i> gene region for Sanger sequencing.....	53
Table 3. 10: Reagents used to synthesize gene specific cDNA.....	56
Table 3. 11: Primer sequences used to generate <i>in situ</i> hybridization RNA probes. T7 promoter sequences are underlined.	57
Table 3. 12: RT-PCR program used to create gene specific cDNA.....	59
Table 3. 13: Reaction mixture used to synthesize probes for <i>in situ</i> hybridization.....	60
Table 3. 14: Embryo life stages used for in situ hybridization experiments for each gene probe	63
Table 3. 15: cDNA synthesis reagents.....	71
Table 3. 16: Thermocycler program for cDNA synthesis.....	71
Table 3. 17: Reagents used for qPCR analysis.....	73

List of Figures

Figure 1. 1 The Zebrafish Anatomy.....	3
Figure 1. 2 Origin of hematopoietic and endothelial cells.....	6
Figure 1. 3 Vasculogenesis in the vertebrate embryo.....	7
Figure 1. 4 Blood vessel schematic.....	10
Figure 1. 5 Schematic of morpholino use in zebrafish embryos.....	17
Figure 1. 6 Schematic of CRISPR mechanism.....	20
Figure 1. 7 The fucosylation pathway.....	27
Figure 1. 8 Lateral line neuromast anatomical map.....	33
Figure 1. 9 Anatomy of hair cells.....	34
Figure 3. 1 Flow chart depicting the generation of the <i>gmds</i> mutant line.....	49
Figure 3. 2 CRISPR targeting sites.....	52
Figure 3. 3 qPCR sample plate.....	74
Figure 4. 1 F0 mutation rate.....	77
Figure 4. 2 Sequence alignment of wildtype and <i>gmds</i> ⁿ¹⁰⁰² mutant zebrafish.....	77
Figure 4. 3 Predicted protein sequence of <i>gmds</i> in wildtype and mutant zebrafish.....	78
Figure 4. 4 Hemorrhaging and circular swimming rates of wildtype embryos injected with a control or <i>gmds</i> morpholino.....	80
Figure 4. 5 Hemorrhaging and circular swimming rates of embryos positive or negative for <i>gmds</i> mutations.....	81
Figure 4. 6 Localized <i>gmds</i> gene expression.....	83
Figure 4. 7 Salvage pathway genes contribute to the hemorrhaging phenotype.....	85
Figure 4. 8 Cerebral hemorrhage and curled tail rates after GDP-Fucose and fucose injections.....	87
Figure 4. 9 Expression patterns of notch dependent mural cell markers: <i>foxc1b</i> , <i>foxc1a</i> , <i>pdgfra</i> , <i>pdgfrb</i>	89
Figure 4. 10 qPCR expression profiles of <i>gmds</i> mutants and wildtype embryos.....	90
Figure 4. 11 Expression patterns of general mural cell markers: <i>tagln</i> , <i>myocd</i> and <i>fbln5</i>	92
Figure 4. 12 Expression patterns of endothelial cell markers: <i>cldn5b</i> , <i>kdrl</i> and <i>pecam1</i>	94
Figure 4. 13 Smooth muscle actin coverage in zebrafish cerebral vasculature.....	96
Figure 4. 14 Smooth muscle actin coverage in zebrafish.....	97
Figure 4. 15 Investigation of neuromast and ear morphology.....	99
Figure 4. 16 Measurements of hair cell morphology.....	100
Figure 4. 17 Expression markers of ear and lateral line neuromasts: <i>sox2</i> , <i>fut9b</i> , <i>slc17a8</i> , and <i>pho</i>	101
Figure 5. 1 Theoretical pathway interaction.....	113

List of Videos

Video 1	Three-day old wildtype embryos in a petri dish are stimulated to initiate swimming, which is straight-lined and rapid.....	121
Video 2	Three-day old <i>gmds</i> mutant embryos in a petri dish are stimulated to initiate swimming, which is circular, unbalanced and erratic.....	121

List of Abbreviations

bp	Base pairs
dpf	Days post fertilization
DSB	Double stranded breaks
<i>cldn5</i>	Claudin-5 (zebrafish gene)
CRISPR	Clustered regularly interspaced short palindromic repeats
CSVD	Cerebral small vessel disease
Gfp	Green fluorescent protein
<i>gmds</i>	GDP-mannose 4,6-dehydratase (zebrafish gene)
GWAS	Genome wide association study
<i>fbln5</i>	Fibulin 5 (zebrafish gene)
<i>fcsk</i>	Fucose kinase (zebrafish gene)
<i>foxc1a/b</i>	Forkhead box C1-a/b (zebrafish gene)
<i>fpgt</i>	Fucose-1-phosphate guanylyltransferase (zebrafish gene)
hpf	Hours post fertilization
Indel	Insertion or deletion
<i>kdr1</i>	Vascular endothelial growth factor receptor (zebrafish gene)
Mbp	Mega base pairs
mRNA	Messenger ribonucleic acid
<i>myocd</i>	Myocardin (zebrafish gene)
NaOH	Sodium Hydroxide
NHEJ	Non-homologous end joining
<i>p53</i>	Tumor antigen p53 (zebrafish gene)
PBST	Phosphate buffered saline
<i>pecam</i>	Platelet/endothelial cell adhesion molecule (zebrafish gene)
<i>pdgfra/b</i>	Platelet-derived growth factor A/B (zebrafish gene)
PFA	Paraformaldehyde
<i>Pho</i>	Phoenix (zebrafish gene)
PKD	Polycystic kidney disease
PTU	N-Phenylthiourea
RNA	Ribonucleic acid
<i>slc17a8</i>	Solute carrier family 17 member 8 (zebrafish gene)
SNP	Single-nucleotide polymorphism
<i>sox2</i>	SRY-box transcription factor 2 (zebrafish gene)
SSC	Saline sodium citrate
TALEN	Transcription activator like effector nucleases
<i>tagln</i>	Transgelin (zebrafish gene)
UTR	Untranslated region
vSMC	Vascular smooth muscle cell

1.Introduction

1.1 Zebrafish as a Model of Blood Vessel Development

1.1.1 Zebrafish as a Vascular Model

The use of zebrafish, *Danio rerio*, as a model of vertebrate genetics was pioneered by Dr. George Streisinger in the 1980s¹. Dr. Streisinger understood the implications and value of a vertebrate model that possessed a variety of desirable attributes which would prove to be critical in its functional role as a genetics animal model of vertebrate development and disease. His findings, outlining his creation of a homozygous zebrafish mutant, were published on the cover of Nature in 1981¹.

The small size of zebrafish along with the ease of husbandry allows for towered racks of thousands of fish to be maintained for a relatively low cost in a small space^{2,3}. The generation time to reproductive maturity is 3-4 months with a then weekly production of several hundred eggs from a single breeding pair. The embryos are fertilized *ex utero* and develop rapidly. Zebrafish have a closed circulatory system and share a high degree of similarity of the process and anatomy of developing vasculature and molecular mechanisms of vascular formation with humans and other vertebrates⁴. Additionally, the transparency of early embryonic stages in zebrafish permit efficient application of experimental methods and high resolution imaging (such as confocal microscopy) for studying the morphology and vasculature anywhere in the early developing embryo to view internal structures^{4,5} (**Figure 1.1** highlights structures visible in the zebrafish embryo due to its transparency). These experiments can be done in real time and do not require the sacrifice of the animal, facilitating long term monitoring. A transparent chorion and early stage embryo provide multiple unique advantages for studying vasculature. Zebrafish

embryos are approximately 1mm in diameter⁶, allowing them to be sufficiently oxygenated through diffusion which allows normal development and survival despite complete absence of circulating blood flow, facilitating the study of vasculature development or abnormalities *in vivo*⁵. While *Drosophila* have a primitive heart and hemolymph they lack an endothelial lining present in vertebrate vasculature. Zebrafish are particularly advantageous for the study of cerebral vasculature as morphology and function can be observed in the living organism over time⁶. The ability to observe and manipulate all critical developmental stages in zebrafish provides yet another unique advantage over traditional vertebrate models that would not be possible in mice or rats without sacrificing the animal to view internal development⁶. The transparent embryonic stage as well as the accelerated ability to induce genetic conditions with use of gene knockdowns, knockouts or overexpression has led to widespread use of zebrafish as a genetic model especially when studying orthologs of human disease⁷. This facilitates zebrafish experimentation as an easier, more cost effective model (compared to mouse models) of providing verification of gene mutation or activity implicated in a human disease⁷.

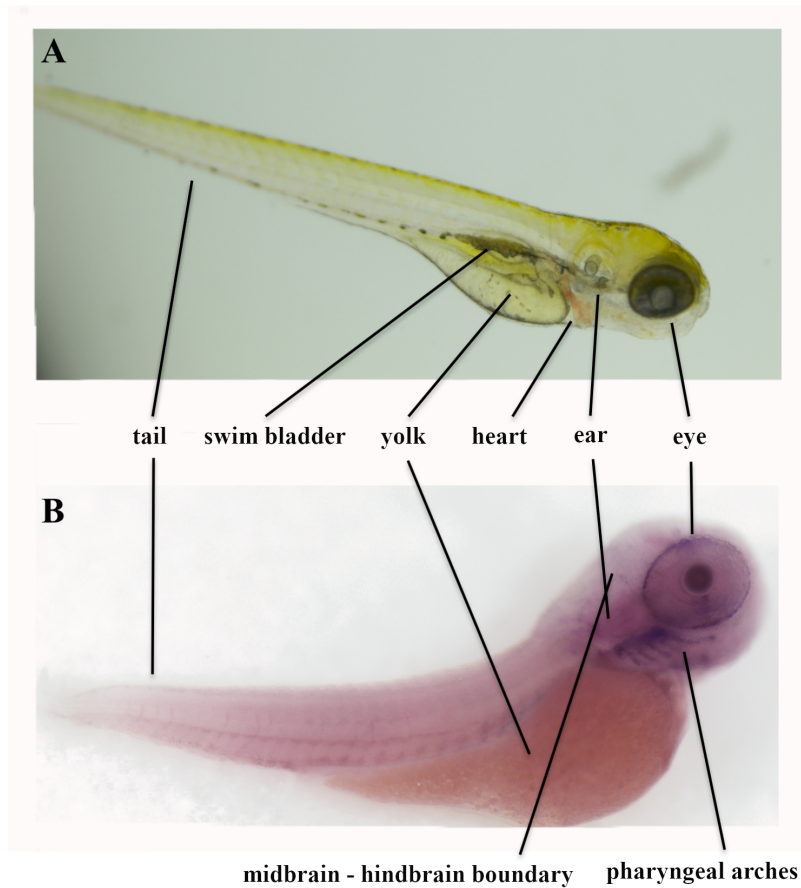


Figure 1. 1 The Zebrafish Anatomy. Some, but certainly not all, structures of the zebrafish embryo have been pointed out in this figure to provide context for the structures I will be mentioning in this thesis. The upper panel (A) is a wildtype embryo that had PTU added to its media to prevent normal pigmentation, allowing for better visualization of internal structures. The bottom panel (B) is a wildtype embryo used in an *in situ* hybridization experiment to stain *foxc1a* gene expression. A number of *in situ* results will be shown, in this thesis, therefore it is necessary to be familiar with structures stained in these experiments but not normally seen in the embryo with the naked eye. The eye and midbrain-hindbrain boundary region have been pointed out in the *in situ* figure provided above, however these areas contain little staining in this particular embryo. These areas will contain much more prominent staining in some embryos seen in the results section.

Ensembl's Gene Tree comparison of the human reference genome found 71.4% of human genes have at least one zebrafish orthologue^{7,8}. Conversely, 69% of zebrafish have at least one human orthologue⁷. Zebrafish are diploid with a genome of approximately 1.7 Mbp's, consisting of 25 pairs of chromosomes with 26,206 protein coding genes^{7,9,10}. As a member of the teleostei infraclass, zebrafish have at least a 20% duplication of gene pairs as a result of a whole genome duplication event in an teleost ancient common ancestor referred to teleost-specific genome duplication^{7,11,12}. The *gmds* gene, the focus of my study, is not duplicated making gene manipulation straightforward and easier to target. A blast alignment search of zebrafish exons sequence data revealed 86.2% identity to human *GMDS*^{13,14}. Taken together, zebrafish are easily maintained and possess a high degree of genetic and developmental conservation with humans making them an ideal model for studying the vascular system and defects that affect it.

1.1.2 Vascular Development

The basic circulatory pathway was first described in a published paper in 1628 by physician William Harvey, who theorized the circular motion of blood from the heart to the lungs through arteries, and finally back to the heart through veins¹⁵. The first scientific recording of angiogenesis was made in 1794 by Scottish anatomist John Hunter, who recognized the relationship between vascularity and metabolic requirements¹⁶. Vasculogenesis is primarily an early embryological process that functions to establish the vascular system, while angiogenesis occurs later in embryonic development and adults. Vasculogenesis is the differentiation of precursor cells, such as angioblasts, into endothelial cells and a vascular network, whereas, angiogenesis is the growth of new blood vessels from pre-existing vasculature. Angiogenesis

occurs throughout life and supplies any metabolically active tissue in the body through a fine network of capillaries¹⁶. Capillaries are essential for delivering nutrients, oxygen and metabolites to tissues throughout the body. Modern investigation into angiogenesis began with Judah Folkman who hypothesized that tumor growth was angiogenesis dependent¹⁶.

Endothelial cells are derived from the mesoderm, line the luminal surface of the blood vessels and are the first organ system to develop in an embryo. Mesoderm stem cells differentiate into hemangioblasts, which give rise to either hematopoietic stem cells or angioblasts (**Fig. 1.2**). Angioblasts can become endothelial cells and with the correct stimulus form blood vessels¹⁶. Vasculogenesis involves cell-cell and extracellular matrix interactions that are directed spatially and temporally by growth factors and chemical cues. These cues drive differentiation of mesoderm stem cells to angioblasts. Angioblasts can become either veins or arteries¹⁶ (**Fig. 1.3**, blue and red respectively). Angioblasts migrate toward stimuli such as vascular endothelial growth factor (VEGF) type A or B to create arteries (**Fig. 1.3**).

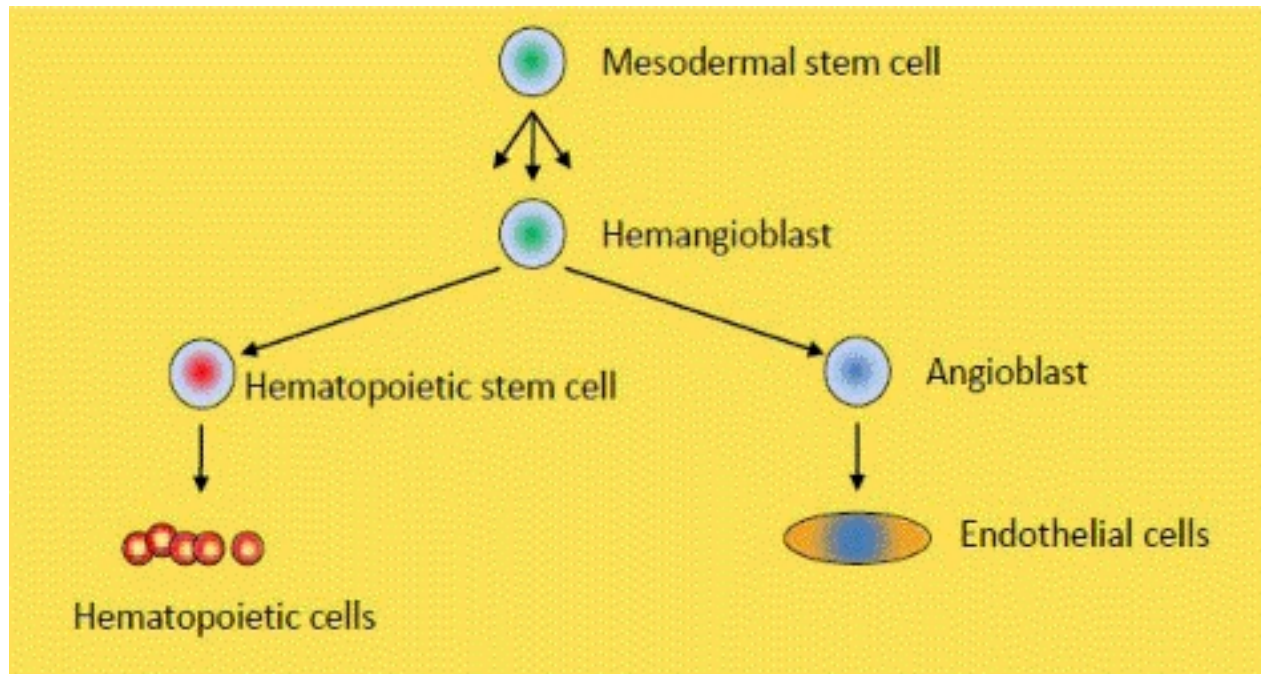


Figure 1. 2 Origin of hematopoietic and endothelial cells. This figure illustrates the lineage of hematopoietic and endothelial cells back to their mutually derived mesodermal stem cell.

Reproduced with permission¹⁶.

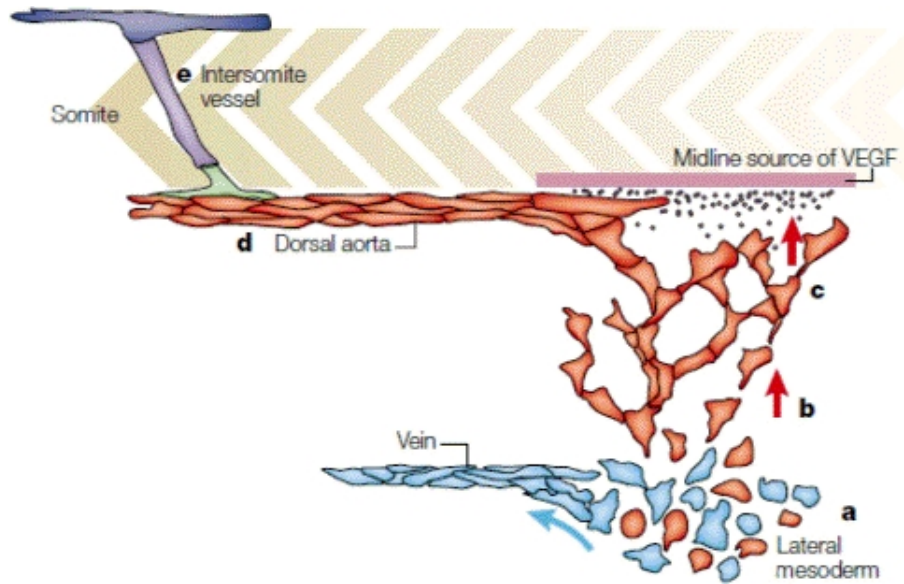


Figure 1. 3 Vasculogenesis in the vertebrate embryo. Vascular endothelial growth factors direct migration of artery precursor cells to the developing dorsal aorta. Reproduced with permission¹⁶.

Blood vessels have multiple layers of specialized cell types. The space in the center of the blood vessels that carries blood to and from the heart is called the lumen. The inside of the lumen is made up of a layer of endothelial cells, followed by a basement membrane, which provides structural support to the vessel. This layer of endothelial cells and basement member is called the tunica interna¹⁷. The next outer layer is referred to as tunica media and is composed of smooth muscle cells. This layer provides control of vascular diameter by means of vasoconstriction or vasodilation. This outer layer termed tunica externa, has its own supply of blood vessels termed the *vasa vasorum* and is coated in nerve fibers, important for regulating vascular tone¹⁷.

The composition of these layers varies between arteries, veins and capillaries. Arteries and arterioles have thick walls and small lumens to withstand the blood pressure and flow supplied by the heart¹⁵. The arteries divide into smaller branches throughout the body in which case the outer tunica externa layer disappears, leaving only the tunica media and interna. As the arterioles expand outwards from the artery the tunica media disappears marking the transition of arteriole to capillary. Capillaries are fine blood vessels composed of a layer of only a single endothelial cell to promote the exchange of nutrients and gases^{15,16}. At this stage the vasculature changes to venuoles by adding a tunica media layer. The basement membrane layer of the microcirculation (capillaries and venuoles) have pericyte cells, a specialized mural cell, that embed and wrap around the endothelial cells to provide structural support to the vessel. Once the tunica externa layer has rejoined the vessel it is termed a vein and they function to carry waste back to the lungs and heart (among other functions), completing the circulation journey¹⁷. Veins have a thinner, weaker tunica media and larger lumens, as the blood pressure initially exerted by the heart has diminished once it reaches this point in the circulatory system. The venous tunica

interna, composed of single celled endothelium like the artery tunica interna, have folds in the epithelium to create valves, to maintain the direct of blood flow towards the heart and prevent blood from pooling in the extremities¹⁵. **Figure 1.4** displays the vessel composition and thickness differences between arties, vessel and capillaries.

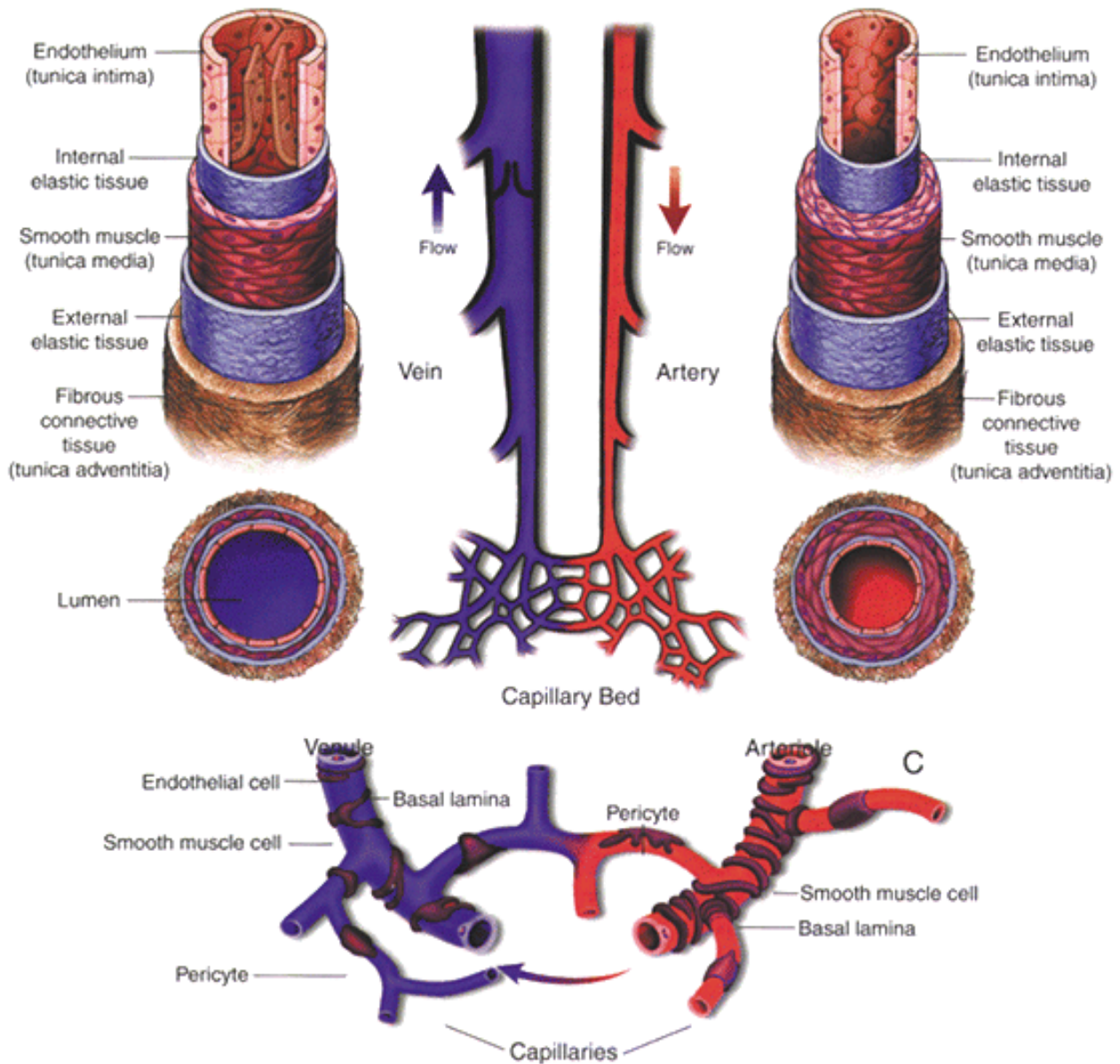


Figure 1. 4 Blood vessel schematic. Blood vessels are composed of an inner tunica interna layer (listed here as tunica intima), a middle tunica media layer and an outer tunica externa layer (listed here as tunica adventitia), which displays the differences in layer thickness between arteries and veins. Reproduced with permission¹⁸.

The way in which existing vessels grow has been categorized into two groups termed, sprouting and intussusceptive (or splitting) angiogenesis. Sprouting of endothelial cells growing towards an angiogenic stimuli, such as VEGF, is termed sprouting angiogenesis¹⁶. Sprouting angiogenesis can create new vessels in tissues devoid of blood vessels and can join multiple capillaries together to form a webbing network of oxygen rich tissue. The vessel wall extending into the lumen to split the blood vessel into two is termed splitting angiogenesis¹⁶.

Sprouting angiogenesis can be broken down into seven steps as defined by Adair & Montani: “enzymatic degradation of capillary basement membrane, endothelial cell proliferation, direction migration of endothelial cells, tubulogenesis, vessel fusion, vessel pruning, and pericyte stabilization”¹⁶. When tissues become hypoxic, chemical cues such as VEGF are dispersed to initiate angiogenesis to resupply the tissue of critical oxygen and nutrients. Endothelial tip cells migrate and grow towards the source of the angiogenesis inducing chemical cue. The developing capillary is guided by the migrating endothelial tip cells through the extracellular matrix towards a chemical stimulus driving angiogenesis, commonly VEGF-A^{16,8}. The tip cells extend filopodia to aid in migration and support of the elongating endothelial stalk cells that proliferate behind the tip cell as it migrates through the extracellular matrix to establish tight junctions and stability of the new vessel¹⁹. The filopodia have VEGF receptors to aid in their migration through the extracellular matrix. Tip cells from two developing vessels converge and fuse to create a lumen. The blood flow through this newly created lumen increases the oxygen supply to this area, thereby decreasing VEGF production, suppressing further angiogenesis. The new vessel is stabilized by pericytes, extracellular matrix, and blood pressure^{4,16}. Sprouting angiogenesis is reliant on functional notch signaling as VEGF-A promotes the production of a notch ligand in tip

cells. This notch ligand binds and activates notch receptors in stalk cells to suppresses VEGF production and thereby the migration of stalk cells compared to tip cells^{4,16}. Therefore, an endothelial cell exposed to the highest levels of VEGF become a tip cell, however they proliferate at a lower rate compared to stalk cells^{4,16}. The production of VEGF is critical for the development of vasculature.

Much less is known about intussusceptive angiogenesis; however, it is thought to occur at a much faster rate compared to sprouting angiogenesis as it only requires reorganization of existing endothelial cells, and therefore does not need to rely on signaling or migration mechanisms. Intussusceptive angiogenesis is predominantly found in a fast-growing embryo when resources are limited from pre-existing capillaries¹⁶.

1.1.3 Vascular Development in Zebrafish & Other Vertebrates

Zebrafish have a closed circulatory system and molecular and genetic mechanisms that control vessel formation is highly conserved between vertebrates, including humans⁴. Circulation in the zebrafish begins at 24 hours post fertilization (hpf) through a simple circulatory loop⁵. Before this, passive diffusion allows essential nutrients and oxygen to navigate throughout the body. This allows normal development even with the presence of circulatory defects, allowing for early stage analysis of zebrafish vasculature and facilitates the analysis of vasculature defects induced by mutations or experimental manipulation^{4,5}. At approximately 20 hpf mark, the lateral dorsal aorta, primordial hindbrain channels and the basilar artery in the hindbrain begin to assemble via vasculogenesis⁴. The formation of cranial vasculature is highly dependent on *vegf*

signaling. Any inhibition of *vegf* signaling results in brain defects localized to the mid-hindbrain boundary⁴. By 36 hpf the circulation throughout the zebrafish is complete and easily observed through a standard light microscope²⁰. By 2 days post fertilization (dpf) most of the trunk and tail have formed vascular lumens and possess active circulation⁵. In zebrafish endothelial and hematopoietic cells are derived from the ventral mesoderm⁴. Cranial neural crest cells migrate to pattern and form the skeletal, neural and connective tissues in the pharyngeal (branchial) arches²¹. The later pharyngeal arches become major aortic vessel supplying the head of circulation. The later pharyngeal arches continue to develop, giving rise to arteries that will supply the gills⁵. Paired lateral dorsal aortae are some of the first vessels to develop and are essential for cranial arterial supply⁴. These aortae along with primordial hindbrain channels and basilar artery make up crucial sections of vascular that supply and drain the mid-hindbrain region. After the primary cranial vessels have been established a smaller network of complex vasculature is formed through angiogenesis and sprouting⁴. All the major blood vessels, including the aortic arches, in the head are formed by 2.5 dpf, with smaller vessels continuing to develop through 7 dpf. Once the embryo reaches 7 dpf all the major cranial vasculature remains relatively unchanged after this period. The smaller capillaries⁵ however, continue to remodel as the embryo grows and develops to compensate for spatial growth and changing oxygen requirements. The primary cranial vasculature is developed through vasculogenesis, while a complex network of vasculature is assembled via angiogenesis and sprouting vessels recruited and stabilized by mural cells⁴.

1.1.3.1 Endothelial cell differentiation in zebrafish

Early hematopoietic and endothelial cells in zebrafish share a common set of genes between zebrafish and mammals⁴. This includes important blood vessel formation genes such as kinase insert domain receptor like (*kdr1*) and vascular endothelial growth factor receptor 2 (*vegfr2*). Endothelial precursor cells (angioblasts) start to express endothelial specific genes during early somitogenesis. ETS transcription factor family play a role in expressing vascular markers for endothelial specification and gene expression. These ETS factors can increase the expression of endothelial genes, *kdr1* and *vegfr2*, and thereby a loss of ETS function can cause endothelial defects⁴. ETS transcriptional regulators also synergistically function alongside forkhead (*FOX*) transcription factors to specify endothelial cell fate⁴.

1.1.3.2 Mural cell development in zebrafish

Mural cells, made up of vascular smooth muscle cells (vSMCs) and pericytes, interact with endothelial cells in the developing vasculature promoting long term vessel stabilization²². Vascular SMCs have a wide variety of developmental origins, with the aorta and proximal branches for example, originating from a mixture of neural crest and somites²³. Cerebral SMCs and pericytes are also neural crest derived²³. Loss of pericyte or vSMCs have been attributed to thoracic aneurysms and dissections, increased brain permeability and hemorrhages²⁴. The endothelium of arteries, arterioles and veins are wrapped with vSMCs and pericytes in the arterioles, venuoles and capillaries, which deposit extracellular matrix proteins²⁴ and interact with the endothelial cells present in the maturing vasculature to strengthen the vessel walls and regulate vascular tone²². The *foxc1* gene is required for the migration of neural crest cells to cerebral nascent vessels. There the neural crest cells express smooth muscle actin positive cells

to become the primary source of mural cells²⁵. Pericytes are primarily found along endothelial cell junctions in smaller vessels, such as capillaries. The recruitment of vSMCs and pericytes to the vessels is reliant on platelet derived growth factor (*pdgf*) signalling, with other signalling pathways, including notch, contribute to mural cell differentiation, recruitment and stabilization²². Whitesell et al. found that in zebrafish specific *foxc1* gene isoforms (*foxc1a, b, c*) are required for vSMCs differentiation²⁴. This study also showed that the expression of *foxc1b* was essential for mesenchymal precursors differentiation into vSMCs and their subsequent expression of smooth muscle actin (*acta2*). Differentiated vSMC then in turn are recruited to the dorsal aorta by *pdgfrb* signalling²². Therefore, it is possible to distinguish vSMC by their expression of *acta2* from pericytes that express *pdgfrb*²⁴.

1.2 Zebrafish and Genetic Modification

In order to implement zebrafish as a pertinent genetics model of disease pathogenesis in humans, a common phenotype is necessary as well as a reasonable degree of genetic similarity, of not only a specific gene of study but at the whole genome level. Forward genetic screens can characterize the phenotypic outcome of drug treatments in zebrafish, which can be indicative of drug effectiveness and adverse symptoms due to a high degree of conservation of drug responses with humans⁶. Reverse genetic screens use targeted gene modification tools to manipulate genes of interest using methods such as morpholinos (morpholino antisense oligonucleotide) and CRISPR/Cas9 (clustered regularly interspaced short palindromic repeats) systems to manipulate gene function. Morpholinos can provide vital insights into gene function by inhibiting genes and studying the resulting phenotypes to better understand the mechanisms and interactions of the

chosen gene. Morpholinos can be splice blocking or translational blocking, the first of which blocks sites involved in splicing pre-mRNA^{26,27} such as intron-exon junctions, which results in misspliced RNA and a defective protein product. The latter simply blocks translation by base complementary binding to the 5' UTR (untranslated region) near the translational start site of mRNA, obstructing ribosomal attachment and therefore translation of the protein²⁸. Once a viable target region of a gene of interest has been identified, designing the morpholino is a relatively straight forward process. An optimal morpholino oligonucleotide will be ~25 bases, targets the 5' cap, has ~50% GC content and no secondary structures. The designing and ordering of morpholinos is a simple process that can be done through commercial companies such as Gene Tools. Morpholinos can then be microinjected into the one cell stage of zebrafish embryos to bind to the targeted mRNA region to inhibit translation of the RNA transcripts^{26,28,29}. Morpholino injections are far easier to accomplish compared to CRISPR injections, as morpholinos are still effective in knocking down gene function whether injected into the cell or into the yolk (a very small target compared to a much larger one). Morpholinos, which partially knock down the gene target and reduces gene expression, can offer a particular advantage compared to total loss and inactivation to gene function methods such as CRISPR, when the gene is critical for development³⁰. In these cases, the amount of morpholino can be diluted to study gene function without being embryonically lethal³⁰. Morpholinos begin to degrade *in vivo* 3-5 days post injection³¹, affecting the ability to affect gene function^{27,32}. However, a large part of the zebrafish embryonic development is completed by this time point³⁰ and the main vessels of the vasculature system are developed by this point to interpret phenotypic changes due to genetic manipulation⁵.

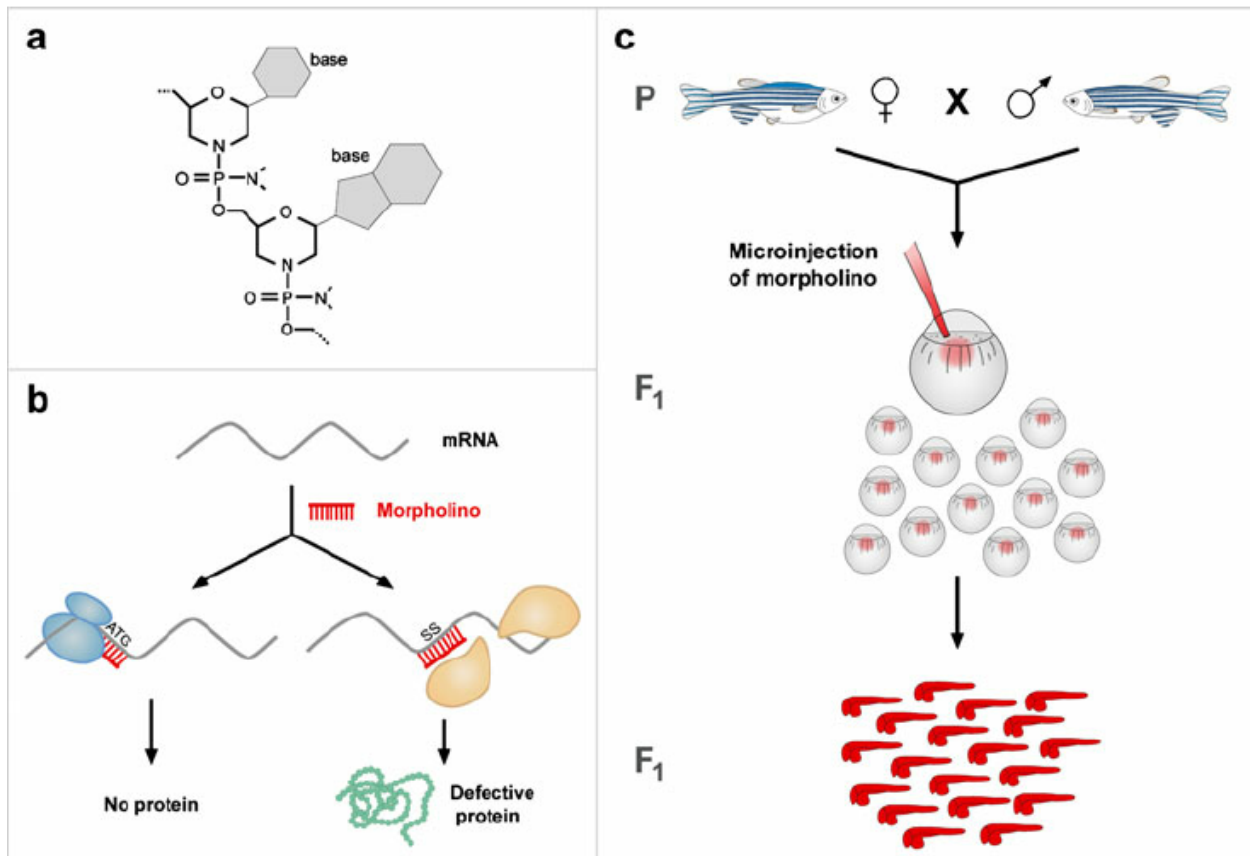


Figure 1. 5 Schematic of morpholino use in zebrafish embryos. A morpholino can bind either to the ATG start codon, blocking translation, or a splice site, which results in misspliced RNA and a defective protein product. Microinjections of morpholino into the one cell stage of zebrafish embryos can be traced through development by co-injecting with a red dye.

Reproduced with permission³³.

Two causes for concern most researchers have regarding the use of morpholinos is the reliability and reproducibility of the morpholino induced phenotype as well as off target effects. There are multiple ways to combat this issue to validate the results of morpholino experiments and ensure the phenotypic outcome is due solely to the knockdown of the targeted gene function and not an interaction with off target RNA. Co-injecting a morpholino targeting the p53 gene can prevent cell death due to off target effects³⁴. Using a second morpholino targeted to the same area with mismatched bases will determine if phenotypic outcome is due to specific targeting or off target RNA knockdown²⁸. To verify if the phenotype is produced by on target knockdown a rescue mRNA can be co-injected. If the abnormal phenotype persists off target knockdowns are the probable cause.

The best way to solidify morpholino phenotypic results is to design a permanent mutation to the same region using gene editing tools such as zinc-finger nucleases (ZFNs), transcription activator-like effector nucleases (TALENs) or the newly developed CRISPR/Cas9 system³⁵. CRISPR/Cas9 refers to the CRISPR locus found in prokaryotic organisms such as bacteria and archaea, that consists of repeated sections of host DNA with intervening spacers of acquired exogenous nucleic acid. The CRISPR locus is flanked by a number of *cas* genes that code for proteins that degrade foreign nucleic acids³⁶. Bacteria and archaea have adapted a unique immune response that utilizes the CRISPR/Cas9 system³⁷. It was discovered that this immunity response could be modified to target specific sections of DNA and therefore could be utilized as a genome editing tool in research and a wide variety of other applications^{38,39}. The current CRISPR/Cas9 system utilized in laboratory conditions is designed with guide RNA (gRNA) targeted to the desired gene modification site attached to a Cas9 protein or can be co-

administered with Cas9 mRNA⁴⁰. When a double stranded break is created at the gRNA binding site, the cells repair machinery attempts to reassemble the break using homologous directed repair (HDR) or non-homologous end joining (NHEJ) (**Fig. 1.6**). Homologous repair relies on template DNA to fix the break, usually in the form of sister chromatids or homologous chromosome, which may not always be available in the cell. In a laboratory setting synthetic DNA can be added to create a specific insertion using the HR machinery⁴¹. NHEJ works quickly to repair DSB, however it is imprecise, often creating insertions or deletion of bases (INDELs) that lead to frameshift mutations if the resulting nucleotide modification is not a multiple of three. Frameshift mutations can lead to a premature stop codon creating a null gene that is particularly useful in reverse genetic studies to observe phenotypic outcome of a gene knockout^{37,41}. If a specific mutation is required the oligonucleotide sequence can be co-injected with the CRISPR/Cas9 system and inserted into the genome using HR. In the absence of a donor oligonucleotide sequence the cell will attempt to correctly repair the DSB using NHEJ and will successfully do so about 99.9% of the time. Once the DSB has been correctly repaired the gRNA can then bind and cut the gene again, this continues until NHEJ makes a mistake and an INDEL has been created. Alternatively, a short oligonucleotide sequence can be co-injected with the CRISPR/Cas9 mechanism to insert a specific desired gene sequence⁴².

1.3 Genetics of Stroke

Stroke is a serious neurologic disorder, which is currently the third leading cause of death behind heart disease and cancer and resulted in over 13,000 deaths in Canada in 2018⁴⁴. Stroke is instigated by a combination of environmental factors and genetic contributions^{45,46}. Ischemic stroke is the most common type of stroke, account for up to 80% of all strokes^{47,48} and it is characterized by a sudden decrease in blood supply to the brain, halted by a blockage of plaque⁴⁶. The less common form of stroke is hemorrhagic stroke, which can be classified as either subarachnoid (SAH) or intracerebral hemorrhages (ICH). Hemorrhagic strokes occur when small penetrating arteries rupture and begin to bleed into the brain⁴⁶. Stroke is a multi-factorial disease caused by risk factors such as hypertension, smoking, obesity and diabetes that account for ~60% of cases with the remaining primarily attributed to genetic factors^{47,49}.

A number of genes have been associated with ischemic strokes, discovered through candidate gene association and GWA studies, although GWAS have become more favorable in recent years⁴⁷. Some lesser known genetic variations found through GWA and candidate gene association studies have been listed in **Table 1.1**.

Table 1. 1: Genes shown to be associated with ischemic stroke and hemorrhagic stroke found through linkage analysis, candidate gene association studies or GWA studies.

Modified and used with permissions from Yamada (2012) and included information gathered from Guo et al. (2010).

Ischemic Stroke Associated Genes		
Chromosomal Locus	Gene Name	Gene Symbol
9q31.1	ATP-binding cassette, subfamily A, member 1	<i>ABCA1</i>
N/A	Angiotensin converting enzyme	<i>ACE</i>
4p16.3	Adducin 1	<i>ADD1</i>
N/A	Arachidonate 5-lipoxygenase activating protein	<i>ALOX5AP</i>
13q12	Arachidonate 5-lipoxygenase-activating protein	<i>ALOX5AP</i>
11q12	Apelin receptor	<i>APLNR</i>
11q23	Apolipoprotein A-V	<i>APOA5</i>
19q13.2	Apolipoprotein E	<i>APOE</i>
9p21.3	CDKN2B antisense RNA 1	<i>CDKN2B-AS1</i>
22q13.3	Cadherin EGF LAG seven pass G-type receptor 1	<i>CELSR1</i>
N/A	C-reactive protein	<i>CRP</i>
14q11.2	Cathepsin G	<i>CTSG</i>
3pter-p21	Chemokine receptor 1	<i>CX3CR1</i>
16q24	Cytochrome b-245, alpha polypeptide	<i>CYBA</i>
8p21-p12	Epoxide hydrolase 2, cytoplasmic	<i>EPHX2</i>
6p25.1	Estrogen receptor 1	<i>ESR1</i>
5q33-qter	Coagulation factor XII	<i>F12</i>
6p25-p24	Coagulation factor XIII, A1 polypeptide	<i>F13A1</i>
11p11	Coagulation factor II	<i>F2</i>
4q28-q31	Fatty acid binding protein 2	<i>FABP2</i>
4q28	Fibrinogen beta chain	<i>FGB</i>
N/A	α -galactosidase A	<i>GLA</i>
12p13	Guanine nucleotide binding protein, beta polypeptide 3	<i>GNB3</i>
17pter-p12	Glycoprotein Ib, alpha polypeptide	<i>GP1BA</i>
5q32-q33.1	Glutathione peroxidase 3	<i>GPX3</i>
11p15.5	Beta globin	<i>HBB</i>
7p21.1	Histone deacetylase 9	<i>HDAC9</i>
19p13.3-p13.2	Intercellular adhesion molecular 1	<i>ICAM1</i>
N/A	Interleukin-6	<i>IL-6</i>
2q14	Interleukin 1, beta	<i>IL1B</i>
2q14.2	Interleukin 1 receptor antagonist	<i>IL1RN</i>
5q31.1	Interleukin 4	<i>IL4</i>
Xq28	Interleukin-1 receptor-associated kinase 1	<i>IRAK1</i>
5q23-q31	Integrin, alpha 2	<i>ITGA2</i>

17q21.32	Integrin, beta 3	<i>ITGB3</i>
19p13.2	Low density lipoprotein receptor	<i>LDLR</i>
6q27	Lipoprotein, Lp(a)	<i>LPA</i>
8p22	Lipoprotein lipase	<i>LPL</i>
6p21.3	Lymphotoxin alpha	<i>LTA</i>
20p12.1	Mono-ADP ribosylhydrolase 2	<i>MACROD2</i>
1p36.3	5,10-methyltetrahydrofolate reductase	<i>MTHFR</i>
12p13	Ninjurin 2	<i>NINJ2</i>
7q36	Nitric oxide synthase 3	<i>NOS3</i>
1p36.2	Natriuretic peptide A	<i>NPPA</i>
5q12	Phosphodiesterase 4D, cAMP-specific	<i>PDE4D</i>
4p25	Paired like homeodomain 2	<i>PITX2</i>
8p12	Plasminogen activator tissue	<i>PLAT</i>
7p21.3	Paraoxonase 1	<i>PON1</i>
3p25	Peroxisome proliferator-activated receptor gamma	<i>PPARG</i>
14q23.1	Protein kinase C	<i>PRKCH</i>
14q22	Prostaglandin E receptor 2, 53kDa	<i>PTGER2</i>
1q25.2-q25.3	Prostaglandin-endoperoxide synthase 2	<i>PTGS2</i>
6q22	c-Ros oncogene 1, receptor tyrosine kinase	<i>ROS1</i>
12p13	Sodium channel, nonvoltage-gated 1, alpha	<i>SCNN1A</i>
1q23-q25	Selectin P	<i>SELP</i>
7q21.3-q22	Serpin peptidase inhibitor, clade E, member 1	<i>SERPINE1</i>
19p13.3	Thromboxane A2 receptor	<i>TBXA2R</i>
19q13.1	Transforming growth factor, beta 1	<i>TGFB1</i>
16p11.2	Vitamin K epoxide reductase complex, subunit 1	<i>VKORC1</i>
16q22	Zinc finger homeobox 3	<i>ZFHX3</i>
Hemorrhagic Stroke Associated Genes		
N/A	Amyloid beta precursor protein	<i>Aβ-PP</i>
6p25-p24	Coagulation factor XIII, A1 polypeptide	<i>F13A1</i>
6q27	Lipoprotein, Lp(a)	<i>LPA</i>
7p21	Interleukin 6	<i>IL6</i>
7q11.23	Lim domain kinase 1	<i>LIMK1</i>
9q34.1	Endoglin	<i>ENG</i>
13q34	Collagen, type IV, alpha 1	<i>COL4A1</i>
14q32.1	Serpin peptidase inhibitor, clade A, member 3	<i>SERPINA3</i>
16p11.2	Vitamin K epoxide reductase complex, subunit 1	<i>VKORC1</i>
17q23	Angiotensin I converting enzyme	<i>ACE</i>
17q23-qter	Apolipoprotein H	<i>APOH</i>
19q13.2	Apolipoprotein E	<i>APOE</i>
1p36.1	Heparan sulfate proteoglycan 2	<i>HSPG2</i>
5q12-q14	Versican	<i>VCAN</i>
5q23-q31	Fibrillin 2	<i>FBN2</i>
6p21.3	Tumor necrosis factor factor	<i>TNF</i>
7q11.2	Elastin	<i>ELN</i>

7q11.23	Lim domain kinase 1	<i>LIMK1</i>
7q21.1	Cytochrome P450, family 3, subfamily A, polypeptide 4	<i>CYP3A4</i>
7q21.3-q22	Serpin peptidase inhibitor, clade E, member 1	<i>SERPINE1</i>
7q22.1	Collagen, type I, alpha 2	<i>COL1A2</i>
7q36	Nitric oxide synthase 3	<i>NOS3</i>
9q34.1	Endoglin	<i>ENG</i>
11q13	Uncoupling protein 3	<i>UCP3</i>
13q34	Collagen, type IV, alpha 1	<i>COL4A1</i>
14q32.1	Serpin peptidase inhibitor, clade A, member 3	<i>SERPINA3</i>
16p13.3-p13.12	Polycystic kidney disease 1	<i>PKD1</i>
17p11.2	Tumor necrosis factor receptor superfamily, member 13B	<i>TNFRSF13B</i>
17q21.32	Integrin, beta 3	<i>ITGB3</i>
20q11.2-q13.1	Matrix metalloproteinase 9	<i>MMP9</i>
22q12	Heme oxygenase 1	<i>HMOX1</i>

N/A = Not available

1.3.1 Ischemic Strokes

Cerebral arteriopathy autosomal dominant with subcortical infarcts and leukoencephalopathy (CADASIL) is an inherited autosomal dominant disease with primary symptoms of reoccurring strokes and progressive dementia^{46,47}. Mutations within the *NOTCH3*, *HTRA1*, and *COL4A1* have been found to be the genetic cause of CADASIL^{25,47}. Disease severity is regulated by environmental and genetic factors and appears to vary significantly even within families, with secondary genes interacting with *NOTCH3* to regulate phenotype⁴⁷. The *NOTCH3* gene codes for a trans-membrane receptor that is highly conserved across species. *NOTCH3* is expressed in SMCs, therefore a mutation in this gene leads to degeneration of SMCs, underlying the cause of CADASIL⁴⁷.

1.3.2 Hemorrhagic Strokes

Hemorrhagic strokes are classified into two disease categories: subarachnoid (SAH) and intracerebral (ICH). SAH usually presents as a rupture of a cerebral arterial aneurysm⁴⁷. ICH however are subdivided into primary and secondary intracerebral hemorrhages, primary accounting for the majority of ICHs. They are attributed to chronic hypertension, the primary risk factor, and other smaller risk factor associated conditions such as small vessel rupture that can often be associated with amyloid angiopathy (a buildup of amyloid proteins along arterial walls in the brain)⁴⁷. Polycystic kidney disease (PKD) is caused by a mutation in the PKD1, PKD2 or PKHD1 gene⁵⁰ and can lead to complications such as high blood pressure. High blood pressure associated with PKD has resulted in cerebral hemorrhages and intracranial aneurysms that presents a cause of mortality in PKD patients⁵¹.

Cerebral small vessel disease (CSVD) is an umbrella term covering several diseases that affect cerebral small arteries, arterioles, venuoles and capillaries⁵². The main manifestation of CSVD is stroke, along with dementia, and motor impairment. MRI scans of the brain look for white matter lesions and normal appearing white matter, a variation in which lead to a spectrum of disease specific symptoms⁵³. Mutations in *FOXC1* and *PIX2* has been associated with cerebral small vessel disease, which is a risk factor for both ischemic and hemorrhagic strokes²⁵. Zebrafish and murine models of *foxc1* and *pix2* defects have exhibited hemorrhaging phenotypes due to reduced smooth muscle actin in cerebral vasculature²⁵.

Mutations in *ACTA2* have been shown to cause coronary artery disease and strokes as well as a predisposition to thoracic aortic aneurysms and dissections⁴⁹. A mutation in this gene

triggers a defect in proliferation of vSMCs and myofibroblasts, leading to arterial occlusion and neighboring abnormal vascular networks in the vicinity of the arterial occlusions⁴⁹.

1.4 Fucosylation and GDP-mannose 4,6 dehydratase (*gmds*)

Fucosylation is the process of transferring a GDP-fucose residue to oligosaccharides and proteins (**Fig. 1.7**). This process is regulated by a number of molecules such as fucosyltransferases and GDP-fucose enzymes⁵⁴. Fucosylated carbohydrates are essential to biological and pathological processes such as, tissue development, angiogenesis, cell adhesion and tumor metastasis in eukaryotic organisms⁵⁵. The fucosylation pathway produces GDP-fucose *in vivo* through two metabolic pathways in the cytoplasm. The *de novo* pathway utilizes cellular GDP-mannose as a substrate, while the salvage pathway produces GDP-fucose using dietary fucose^{56,57}. The post-translational addition of GDP-fucose to proteins, such as glycans, in the Golgi through the fucosylation pathway is essential for proper function of glycans. Any loss of enzymatic function will result in a decrease or complete loss of the product, GDP-fucose, affecting downstream molecules and pathways that rely on fucosylation. For this reason, this study focused on investigating the function of the catalytic enzymes fucose kinase (*fcsk*), and fucose-1-phosphate guanylyltransferase (*fpgt*) in the salvage pathway, and GDP-mannose 4,6-dehydratase (*gmds*) in the *de novo* pathway (**Fig. 1.7**).

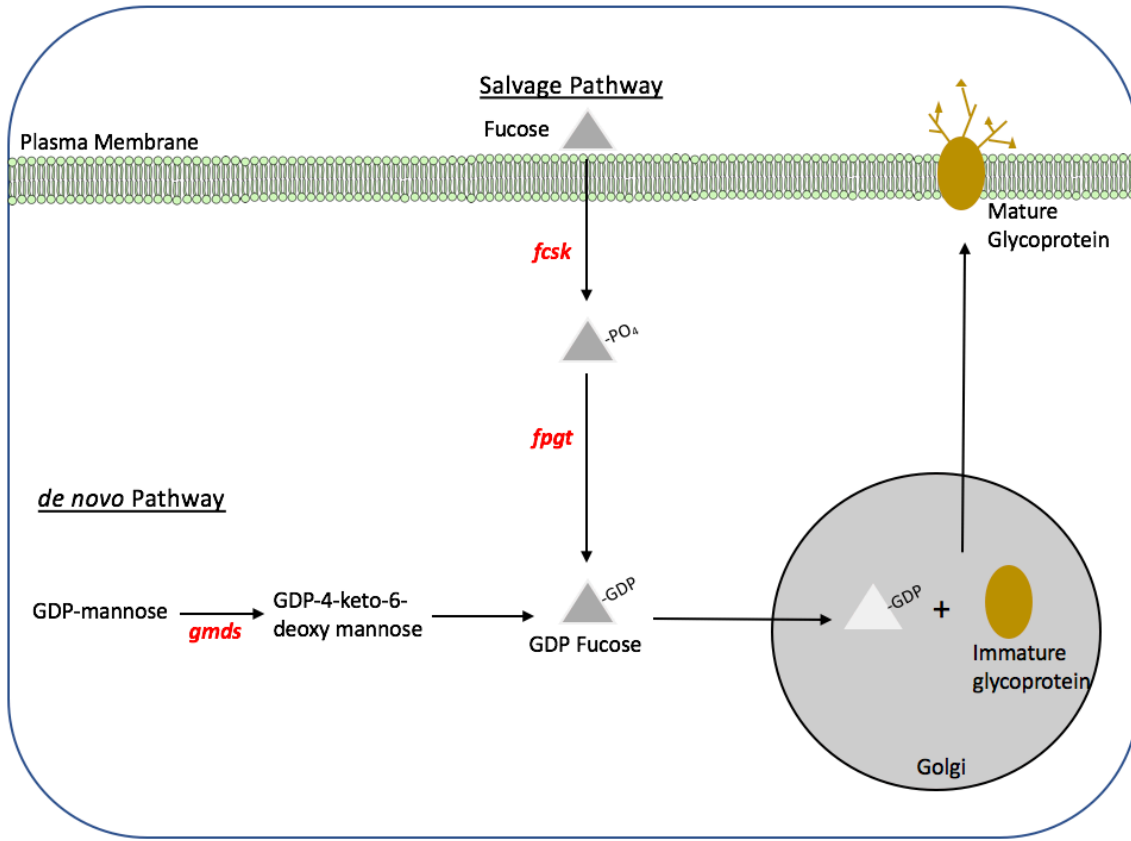


Figure 1. 7 The fucosylation pathway. GDP-fucose can be produced through the *de novo* or salvage pathway. This study investigates the catalytic enzymes highlighted in red, but focuses predominantly on *gmds*.

1.5 Diseases associated with *gmds*

Mutations in the *gmds* gene has been implicated in a number of diseases in humans. Leukocyte adhesion deficiency II (LADII) is a rare autosomal recessive congenital disease caused by a decreased activity of *GMDS* in patients⁵⁸. The result of this decrease in *GMDS* activity means that glycoproteins of endothelium (eg. selectins) and leukocytes are not fucosylated. This results in the premature termination of the inflammatory responses by blocking leukocyte rolling on the vascular endothelium^{58,59}. LADII is characterized by immunodeficiency, mental disabilities, and severe growth retardation^{58,59}. The symptoms are the result of a genetic defect in the Golgi-localized GDP-fucose transporter, which impairs the fucosylation of glycoproteins^{57,59}. One study found deficient notch signalling, a key regulator of epithelial cell differentiation and critical involvement in a number of diseases, to be the cause of secretory cell hyperplasia in murine mutant GDP-4-keto-6-deoxymannose models (the molecular product of the chemical reaction *gmds* catalyzes), specifically in the small intestine and colon⁵⁹. Considering fucosylation is critical to the function of a number of processes in the GI tract they hypothesized that the mechanism leading LADII patients to experiencing poor growth could be attributed to a downstream loss of Notch signaling within the intestinal epithelium due to a loss of fucosylated Notch specific ligands⁵⁹.

The changes in expression of fucosylated oligosaccharides have been associated with certain cancers. Monoclonal antibodies and lectins that recognize cancer associated fucosylated glycoproteins, such as CA19-9 and AFP-L3 are being used as a cancer diagnostic tool⁵⁴. More specific to *GMDS*, mutations in the gene have been associated with colon cancer cells resistance

to tumor necrosis factor-related apoptosis-inducing ligand (TRAIL) apoptosis, thereby increasing tumor and malignancy rates^{60,61}. The binding of TRAIL/Apo-2L to its cognate receptors death receptor 4 and 5 (DR4 and DR5) induces apoptosis in cancer cells by “transmitting a caspase-activating death signal through a cytoplasmic death domain”⁶¹. A deficiency in *GMDS* leads to inhibition of DR4 and DR5 mediated apoptosis as well as CD95 (in the *Fas* receptor family, responsible for programmed cell death) mediated apoptosis by suppressing the formation of complexes (“comprised of the receptor, Fas-associated death domain, and caspase-8”)⁶¹. Multiple GWA studies of glaucoma patient cohorts have discovered an association with SNPs in the *GMDS* gene^{43,62,63} and have associated its neighboring gene, *FOXC1B*, with glaucoma^{64,65}. Zebrafish studies demonstrated decreased cell numbers in the retinal ganglion cell layer of the developing eye in *foxc1a* morphants and *foxc1b* mutants. This study found that *foxc1* was required for the regulation of genes responsible for retinal ganglion cell differentiation and disrupting any of these key genes results in glaucoma⁶⁵.

1.6 Cerebral Small Vessel Disease GWAS

A 2014 study investigating causative genes in cerebral small-vessel disease (CSVD) conducted a meta-analysis of (genome wide association) GWA data around the *FOXC1* gene region from the Cohort for Heart and Aging Research in Genomic Epidemiology (CHARGE)²⁵. Patients had a heterozygous *FOXC1* mutation. The paper found a cluster of 10 SNPs within *GMDS* that were associated with white matter hyperintensities, a stroke risk factor²⁵. This study was prompted by high self-reported incidences of stroke within pedigrees containing *FOXC1* mutations and the genes critical importance in vascular development²⁵. To determine the

potential molecular mechanisms in place, this group evaluated the *pdgfr* pathway as a potential contributor to vascular degradation, as *pdgfr* signaling regulates the recruitment of the neural crest cells to the developing vasculature. Morpholinos directed against the *foxc1* gene injected into zebrafish embryos, found reduced expression of *pdgfra* and *pdgfrb*. A follow up study by the same group found the same trend in *foxc1* mutants, indicating a potentially translational pathway to the pathology of the human disease²⁴. Mutations in *GMDS* had not yet been associated with CSVD and its role was unknown.

1.7 Comparable *gmds* Mutants

Two research groups created *gmds* mutant zebrafish in the past to model leukocyte adhesion deficiency and to study motor neuron migration and axon pathfinding. Leukocyte adhesion deficiency is caused by a mutation within the *FUCT1* gene, a gene responsible for the transport of GDP-fucose from the cytosol to the Golgi¹³. The immunodeficiency characteristic of this disease is thought to be caused by the loss of fucosylated glycans. The *slytherin* (*gmds*) mutant, identified through a forward genetic screen for its swimming defects, was used to study the link between decreased fucosylation and its effects on neuron development, function and synapse formation to provide more insight into molecular mechanisms causative of neurodevelopmental symptoms seen in patients¹³. As Notch-Delta signaling has a critical role in regulating neurogenesis, glial specification and neuronal maturation, this group investigated the fucosylation relationship to Notch signaling and its contribution to downstream neuron and synaptic health; finding that both notch independent and dependent mechanisms contributed to the decreased gliogenesis and abnormal neural patterning in their *slytherin* mutant¹³. Outside of

the neuron related phenotypes reported in this paper, this group also reported that the *slytherin* mutants exhibited a bent tail by 24 hpf, becoming more severe over time, and had a malformed hindbrain. Also provided through the supplemental material are videos of the *slytherin* mutants swimming, which show the bent tail phenotype severely affecting the swimming behavior¹³.

The *towhead* (*gmds*) mutant was utilized to investigate vagus motor neuron migration in the zebrafish hindbrain. The development of the nervous system and expansion of the brain is dependent on neural migration, which is controlled by a number of molecular pathways and genes⁵⁷. This study discovered fucosylated glycans expressed in neuroepithelial cells were required to guide motor neuron migration. Along the same reasoning as the *slytherin* research group, the *towhead* group tested gene expression levels of Notch targets in their *towhead* mutants, given that Notch signaling pathway is a key regulator of neurogenesis, and notch ligands require fucosylation to bind to the extracellular notch domain. However, the *towhead* mutant exhibited no significant decrease in Notch signalling. The *towhead* mutants also exhibited a curled tail by 2 dpf and died by 7 dpf⁵⁷. No additional phenotypes were reported by either research group.

Any loss of GDP-fucose, through a mutation in *gmds*, could affect vascular formation, maintenance or stability causing cerebral hemorrhaging. The abnormal swimming behavior and curled tails present in the *towhead* and *slytherin* mutants could be indicative of a defect in the lateral line neuromasts as circular swimming is a typical phenotype in defective neuromast mutants, in addition to the neuronal mechanisms they had described. Both mutants had a single missense mutation in the *gmds* gene.

1.8 Neuromasts

In vertebrates, sound and movements of the head are detected by the inner ear⁶⁶. During the development of the inner ear, neuroepithelial cells specialize into hair and support cells to detect vestibular and auditory stimuli^{66,67}. Hair cells are a mechanoreceptor that function to transmit sound waves in the cochlea and head movements in the vestibular organ into electrical signals sent to the brain, which is termed mechanotransduction^{66,67}. Fish have an additional mechanosensory organ along the length of each side of the body termed the lateral line with neuroepithelium termed neuromasts (**Fig. 1.8**)⁶⁷.

These neuromasts also possess hair cells, surrounded by support cells, that project from the body to detect motion in the water, aiding in orientation in the water column and facilitating predatory avoidance, prey capture and mating^{67,68}. Neuromasts are surrounded by two support cell populations, inner support cells and mantle cells, that form a ring around the neuromast and the protruding hair cell (**Fig. 1.9**)^{68,69}.

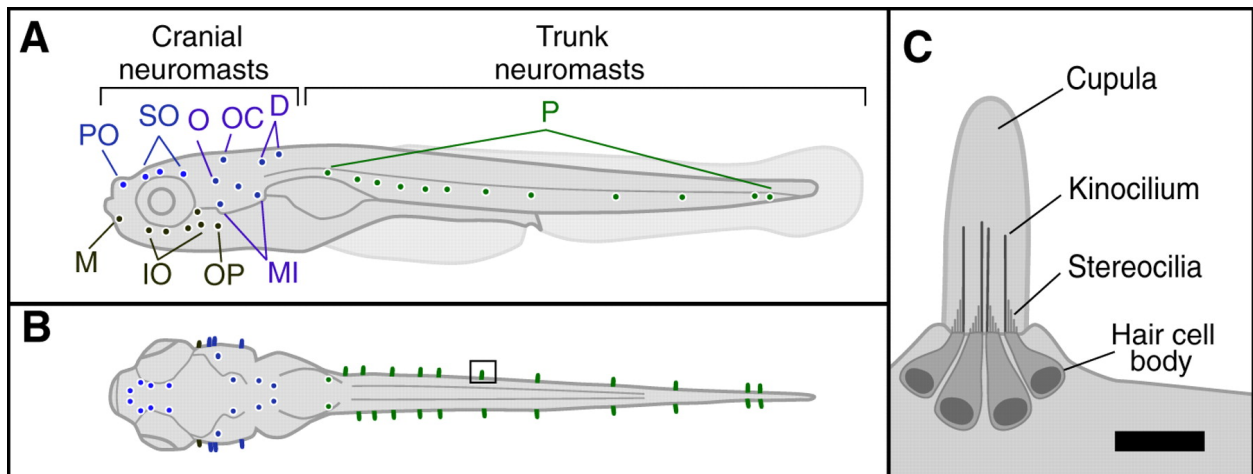


Figure 1. 8 Lateral line neuromast anatomical map. Lateral line neuromasts have protruding hair cells that detect water movement that are present in the inner ear and run along the body. Abbreviations in (A) refers to names given to these neuromasts, which specifies their anatomical location. Reproduced with permission⁷⁰.

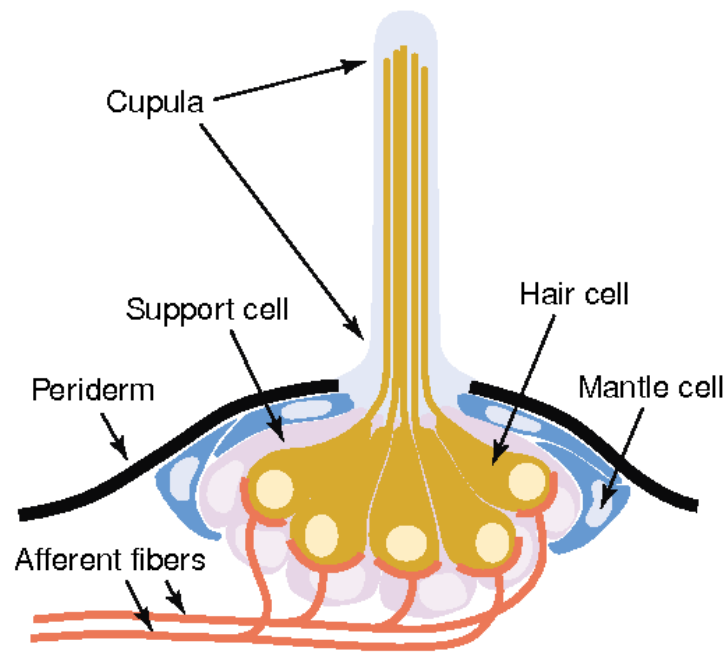


Figure 1. 9 Anatomy of hair cells. The hair cells come together to form a bundle termed the cupula, which is surrounded under the skin by support and mantle cells. The hair cells are connected to afferent nerve fibers that send signals to the brain. Reproduced with permission⁶⁹.

While some evidence shows mantle cells may lend support to regeneration of hair cells, the support cells are the primary contributor of hair cell regeneration through gene regulation. The phoenix (*pho*) gene is expressed in the support cells of the neuromast and is required for hair cell regeneration after inflicted damage⁶⁷. The retinoic acid signaling pathway mediates hair cell regeneration in neuromasts by regulating the transcription of p27^{kip} and transcription factor SOX-2 (*sox2*) in the support cells of the inner ear and lateral line⁷¹. The *sox2* gene is expressed in sensory progenitors, predominantly in support cells, and is essential for sensory development. Notch signaling acts to inhibit regeneration during development to maintain the optimal numbers of support and hair cells throughout the lateral line and inner ear. Notch has been shown to regulate the expression of *sox2* and its antagonist gene *atoh1*, to regulate hair cell specification, differentiation and regeneration^{68,71}. Zebrafish mutagenesis screens have been used to identify genes implicated in hair cell function, categorizing their role into three classes: (1) genes required for mechanotransduction, (2) genes required for synaptic transmission and (3) genes required for protein processing and sorting that could disrupt both of the previous processes⁶⁶. For example, the solute carrier family 17 (vesicular glutamate transporter), member 8 (*slc17a8*) gene is responsible for the function and recycling of glutamatergic synaptic vesicles within the hair cells^{66,72}. Zebrafish with defects in the mechanosensory organs of the auditory system exhibit the inability to maintain balance in the water column and characteristic circular swimming behaviors⁷³.

The supporting cells are predominantly responsible for the development of hair cells and their regeneration after damage⁶⁷. Damage to the inner ear hair cells in both humans and non-mammalian vertebrates leads to deafness and balance defects^{68,71}, with a large portion of

deafness in humans attributed to hair cell damage⁶⁷. Hearing loss due to hair cell deficits can be acquired or inherited, with acquired damage commonly attributed to prolonged noise exposure, or treatment with ototoxic drug such as antibiotics and chemotherapy^{68,74}. While humans cannot regenerate damaged inner ear epithelia hair cells, many other non-mammalian species such as birds, amphibians, reptiles and fish can regenerate new hairs by transdifferentiation of support cells to hair cells^{67,68,71}. A number of genes are responsible for vestibular and neuromast support cell proliferation after injury, studying of these genes have become a growing field for its potential applicability to treat hearing loss in humans⁷⁴. Zebrafish provide a valuable tool for studying hair cell development, regeneration and causative genes as the transparency allows real-time visualization and manipulation of inner ear hair cells⁶⁸. Lateral line neuromasts can also be used for studying hair cells, in which case zebrafish provide significant benefits over other animal models as the hair cells reside on the outside of the body. The lateral line neuromasts on the head begin to appear by 2 dpf, with hair cells becoming fully functional by 4 dpf⁷¹. Additionally, hair cells in both the inner ear and lateral line neuromasts are functionally and morphologically analogous and developmentally conserved to mammalian inner hair cells⁶⁸.

2. Rationale, Hypothesis and Research Objectives

2.1 Rationale

SNP clusters within the *gmds* gene have been shown to be associated with cerebral small vessel disease, which is a stroke risk factor²⁵. The *gmds* gene, which is a part of the fucosylation pathway, has never been associated with vascular phenotypes. This thesis focused on investigating the function of the catalytic enzymes fucose kinase (*fcsk*), and fucose-1-phosphate guanylyltransferase (*fpgt*) in the salvage pathway, and GDP-mannose 4,6-dehydratase (*gmds*) in the *de novo* pathway of the fucosylation pathway (**Fig. 1.7**). This project utilized a zebrafish model to investigate the phenotypic effects of a *gmds* mutation and whether a dysfunction in this gene in zebrafish would recapitulate the human phenotype. Little is known about the disease pathology, particularly the genetic contribution of this disease, which exemplifies the unprecedented importance of creating an animal model which is easily genetically manipulated and experimentally studied. A *gmds* CRISPR mutant was created to study its contribution to cerebral phenotypes, which exhibited cerebral hemorrhages and irregular swimming behaviors.

2.2 Hypothesis

The loss of function of *gmds* through a CRISPR induced mutation causes a downstream downregulation of mural cell markers in the cerebral vasculature in zebrafish resulting in cerebral hemorrhaging. Secondly, the loss of *gmds* also results in abnormal swimming behavior due to neuromast dysfunction and lack of swim bladder development.

2.3 Research Objectives

By creating a zebrafish model of *gmds*, I sought out to explore:

1. The expression of *gmds* and other fucosylation pathway genes in wildtype zebrafish and the effect of any disruption to GDP-fucose production on phenotype.
2. To investigate the molecular mechanisms and genetic contributions of the hemorrhaging phenotype observed in *gmds* mutants.
3. To examine the cause of circular swimming and balance defects present in *gmds* mutants and whether it can be attributed in part to a defect in lateral line neuromasts.

3. Methods

3.1 Fish Husbandry

All experiments were performed in compliance with the standards set by Memorial University of Newfoundland Animal Care Committee and the Canadian Council on Animal Care. Adult zebrafish were maintained in a recirculation housing system (Aquaneering Inc., San Diego, California) with a pH of 7.2-8.0, conductivity of 600-700 μ S, temperature of 28°C, and a light/dark cycle of 13:11 hr. Fish were fed a diet of GEMMA Micro 300 diet (Skretting, Tooele, Utah) and live hatched brine shrimp (Brine Shrimp Direct, Ogden, Utah).

3.2 Breeding and Fixation

Zebrafish pairs were placed in beach style breeding tanks, and were induced to breed using light. Zebrafish take seven days to reconstitute their ovaries, however we have found waiting two weeks between breeding cycles gave optimal breeding productivity. Newly fertilized embryos were collected after 2-3 hours, staged according to a previous study by Kimmel et al. (1995)⁷⁷, and raised at 28°C in embryo media (Appendix A) in petri dishes. Embryos were dechorionated and fixed overnight using 4% Paraformaldehyde/PBS (PFA, Appendix A) at the desired embryonic stages, expressed as hpf or dpf. The embryos were left in 4% PFA at room temperature on a shaker for at least 4 hours or overnight at 4°C on a shaker. Embryos could then either be used directly or placed into methanol for long term storage. For methanol storage, 4% PFA was removed and embryos were washed in 100% methanol and stored in 100% methanol at -20°C. In order to use the embryos, they were rehydrated transferring through decreasing

concentrations of methanol diluted in PBS-Tween-20. The embryos are washed in 1 ml of a 75% methanol/25% PBST mixture for 5 minutes, a 50% methanol/50% PBST mixture for 5 minutes, and a 25% methanol/75% PBST mixture for 5 minutes.

3.3 Microinjections of Morpholinos, Fucose and GDP-fucose

Morpholino antisense oligonucleotides targeting the intron-exon junction of *gmds* were injected into the one cell stage of wildtype embryos to knockdown the function of this gene. Likewise, a *fcsk* morpholino was injected into the one cell stage of *gmds* mutants and wildtype embryos to knockdown the function of this genes. A standard oligonucleotide (adjusted to experimental morpholino concentration), with no specific target in the zebrafish genome, was injected to act as a negative injection control. A p53 targeted morpholino was also co-injected to circumvent cell death. All morpholino sequences can be found in **Table 3.1**. Capillary needles used for microinjections were pulled using a Sutter P-97 Micropipetter Puller (Sutter Instrument Co.), under the following settings: Heat= 650, Pull= 150, Velocity= 75 and Time=150.

Table 3. 1: Sequences of oligonucleotides used for microinjections

Target	Oligo Sequence – All supplied by Gene Tools	Injected Concentration (ng/μl)
<i>gmds</i>	5'-CGTATGTTTGCTGACCATAAGGCGA-3'	4.25
<i>fcsk</i>	5'-TGTATAAAAGTTGCTCACCTGTCG-3'	2.1
Standard Oligo	5'-CCTCTTACCTCAGTTACAATTTATA-3'	4.25/2.1
<i>p53</i>	5'-GCGCCATTGCTTTGCAAGAATTG-3'	1.0

An incross of *gmds* heterozygous mutants and AB embryos were bred for the salvage pathway experiment (Section 4.4) and were injected at the one cell stage with *fcsk* morpholino. Uninjected *gmds* heterozygous mutants were used as a comparative control. Keep in mind this control group consists of a heterozygous cross and therefore contains a mix of wildtype, heterozygous and homozygous embryos. The cerebral hemorrhage incidence was recorded for each control and experimental group.

gmds mutant embryos were injected with either 10mM GDP-fucose, 50mM GDP-fucose, 10mM fucose and 50mM fucose (Sigma-Aldrich, St. Louis, Missouri) at the one cell stage. The cerebral hemorrhaging and curled tail rates were compared to uninjected *gmds* mutants to determine if these phenotypes could be rescued by supplementing the fucosylation pathway with a replacement of dietary fucose (fucose) or the end product of the salvage and *de novo* pathway (GDP-fucose). The p-value was calculated using a Chi-Square test with a statistical significance of <0.05, along with standard error.

Embryos were raised in petri dishes in embryo media and visualized from 2-3 dpf to assess cerebral hemorrhaging rates, which presented as stationary patches of blood typically in the midbrain-hindbrain boundary region. The incidence of cerebral hemorrhage was recorded for mutants, morphants, and wildtype embryos to determine if the phenotype was statistically significant.

3.4 CRISPR-Cas9 Design

3.4.1 Annealing of Oligonucleotides

The CRISPR technology designed for gene editing use in a laboratory is made up of a guide RNA (gRNA) and a Cas9 protein. The gRNA is a 17-20 nucleotide sequence complementary to the desired target DNA region, in this case targeting exon 6 of the long transcript of *gmds*. Two oligonucleotides (Integrated DNA Technologies, Coralville, Iowa), both complementary to exon 6 of *gmds*, were diluted to a 200 μ M working stock. The oligonucleotides were annealed using the reaction protocol outlined in **Table 3.2**. Reactions were placed in boiling water and allowed to cool to room temperature in a breaker on the bench overnight.

Table 3. 2: Annealing oligonucleotides reaction protocol

Reagent	Per reaction volume (μ l)
Oligonucleotide A (Integrated DNA Technologies, Coralville, Iowa)	7
Oligonucleotide B (Integrated DNA Technologies, Coralville, Iowa)	7
10x NEB Buffer (New England Biolabs, Ipswich, Massachusetts)	2
RO water	4

3.4.2 Vector-Oligonucleotide Ligation

The oligonucleotides were ligated in the Dr274 vector (Addgene, Watertown, Massachusetts) using the following reaction protocol outlined in **Table 3.3**. Wrapped in Parafilm (Sigma-Aldrich, St. Louis, Missouri) and left overnight at room temperature. The Dr274 (Addgene, Watertown, Massachusetts) construct contains the sequence for the Cas9 protein.

Table 3. 3: Ligation of Dr274 vector and oligonucleotide protocol

Reagent	Per Reaction Volume (μ l)
Bsal digested Dr274 vector (10ng/ μ l) (Addgene, Watertown, Massachusetts)	1
Annealed Oligonucleotides	5
10x NEB DNA Ligase (New England Biolabs, Ipswich, Massachusetts)	1
NEB T4 DNA Ligase (New England Biolabs, Ipswich, Massachusetts)	0.5
RO Water	2.5

This entire protocol takes place on ice. Competent cells (New England Biolabs, Ipswich, Massachusetts) were divided into two tubes (~25 μ l each) and 4 μ l of the ligation mixture was added. Pipetting to mix would shear competent cells. Reactions were left on ice for 20 minutes, heat shocked in a water bath at 42°C for 30 seconds and placed back on ice for 2 minutes. The tubes were taken off ice and 200 μ l of SOC Outgrowth Media (New England Biolabs, Ipswich, Massachusetts) was added to each tube and incubated on a thermomixer for 1 hour at 250 rpm at 37°C. The tubes were centrifuged at 3500 rpm for 3 minutes to pellet the cells. The majority (150 μ l) of SOC medium was removed, with the remaining 75 μ l mixed with the pellet that had been formed and plated on agar plates (Appendix A). Agar plates were parafilmmed to prevent dehydration and left to incubate overnight in a convection incubator (Benchmark) at 37°C.

3ml of LB liquid media (Bio Basic Canada Inc., Toronto, Canada) containing 50 μ g/ml Kanamycin (Sigma-Aldrich, St. Louis, Missouri) was added to a 15ml conical tube along with a colony from the grown agar plates. Multiple colonies were selected as some plasmids may not have taken up the vector-oligonucleotide compound and would remain empty. A flame was used

throughout to ensure sterilization and prevent contamination. Tubes were placed on a thermomixer shaking at 250 rpm overnight at 37°C.

The QIAprep Spin Miniprep Kit (Qiagen, Hilden, Germany) was used to purify the inoculated cells. This Qiagen kit uses columns containing silica membranes that bind up to 20µg of DNA and utilizes alkaline lysis based DNA recovery, providing an advantage over traditional phenol-chloroform extraction methods.

The 3mls of mixture in the conical tubes were split between two 1.5ml centrifuge tubes (Lifegene, Mevo Horon, Israel) and centrifuged at 14,000g for 1 minute. The supernatant was discarded and the cell pellets from the two tubes of the same sample was combined into one tube. The mixture was centrifuged at 14,000g for 1 minute and supernatant discarded. 200µl of PD1 Buffer (Qiagen, Hilden, Germany) and 2µl of True Blue Lysis Buffer (Qiagen, Hilden, Germany) was added and pipetted to mix, to lyse the bacterial cells open. 200µl of PD2 Buffer (Qiagen, Hilden, Germany) was added and mixed by inverting. The mixture was left at room temperature for 2 minutes. 300µl of PD3 Buffer (Qiagen, Hilden, Germany) was then added and mixed by inverting until the blue color had disappeared. The samples were centrifuged at 16,000 g for 3 minutes and again at 20,000g for 8 minutes. To bind DNA to the filter column the supernatant was transferred to a PDH column (Qiagen, Hilden, Germany) placed in a 2ml collection tube, centrifuged at 14,000g for 30 seconds and flow-through discarded. 400µl of W1 Buffer (Qiagen, Hilden, Germany) was added, tubes were centrifuged at 14,000g for 30 seconds and flow-through was discarded. 600µl of Wash Buffer (Qiagen, Hilden, Germany) was added to the column and centrifuged at 14,000g for 30 seconds. The flow-through was discarded and

tubes were centrifuged for an additional 3 minutes at 14,000g. The column was transferred to a new 1.5ml centrifuge tube and 30ul of Elution Buffer (Qiagen, Hilden, Germany) was added to the center of the filter membrane and left to soak into the filter for 2 minutes. The DNA was washed off the filter and into the collection tube by centrifuging at 16,000g for 3 minutes.

Samples were quantified using a Nanodrop Spectrophotometer (Nanodrop 1000 Spectrophotometer, ThermoFisher Scientific, Waltham, Massachusetts Scientific), calibrating the device with 1.5 µl of Elution Buffer (Qiagen, Hilden, Germany). DNA samples were deemed successfully isolated and of acceptable with a concentration of > 50 ng/µl and a ratio absorbance reading of 230 nm and 260 nm (230/260), 260 nm and 280 nm (260/280) of 1.7-2.1.

Vectors containing the oligonucleotides were digested to become linear by using the following reaction protocol in **Table 3.4**, and incubated in a water bath for 2.5 hours at 37°C. A digested Dr274 and undigested Dr274 vectors with no inserts were used as controls.

Table 3. 4: Reagents used for Dral digest

Reagent	Reaction Volume Per Sample of Mini Preparations (µl)	Reaction Volume Per Sample for Dr274 Vector (µl)
DNA	8	1
Dral (New England Biolabs, Ipswich, Massachusetts)	2	2
10 x CutSmart Buffer (New England Biolabs, Ipswich, Massachusetts)	2.5	2.5
Nuclease Free Water (Life Technologies, Carlsbad, California)	12.5	19.5

Digests were run on a 0.8% TAE agarose gel (Appendix A) by loading samples mixed with 4µl of x6 Loading Dye (New England Biolabs, Ipswich, Massachusetts) and comparing the

linearized samples to 5µl of 1kb ladder (FroggaBio, Toronto, Ontario). Gels were run for ~30 minutes at 100V.

The bands on the agarose gel were extracted using the Qiagen Gel Extraction Kit in 1.5ml centrifuge tubes (Lifegene, Mevo Horon, Israel). The bands were cut from the gel using a scalpel on a BLook LED Transilluminator® (GeneDireX, Taoyuan, Taiwan). The tube was weighed first empty, and then with the addition of the gel to determine the weight of the gel in order to add 3 volume of Buffer QG (Qiagen, Hilden, Germany) to the tube. The tubes were incubated in a water bath for 15 minutes at 55°C, until gel has been completely dissolved, with intermediate vortexing to help degrade the gel. One volume of isopropanol (Fischer Scientific) was then added to each sample, which was then transferred into a spin column (Qiagen, Hilden, Germany) placed in a 2ml collection tube (Qiagen, Hilden, Germany). The tubes were centrifuged for 1 minute at 16,000g to bind DNA to the column filter, thereafter the flow-through was discarded. To wash the DNA of contaminates, 750µl of Buffer PE was added to the column and let to stand for 2 minutes before centrifuging for 1 minute at 16,000g. This step was repeated 4 times. The tubes were centrifuged for another minute at 16,000g to dry the filter column. The column was then placed in a new 1.5ml collection tube (Lifegene, Mevo Horon, Israel) and 30µl of warmed Elution Buffer (Qiagen, Hilden, Germany) was added to the center of the filter column and left to absorb for 3 minutes. The tube was centrifuged for 1 minute at 16,000g and concentrations were measured using a nanodrop spectrophotometer (ThermoFisher Scientific, Waltham, Massachusetts) using Elution Buffer to blank the device. The samples were sent for sequencing at Memorial University of Newfoundland's Genomics and Proteomics Laboratory, providing

them with 600ng of sample. The samples were sequenced to ensure the samples contained the correct oligonucleotide sequence.

3.4.3 sgRNA

The oligonucleotides were assembled into a gRNA using the Maxiscript T7 Kit (Ambion, ThermoFisher Scientific, Waltham, Massachusetts). The reagents were assembled as per **Table 3.5**. The gRNA was designed to target exon 6 (target site: GGAGGCCTGGTAGAAGCGGA) of the *gmds* gene using the following oligos (TAGGTTGGAACCCTTCGGCTGC, TAGGAGGCCTGGTAGAAGCGGA).

Table 3. 5: Reagents used to synthesize gRNA

Reagent	Per Sample Volume (μ l)
DNA Template	20
10x Transcription Buffer (Ambion, ThermoFisher Scientific, Waltham, Massachusetts)	4
10mM ATP (Ambion, ThermoFisher Scientific, Waltham, Massachusetts)	2
10mM CTP (Ambion, ThermoFisher Scientific, Waltham, Massachusetts)	2
10mM GTP (Ambion, ThermoFisher Scientific, Waltham, Massachusetts)	2
10mM UTP (Ambion, ThermoFisher Scientific, Waltham, Massachusetts)	2
T7 Enzyme Mix (Ambion, ThermoFisher Scientific, Waltham, Massachusetts)	2
RO water	6

This mixture was incubated for 1.5 hours at 37°C in a thermocycler. To remove excess template DNA 2µl Turbo DNase (ThermoFisher Scientific, Waltham, Massachusetts) digestion was added to the reaction mixture and incubated for an additional 15 minutes at 37°C. 4µl of 0.5M EDTA (pH 8, Appendix A) was added to stop the reaction.

Sigma-Aldrich Prep™ spin columns (Sigma-Aldrich, St. Louis, Missouri) were centrifuged for 30 seconds at 750g and then the base of the column was broken off to allow flow-through. The columns were centrifuged for 2 minutes at 750g in a collection tube to remove storage buffer. The column was placed in a new collection tube, the RNA template from above was added to the column and centrifuged for 4 minutes at 750g. The column was discarded and 2µl of 0.25M EDTA (pH 8, Appendix A) was added to the sample. The samples were quantified using a nanodrop spectrophotometer (ThermoFisher Scientific, Waltham, Massachusetts) and run on a 2% TAE agarose gel to ensure inclusion of the insert was present. The gel contained 100µl of bleach to prevent RNA degradation⁷⁸.

3.5 Microinjections of CRISPR/Cas9

Microinjections of two gRNA (6.2 ng/µl and 27.4 ng/µl) and nuclear localized Cas9 protein (347 ng/µl) were injected into the one cell stage of the wildtype zebrafish embryos. A small portion of injected fish were set aside for genotyping (as described in section 3.6 and 3.7 below), to ensure the CRISPR mechanism was inducing an INDEL in the correct gene/gene region (**Fig. 3.1**). The remainder were grown to sexual maturity and outcrossed with the wildtype fish to establish a heterozygous founder population. Again, a small sampling of embryos from

this outcross were genotyped to ensure the fish did in fact carry a *gmds* mutation. The remainder were raised until sexual maturity and were used for all further experiments.

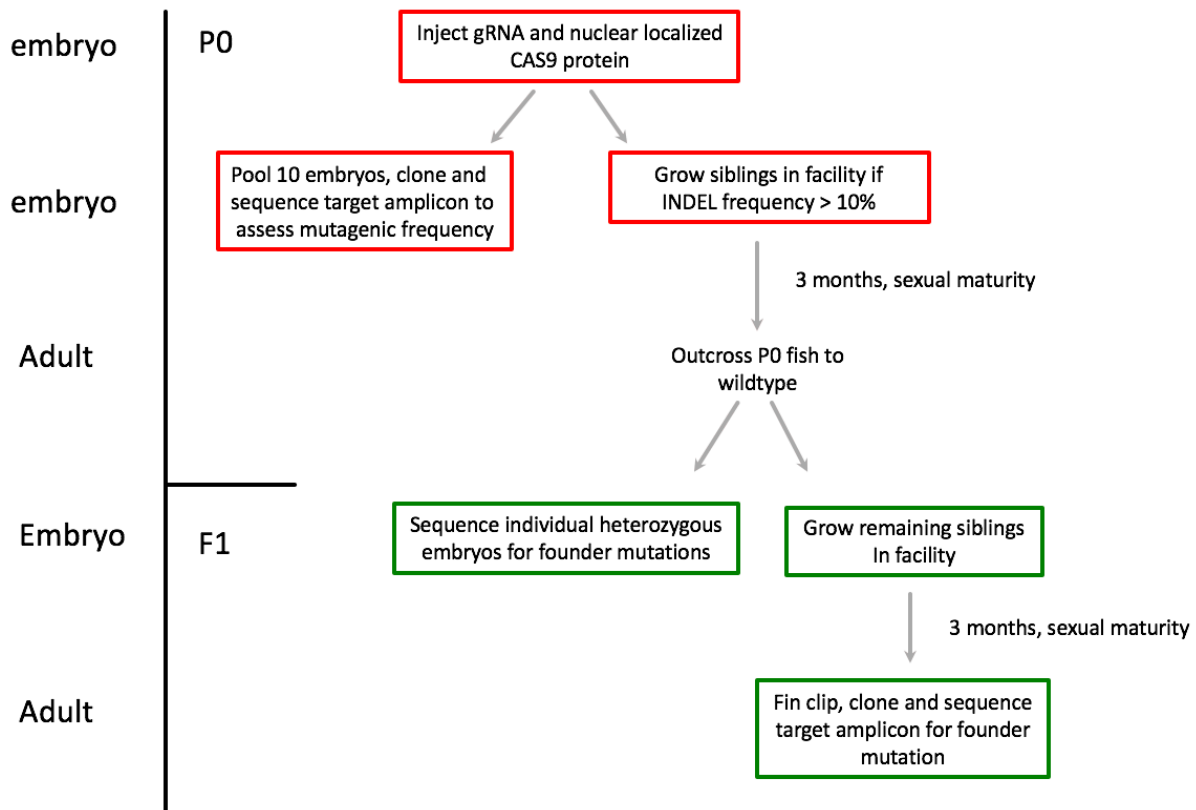


Figure 3. 1 Flow chart depicting the generation of the *gmds* mutant line. Wildtype zebrafish embryos were injected with the CRISPR construct targeting the *gmds* gene and Cas protein at the one cell stage. Ten embryos were selected for genotyping to ensure an INDEL was introduced in the correct gene. Siblings were grown to reproductive maturity and outcrossed to wildtype fish to establish the F1 generation. A small subset of embryos were taken aside for genotyping to ensure a *gmds* mutation was present, while the remaining siblings were grown to reproductive maturity.

Once the embryos were large enough, they were fin clipped and sequenced with *gmds* mutants used for all further experiments.

3.6 Characterization of Genotype and Phenotype of Mutants

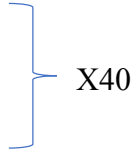
Adult mutants were anesthetised using 4.2% Tricane (Appendix A) until fish became immobilized and the rate of gill beats slowed to indicate sedation, in order to clip a small section of caudal fin for DNA isolation. Fish were recovered in system water and monitored until normal swimming behavior resumed. Each fin clip was placed in a 0.2 mL tube, labelled with a number corresponding to the isolated tank each fish would reside in until individual genotypes were identified. DNA was isolated from the fin clip by incubating in 50 μ l 50mM NaOH (Appendix A, ACP Chemicals) for 20 minutes after which, 5 μ l 1M Tris-HCl (Appendix A) was added. The *gmds* gene was amplified from this using polymerase chain reaction (PCR) using the outlined primers (**Table 3.6**). The PCR program used to amplify *gmds* is outlined in **Table 3.7**. DNA isolation of mutant progeny was performed using the whole embryo and genotyped in the same fashion.

Table 3. 6: *gmds* forward and reverse primers used to amplify the *gmds* region for PCR and Sanger sequencing

Gene Primer	Sequence	Tm (°C)	Size (bases)
<i>zGMD</i> SampF	5'-CTGCATTGCTTATGTTACCGGG-3'	56.4	22
<i>zGMD</i> SampR	5'-AATGCGTATGTTTGCTGACCAT-3'	55.4	22

Table 3. 7: The PCR program used to amplify the *gmds* gene for genotyping

Procedure	Temperature (°C)	Time
Initialization	95	4 minutes
Denaturation	95	30 seconds
Annealing	54.5	30 seconds
Extension	72	30 seconds
Final Elongation	72	5 minutes



The PCR products were then run on a 1% agarose gel to verify that the correct gene was amplified by looking for a band of approximately 307 bp (**Fig. 3.2**). DNA fragments were cleaned up using ExoSAP-IT™ (ThermoFisher Scientific, Waltham, Massachusetts), by adding 2 µl of ExoSAP-IT™ to 5 µl of DNA fragment and run on a thermocycler at 37°C for 15 minutes and 80°C for 15 minutes. Samples were also read on a nanodrop spectrophotometer (ThermoFisher Scientific, Waltham, Massachusetts) to ensure purity and concentration, as described in section 3.5.8. Considering that the CRISPR mutation screened and selected as the most efficient mutation to breed the next generation of the *gmds* mutant line was only a 1 base pair insertion (1BPI), genotyping based on band separation on agarose gel was not possible, which could otherwise be achieved with a mutation of a larger insertion/deletion. Therefore, to genotype the individual fish Sanger sequencing was used.

TAAAAATATCGATGCTGTAATAAATCAATCGTATAAAAATTGAGTCACATTAACCGGTTACTGA
AAGTTTATCGGTAGAGGAACTAGCTGTGCATATACCCTATTTAACAGAATACGGAGTTG
GGGTGGAGCTTTCTTTTTGTGCAGCATTCTTTATAGCAAACAACAATAAGAAGGGCAG
AGTAAAGAATATAGTCGGCGAACTGATGTCAACACAGGCACCACCCTCAAAAACAAGGAA
GCAACTGGTAACCTGGTCATATTTTGAAGAACAACCTGTTTTTTTGTTCACAACAACGTGA
CAATAGCAAAAATAAAAAATTTAATTTTGATTTTACACATATTTTCGACAGAATTTGTAT
TCTTTGCCACTATCAAAACCCTTGATTTTAGCCATTTGTCAAGGGGTTTTTAAACATTTA
AAATAAAATCCAGTGAAGTATGATCACTTCTCCTTTCATAAATTTTCATTAATAAATTATA
TATTAATACATGTTAATAGAATAAAGATGGAACATTTTACATTTATTTAGACTATTTAGG
TAATTTGAAACATTAAGTATACACTTGCCTTTAATAACATTTTGTATATACATAACAATTT
GCTTTTGTAAATTTAATTTGACCAAATCATTAAATTTGATTTGGACACTAAATCTACTCT
CATCTGACTGTTTTTACATTTGTTCTATATGATAACAGTGAATTGAATTTAAAGAAAAATG
TTTCAAAGCACAATAAAAGTGTATAGATAGAAAATATTTCTTTAAACTATGCTTTTCATA
TGATTTGATTAGTATCAAGAACAGGCTGAAATTATTATTATGTTTTCTCCTGAAATCAGTG
TTTGTCTCTTTCTACATTCATAAGGGAGTAATTGCCTGATTTGTGTACAGATTGTTTTT
TTTGCCTCAAGACTTTTTCAGTGAACGCTTTGAGATTCAAATTTTCATTTTAAAGTTCAGTT
TTGCTTTTATTATTTATTTTAAAGACACTGTAAAATTTAAAATGTAGCACACATACAATG
TAAATCAAACACTCACAGAATGCAGCCCTTTATATACAGGATTTTCATTTGTTGACCTGGTTT
ACATGAGCAAACCCCTTTGATGTTCTTTGTTGTTTTCCCTCACTGCAAAGCATGCAGTTCT
GTGCAAACAAGTCACTTGATATCAACTGTCAAAGACAAGAATCCTTCTCTCCGCTAAGA
CAGTTTTATTACCAGACAGTTTTTCATATCCCTTAAATTAGATTTATGTTTATCCCGGCA
GCTGCATTGCTTATGTTACCGGGTTAAGTCATTATACTTGTATGCTTGTGTACTTGAGCG
TTAAGTCTTATGCGTAAATGCTTTGTTGTTGTCAG ICTCCTTTGACCTGGCCGAGTAC
ACAGCAGATGTGGACGGGGTTGGAAACCCTTCGGCTGCTGGATGCAGTGAAGACCTGCGGT
TTAACTGACACCGTCCGTTCTAGCAGGCTCCACCAGCGAGCTCTATGGGAAAGTACAG
GAAATTCGCCAGAAAGAAACCAGCCATTTTACCAGCGATGCGCTTATGGTCAGCAAACA
TACGCATTAAATCAAACACTTAAAGATTACATTTTCTGCTTTTTTAAATAAGACTAATT
TCTTTTGCACAATTGATGAAATATCATTTCAGTTTAAAAATATATTATTGGAACCAAAAA
TGCTAATTATTCTAAATAGTTATACTTTGTAATGCATAGTAATTCCTATTTTATTTTATT
ACTATTTGACATATTCACACTATAAAATATACAAAATGTTTTAATGGCATAAGAAGATAT
TCTTGTATTCTAATAATTTAATAATTTTAAAGGAAAAAATCTAGTATTTTCGACCCAG
GGAATGTATTTTTCAGCGTTTTGCAAGAAATATACCCATGCAACTGATGACTGGTTTTGGT
CCAGGGTCACATATAATCAAATATGGTACTGTATGTTTCATATTAATGTATAGTATACAGA
TCAAAATCAAATATGTTGTTTCATTTGTATATTATAATATGGGTAATTAACAATGCAA
CATTTCCCATATTTCTTTTTCGTACCATTTTTATTTAAAAAATGTGAAGCATATGCA
TTACTTGCACTTACTATGCTATGTACAGCGTATATTGTACACCCCTTACAAATCT
CTCATTTAAATGAATATTTCTATAGGAAGCTTTACAATAATATATTGTGCATATACAT
TCCATTAGTCAGTACTAAAGCCAAATCTGGAGATAATCTTTATTTAAAGTTGAAGTTAGA
ATTATTAGCCCCCTGTTAACTTTTTTCCCAAGATTTTTTCAACACATTTTAAACATA
ATAGTTTTAATAACTCATTCTAATAATTTGATTTATTTATCTTTGCCTTGATGACA

legend: - Target Sites - Primers for amplicon
 - Missense Mutation - Insertion Mutation

Figure 3. 2 CRISPR targeting sites. Two CRISPR targeting sites were designed (highlighted in blue) to target exon 6 of the *gmds* gene. The second targeting site was a much more efficient target and mutations were created more frequently here, including the introduced missense mutation (highlighted in pink) and the one base pair insertion (highlighted in red) used to create our mutant line. The first targeting site region exhibited no mutations, indicating its inefficiency as a target sequence site. The primers used to amplify this region, highlighted in yellow, in PCR result in an amplicon size of 307 base pairs.

3.7 Sanger Sequencing

Exo-SAPped samples were prepared for sequencing in 96 well plates (ThermoFisher Scientific, Waltham, Massachusetts) by adding 2 μl of Exo-SAPped DNA to 8 μl of the following sequencing recipe in **Table 3.8**. The sequencing plate was spun in a (ThermoFisher Scientific, Waltham, Massachusetts) centrifuge at 1250 rpm for ~5 seconds and then placed on a cycle sequencing thermocycler program (**Table 3.9**) to amplify the specific gene region of interest with integrating fluorescently tagged dideoxynucleotides.

Table 3. 8: Sequencing reaction ingredients

Reagent	Volume per reaction
Nuclease Free Water	6.59 μl
ABI 5X Sequencing Buffer (ThermoFisher Scientific, Waltham, Massachusetts)	1.0 μl
F <i>gmds</i> primer	0.16 μl
ABI BigDye Terminator 3.1 cycle sequencing kit (ThermoFisher Scientific, Waltham, Massachusetts)	0.25 μl

Total: 8.0 μl

Table 3. 9: Cycle sequencing program used to amplify the *gmds* gene region for Sanger sequencing

Procedure	Temperature ($^{\circ}\text{C}$)	Time
Initialization	96	1 minute
Denaturation	96	10 seconds
Annealing	50	5 seconds
Extension	60	4 minutes

} x25

The plate was spun again at 1250 rpm then 5 μ l of 0.125M EDTA (Appendix A) and 65 μ l of 95% Ethanol (Commercial Alcohols, Toronto, Ontario) was added to each well. The plate was incubated in the dark for at least 30 minutes (the plate can be stored in the freezer at this stage) and then spun for 30 minutes at 3000x g. The plate is quickly inverted over a sink and patted to remove all ethanol. Co-precipitated salts were removed by adding 70 μ l of 70% ethanol to each well and spinning the plate for 15 minutes at 3000x g. The plate was inverted over a sink and patted to remove all ethanol. The inverted plate, with a napkin underneath, was spun in a centrifuge for 1 minute at 180x g to ensure all ethanol was removed to prevent ethanol contamination. The plate was then placed in the dark for 20 minutes with a Kim Wipe (KimTech, Irving, Texas) on top to allow any remaining ethanol to evaporate off. 15 μ l of Hi-Di™ Formamide (HDF) (ABI Scientific Inc., Sterling, Virginia) was then added to each well and spun at 1250 rpm for ~ 5 seconds. The plate was placed on a thermocycler for 2 minutes at 95°C to denature the DNA giving single stranded DNA (ssDNA) and the appropriate input for sequencing. The plate was again spun at 1250 rpm for ~ 5 seconds and run on a 3130x Genetic Analyzer (Applied Biosystems, Foster City, California). Sequencing files (ab1 format) were analyzed using 4Peaks (Nucleobytes, Aalsmeer, Netherlands) software to identify the introduction of an INDEL into the *gmds* gene.

3.8 Probe Generation and Whole Mount *in situ* Hybridization

3.8.1 Complementary DNA synthesis (cDNA)

The protocol used for anti-sense probe synthesis and *in situ* hybridization was modified from Thisse and Thisse (2008)⁷⁹. To prepare embryos for cDNA anti-sense probe synthesis a pool of ~30 2, 3 and 5 dpf AB embryos were lysed in 500 µl of Trizol (Life Technologies, Carlsbad, California; ThermoFisher Scientific, Waltham, Massachusetts). RNA was kept on ice throughout the protocol to prevent degradation. Embryos were homogenized using a pestle and vigorous pipetting and incubated for 5 minutes at room temperature. 200 µl of chloroform was added, lightly vortexed and incubated at room temperature for 3 minutes. To separate RNA, tubes were centrifuged at 4°C at 12,000x g for 15 minutes. The upper aqueous layer containing the RNA was removed and placed in a new tube. Equal parts isopropanol (ThermoFisher Scientific, Waltham, Massachusetts) was added and incubated at room temperature for 10 minutes to precipitate RNA. The RNA was further pelleted by centrifuging at 4°C at 12,000x g for 10 minutes. The supernatant was removed and the pellet was washed with 500 µl of 75% ethanol and centrifuged again at 4°C at 12,000x g for 5 minutes. The pellet was air dried for 20 minutes to ensure all ethanol had evaporated off the sample. RNA concentrations and purity were measured using nanodrop spectrophotometry (Nanodrop 1000 Spectrophotometer, ThermoFisher Scientific, Waltham, Massachusetts Scientific). The nanodrop was calibrated with 1.5 µl of RNA free water. RNA samples were deemed successfully isolated with a concentration of > 40 ng/µl and an absorbance of 230 nm and 260 nm (230/260), 260 nm and 280 nm (260/280) ratio readings of 1.7-2.1. The isolated RNA was stored at -80°C to prevent degradation.

Gene specific cDNA was generated from the total RNA extracted from the wildtype zebrafish embryos using the SuperScript One-Step RT-PCR with Platinum *Taq* Kit (ThermoFisher Scientific, Waltham, Massachusetts) using the reaction mixture in **Table 3.10** and the following primers (**Table 3.11**). A T7 RNA polymerase promoter sequence, 5' TAATACGACTCACTATAGGG 3', was added to the 5' end of the reverse primer to the 5' end of the reverse primer to allow for downstream antisense probe synthesis. Primers listed in **Table 3.11** without an underline do not have a T7 promoter site attached to the reverse primer because they were cloned into a vector that contained a T7 promoter. The program used for this One-Step kit is listed in **Table 3.12**; annealing temperatures differ based on primer melting temperature.

Table 3. 10: Reagents used to synthesize gene specific cDNA

Reagent	Volume per reaction (μl)
2x Reaction Mixture (Life Technologies, Carlsbad, California)	12.5
RNA Template	4.0
Sense Primer (10 μM)	0.5
Antisense Primer (10 μM)	0.5
RT/Platinum Taq Mixture (Life Technologies, Carlsbad, California)	0.5
RNase Free Water (Life Technologies, Carlsbad, California)	7

Table 3. 11: Primer sequences used to generate *in situ* hybridization RNA probes. T7 promoter sequences are underlined.

Primer Name	Sequence 5'-3'	Tm (°C)	PCR Product Size (bases)
<i>Cldn5</i> Forward Primer	CCTCAAGTTCCTACGCCAA	59.68	902
<i>Cldn5</i> Reverse Primer	<u>TAATACGACTCACTATAGGG</u> TATGGACCCTCCCTTCACCC	60	
<i>Fbln5</i> Forward Primer	TGGGCCGAGTACGGAATACA	60.68	1037
<i>Fbln5</i> Reverse Primer	<u>TAATACGACTCACTATAGGG</u> GACACTCGTCCACATCTTGG	65.5	
<i>Fcsk</i> Forward Primer	CTGCCACCTAAAGGGTCCAATC	57.8	1051
<i>Fcsk</i> Reverse Primer	<u>TAATACGACTCACTATAGGG</u> CAGTCCACCATGTTCAAAGGCT	67.7	
<i>Foxc1a</i> Forward Primer	GTTTTGGAGAGCAGTCATGCAG	56.5	1032
<i>Foxc1a</i> Reverse Primer	<u>TAATACGACTCACTATAGGG</u> GCGTTGGAGGTAGTCGAGATAG	64.2	
<i>Foxc1b</i> Forward Primer	TGAAGCAAAGGGAGGAAGAGAC	56.7	1139
<i>Foxc1b</i> Reverse Primer	<u>TAATACGACTCACTATAGGG</u> GATAGAGGAGGCGTTTGTGTGT	64	
<i>fpgt</i> Forward Primer	CAGAACGCGGAAACGTCTATCT	57.0	1053
<i>fpgt</i> Reverse Primer	GGTCGGCTGTTAAGTGAACAA	57.6	
<i>Fut9b</i> Forward Primer	GCAACACCACACTACATGCTTT	56.2	1001

<i>Fut9b</i> Reverse Primer	<u>TAATACGACTCACTATAGGG</u> GATACGCAACGTCATCCCTATCC	66.1	
<i>gmds</i> Forward Primer	CTGCATTGCTTATGTTACCGG	59.97	978
<i>gmds</i> Reverse Primer	AATGCGTATGTTTGCTGACCAT	59.25	
<i>Kdrl</i> Forward Primer	CCCACACATGGTCATTGAGAGA	56.8	943
<i>Kdrl</i> Reverse Primer	<u>TAATACGACTCACTATAGGG</u> AACAGGATACGCTCCTCTGGT	64.2	
<i>Myocd</i> Forward Primer	GAAGCCCAAAGACATGAAGCC	59.8	1161
<i>Myocd</i> Reverse Primer	<u>TAATACGACTCACTATAGGG</u> TGCTCAGACGAGTACGAACAG	63.7	
<i>Pdgfra</i> Forward Primer	ATCATCCTCCCTCTCACAGACA	57.1	1178
<i>Pdgfra</i> Reverse Primer	<u>TAATACGACTCACTATAGGG</u> TAGAGTCCTGCTCATTCTCCA	65.4	
<i>Pdgfrb</i> Forward Primer	AGCCAGCATCAACATCACTGTA	56.5	1058
<i>Pdgfrb</i> Reverse Primer	<u>TAATACGACTCACTATAGGG</u> TGTTGATGTGAGGACCCAGATG	67.6	
<i>Pecam</i> Forward Primer	GAGGGCTCTTACCCAATCACC	60.13	884
<i>Pecam</i> Reverse Primer	<u>TAATACGACTCACTATAGGG</u> CCTGTTCCCTCGCAGTCCTTAG	65.4	
<i>Pho</i> Forward Primer	GGTTGCCAGACTTTATCAGGGA	60.06	965
<i>Pho</i> Reverse Primer	<u>TAATACGACTCACTATAGGG</u> TGGTGTCTTGGCTCAAACCT	66.1	
<i>Slc17a8</i> Forward Primer	AAACGAAGCCCACCCCTATTG	60.2	1031

<i>Slc17a8</i> Reverse Primer	<u>TAATACGACTCACTATAGGGG</u> CTCCATTCCAAAACCTCCA	69.4	
<i>Sox2</i> Forward Primer	GCTGGTGGGGTAGACTTTCG	60.3	930
<i>Sox2</i> Reverse Primer	<u>TAATACGACTCACTATAGGG</u> CGCTCTGGTAATGTTGGGACA	67.4	
<i>Tagln</i> Forward Primer	GCCGTGCTGAACATAAAGCTG	60.47	705
<i>Tagln</i> Reverse Primer	<u>TAATACGACTCACTATAGGG</u> TGAGTGTGTGTTTCAGGGGTTTC	65.5	

Table 3. 12: RT-PCR program used to create gene specific cDNA

Procedure	Temperature (°C)	Time
cDNA Synthesis	55	30 minutes
Pre-Denaturation	94	2 minutes
Denaturation	94	15 seconds
Annealing	54.5	30 seconds
Extension	68	1 minute
Final Elongation	68	5 minutes

} X40

The amplification of the correct cDNA gene region was confirmed by separating the RT-PCR products on a 1% agarose gel. High quality cDNA would show a distinct bright band of the correct gene region size with no double banding or smears when viewed under the UV imager (Alpha Innotech, Palo Alto, California & UGenius, Sandy, Utah). cDNA fragments were cleaned up using ExoSAP-IT™ (ThermoFisher Scientific, Waltham, Massachusetts) as described previously in the Genotyping section (Section 3.6).

3.8.2 Antisense mRNA Probe Synthesis

Table 3. 13: Reaction mixture used to synthesize probes for *in situ* hybridization

Reagent	Volume per reaction (μ l)
10X RNA Polymerase Reaction Buffer (10x) (New England Biolabs, Ipswich, Massachusetts)	2.0
DTT (0.1M) (Life Technologies, Carlsbad, California)	2.0
DIG RNA Labeling Mix (10x) (Roche, Basel, Switzerland)	2.0
T7 RNA Polymerase (New England Biolabs, Ipswich, Massachusetts)	1.0
RNAse Out (Life Technologies, Carlsbad, California)	1.0
cDNA Template	7.0
RNAse Free Water (Life Technologies, Carlsbad, California)	5.0

Total = 20 μ l

Antisense probes were synthesized using a T7 RNA polymerase using the following reaction mixture, **Table 3.13**. The mixture is incubated in the thermocycler (Bio Rad, Hercules, California) at 37°C for 2 hours. After one hour has elapsed an additional 1.0 μ l of T7 RNA Polymerase was added to ensure this limiting reagent does not deplete. After the 2-hour cycle has concluded, 2 μ l of TURBO DNase (Life Technologies, Carlsbad, California) was added and incubated for an additional 20 minutes at 37°C. To stop the action of TURBO DNase 2 μ l of (0.25M) EDTA was added. To remove unincorporated ribonucleotides, the mRNA was run through the Sigma Spin Post-Reaction Clean-Up (Sigma-Aldrich, St. Louis, Missouri) columns. The columns were spun in a centrifuge for 15 seconds at 750 g. The base of the column was broken off and the lid loosened to allow flow-through of buffer, facilitated by spinning for 2 minutes at 750g. The column was placed in a new collection tube and the mRNA sample was

added and spun for 4 minutes at 750g. To the collection tube 2.0 µl of 0.25 M EDTA (Appendix A), 1.0 µl of RNase Later (Sigma-Aldrich, St. Louis, Missouri, Life Science), 2.0 µl RNase Out (Life Technologies, Carlsbad, California), and 6.0 µl of DEPC water was added to the mRNA. To confirm correct amplicon size, the sample was run on a 1% TAE agarose gel (described as above) containing 100 µl of bleach (Old Dutch) to prevent degradation during gel electrophoresis run time. The purity and concentration of mRNA was checked using a nanodrop spectrophotometer (described as above, ThermoFisher Scientific, Waltham, Massachusetts). mRNA probes were stored at -80°C. Probes were diluted to a 1/200 working stock by adding 100 ng of mRNA probe to 1000 µl of hyb mixture containing tRNA. Embryos intended for *in situ* hybridization had 1-phenyl 2-thiourea (PTU; Sigma-Aldrich, St. Louis, Missouri) added to their embryo media to prevent pigment formation. Pigment formation could mask *in situ* staining within the embryos tissues, preventing visualization of gene specific staining in these pigmented areas.

3.8.3 In Situ Hybridization Protocol

Considering the *gmds* gene has not been linked to having a role in blood vessel development or stability, I had limited information to utilize to drive my investigation of its functional role and any interactions it may have with genes responsible for blood vessel development. From the French *et al.* (2014)²⁵ study, it was discovered that SNPs within *gmds* were associated with increased stroke risk, but also that *gmds* was in linkage equilibrium with its neighbouring gene *foxc1*. *Foxc1* mutants have been known to hemorrhage due to a lack of *pdgfr* gene expression. Therefore, we examined the expression of *foxc1a*, *foxc1b*, *pdgfra*, and *pdgfrb* in *gmds* mutants, as any differential expression of these genes could indicate an interaction of *gmds*

in a pathway that involves *foxc1* or *pdgfr* and the resulting hemorrhaging phenotypes seen in these mutants. A number of endothelial cell marker genes (*cldn5b*, *kdrl*, and *pecam*) and mural cell marker genes (*foxc1a*, *foxc1b*, *pdgfra*, *pdgfrb*, *tagln*, *myocd*, and *fbln5*) were tested in *gmds* mutants to determine if *gmds* was affecting the expression of genes responsible for blood vessel development and stability. The observed curled tail and abnormal swimming phenotype prompted me to look for a link between *gmds* and genes responsible for neuromast development and function (*sox2*, *slc17a8* and *pho*) using *in situ* hybridization. Genes in the fucosylation pathway (*gmds*, *fcsk*, *fpgt*, and *fut9b*) were also examined using *in situ* hybridization to determine if they were expressed in areas that contribute to blood vessel formation.

Day one: Embryo Fixation

Embryos are able to break out of their chorion by ~3 dpf. If embryos were needed at an earlier time point they were dechorionated manually. The chorion encasing the embryo was removed using fine tip tweezers. Embryos were dechorionated and placed in 4% PFA (Sigma-Aldrich, St. Louis, Missouri) at the desired time point to fix them in the selected developmental stage (as described in breeding section). Embryos were separated into wildtype and mutant tubes based on phenotype, with each tube containing 15-30 embryos. A set of tubes was used for each time point and/or probe desired. The time points used for each probe are listed in **Table 3.14**.

Table 3. 14: Embryo life stages used for in situ hybridization experiments for each gene probe

Gene	Time point (hpf)
<i>cldn5</i>	72
<i>fbln5</i>	72
<i>fcsk</i>	48
<i>foxc1a</i>	72
<i>foxc1b</i>	72
<i>fpgt</i>	24
<i>fut9b</i>	72
<i>gmds</i>	2, 24, 48, 72
<i>kdrl</i>	48
<i>myocd</i>	72
<i>pdgfra</i>	48, 72
<i>pdgfrb</i>	48, 72
<i>pecam</i>	48
<i>pho</i>	72
<i>slc17a</i>	72
<i>sox2</i>	72
<i>talgn</i>	48, 72

Each tube of embryos was washed in PBST (PBS/0.1% Tween-20- Sigma-Aldrich, St. Louis, Missouri, Appendix A) 5 times for 5 minutes each. The embryos were permeabilized in PBST containing 10 µg/ml Proteinase K (Appendix A) for varying time frames based on the age of the embryo. The 24 hpf, 48 hpf, and 72 hpf embryos were permeabilized using Proteinase k for 3 minutes, 15 minutes, and 30 minutes, respectively. The 2 hpf embryos were too fragile for Proteinase k, therefore this step was skipped. Embryos were re-fixed in 4% PFA for 20 minutes

at room temperature and rinsed in PBST 5 times for 5 minutes. The embryos were placed in 500 μ l of hybridization mixture (Appendix A) for at least one hour at 65°C in a water bath (ThermoFisher Scientific, Waltham, Massachusetts). The hybridization mixture was removed and replaced with the warmed probe (1/200) working stock and left overnight at 65°C. Challenging probe targets, that were expressed at low levels, were left in the probe mixture for two days.

Day two: Washes & anti-digoxigenin-alkaline phosphatase binding

Embryos were washed with a series of pre-warmed 66% hybridization/33%2x SSC mixture, 33%hybridization/66% 2x SSC, and 2x SSC solutions for 5 minutes each at 65°C (recipes in Appendix A). Embryos were then washed in 0.2x SSC/0.1% Tween-20 (Sigma-Aldrich, St. Louis, Missouri) and twice in 0.1x SSC/0.1% Tween-20 for 20 minutes each at 65°C. Embryos were then washed through 66% 0.2x SSC/33% PBST, 33% 0.2x SSC/66% PBST, and 100% PBST for 5 minutes each at room temperature.

Embryos were then incubated in fresh blocking solution (PBST, 2% sheep serum, 2 mg/mL bovine serum albumin, Sigma-Aldrich, St. Louis, Missouri) for 1 hour at room temperature on a horizontal shaker. Embryos were then incubated in a 1/5000 solution of anti-digoxigenin-AP antibody (Roche, Basel, Switzerland) in blocking solution on a horizontal shaker overnight at 4°C.

Day three:

Embryos were washed to remove the antibody solution using 5 x 15 minute washes of PBST on a horizontal shaker at room temperature.

Coloration reaction – NBT/BCIP

Embryos were washed in coloration buffer (Appendix A) 4 x 5 minutes. The coloration reaction was achieved by placing embryos in a solution of coloration buffer with 45 μ l nitro-blue tetrazolium (NBT, Roche, Basel, Switzerland) and 35 μ l of 5-bromo-4-chloro-3-indolyl phosphate (BCIP, Roche, Basel, Switzerland) in a ceramic dish in the dark at room temperature until appropriate levels of specific staining had been achieved.

Coloration reaction – BM Purple (alternate coloration method)

BM Purple coloration buffer was also used for a number of *in situ* experiments, however we opted to revert back to the NBT/BCIP protocol as the BM purple solution was resulting in higher background staining for some probes. After the mentioned PBST washes, embryos were washed with reverse osmosis water (M Ω 18.2), twice for ~5 seconds. The embryos were then resuspended in 1 ml of BM Purple (Roche, Basel, Switzerland) in a ceramic dish in the dark at room temperature until appropriate levels of specific staining had been achieved. The BM Purple coloration reaction tended to colorize in a shorter time frame compared to the NBT/BCIP reaction protocol.

To stop the coloration reaction for the NBT/BCIP or BM Purple protocols, embryos were washed in PBST (pH 5.5) stop solution (Appendix A) 2 x 10 minutes. Embryos were stored in PBST until microscopic imaging.

3.9 Screening mutant generations

Zebrafish with a potential *gmds* mutation were screened for mutant phenotypes starting at 2 dpf. Initially mutant phenotypes were characterized by recording and photographing bent tail and cerebral hemorrhaging phenotypes and individually genotyping zebrafish embryos using Sanger sequencing. Through sequencing embryos and matching their phenotypes to their genotype, it was determined that only homozygous mutants exhibited these phenotypes. A phenotype based screening method was used to characterize embryos as wildtype or mutant for experiments.

3.10 Fucosylation Measurement

Fucosylated proteins were stained using *Aleuria aurantia* Lectin (AAL, Vector Labs, Burlingame, California) stain and described. Live wildtype and *gmds* mutant embryos, at 24 hpf and 48 hpf time points, were placed in a centrifuge tube containing 1 mL of 20 ug/mL AAL for 10 minutes and washed twice in PBST (Appendix) for 5 minutes.

3.11 Scanning Electron Microscopy (SEM)

SEM was performed on the 6 dpf mutant and wildtype embryos to photograph the lateral line neuromasts and determine any potential morphological differences caused by the *gmds* mutation. Embryos were categorized as either mutant or wildtype based on the presence or absence of cerebral hemorrhaging that appeared over the six days.

Whole embryos were fixed in 2.5% glutaraldehyde (Electron Microscopy Sciences, Hatfield, Pennsylvania) and 2.5% PFA (Sigma-Aldrich, St. Louis, Missouri, Appendix A) in a 0.1M Sodium Cacodylate buffer (Electron Microscopy Sciences, Hatfield, Pennsylvania) overnight. They were then washed 3 times in 0.1M Sodium Cacodylate buffer for 10 minutes. Embryos were then placed in 1% OSO_4 (Sodium Tetroxide) in a 0.1M Sodium Cacodylate buffer for 1 hour, and subsequently washed twice with 0.1M Sodium Cacodylate buffer for 10 minutes. The embryos were then dehydrated using increasing graded series of ethanol washes. First, they were washed in 25%, 50% and 75% EtOH (Commercial Alcohols, Toronto, Ontario) at 15 minutes for each wash (varying concentrations of stocks were made using reverse osmosis water). Then, the embryos were washed for 10 minutes in 100% EtOH, followed by another 15 minute wash in 100% EtOH. The ethanol was gradually replaced using a series of hexamethyldisilazane (HMDS, Electron Microscopy Sciences, Hatfield, Pennsylvania)/EtOH solutions. Solutions of 75:25, 50:50, 25:75 were prepared, and embryos were washed in each for 15 minutes⁸¹. The remaining ethanol was rinsed from the embryos using two, 15 minute 100% HMDS washes. The HMDS was poured off and the embryos were left to dry overnight in the fume hood. A selection of mutant and wildtype embryos were mounted on separate SEM stubs,

gold plated by the Scanning Electron Microscopy Laboratory (Memorial University of Newfoundland), and imaged in a partial vacuum.

Images of lateral line neuromasts were captured at 12,355x magnification. The neuromast length and width were measured using ImageJ's freehand tool and averaged for mutants and wildtypes. Statistical significance was determined by averaging length and width measurements and performing an unpaired Student's t-test along with the standard error.

3.12 Confocal Imaging of Transgenic Line

The *gmds* mutant line was crossed with a *acta2:gfp* line to localize mural cells within the context of the *gmds* mutation, which can be viewed under a confocal microscope. Embryos were screened for the presence of *gfp* and then separated as wildtype or mutant based on the presence or absence of cerebral hemorrhages. The embryos were fixed in 4% PFA (Sigma-Aldrich, St. Louis, Missouri, Appendix A) for 2 hours on a shaker at room temperature, in the dark to prevent *gfp* photobleaching. The embryos were washed twice with PBST (Appendix A) for 10 minutes. A small layer of nail polish (Claire's) was used to draw a box slightly smaller than the coverslips to prevent the solution from leaking out while setting. The embryos were de-yolked and placed on a microscope slide (StatLab, McKinney, Texas) on their backs, careful to remove all PBST from the slide. Grease was applied to the slide using a syringe to create four pillars to support the cover slip. Once the coverslip (Sigma-Aldrich, St. Louis, Missouri) was placed on, the Fluoroshield with DAPI Histology Mounting Solution (Sigma-Aldrich, St. Louis, Missouri) was added to coat the underside surface area of the coverslip. Slides were left to dry overnight, in the

dark, to prevent gfp degradation. Confocal images were taken on a Nikon A-1 confocal microscope using the operating NIS-Elements AR 4.50 program provided by the Cold-Ocean Deep-Sea Research Facility at Memorial's Ocean Science Centre.

3.13 RNA Isolation and cDNA Synthesis for qPCR

3.13.1 RNA Isolation

Fertilization of *gmds1bpi* mutants and AB wildtype embryos were synchronized to ensure simultaneous collection of matching aged embryos. Embryos were grown for three days, at which point the *gmds* mutants with cerebral hemorrhaging were selected as the mutant group going forward. RNA was isolated from each genotype group using the PureLink™ RNA Mini Kit (ThermoFisher Scientific, Waltham, Massachusetts). All steps are performed at room temperature. Embryos of the same genotype were pooled in a tube and 3µl of 2-mercaptoethanol (Sigma-Aldrich, St. Louis, Missouri) and 300µl to Lysis Buffer (ThermoFisher Scientific, Waltham, Massachusetts) was added to each sample. The mixture was pipetted to mix with a 100µl pipette tip to mince and lyse tissues. The lysate was transferred to a 1.5ml centrifuge tube and centrifuged for 2 minutes at 12,000g. One volume of 70% ethanol (Commercial Alcohols, Toronto, Ontario) was added to the tissue homogenate and then vortexed to disperse any formed precipitate. The sample was transferred to the Spin Cartridge (ThermoFisher Scientific, Waltham, Massachusetts) and centrifuged for 15 seconds at 12,000g, the flow-through was discarded. 700µl of Wash Buffer I (ThermoFisher Scientific, Waltham, Massachusetts) was added to the Spin Cartridge and centrifuged for 15 seconds at 12,000g, flow-through discarded. The Spin Cartridge was added to a new collection tube and 500µl Wash Buffer II with ethanol

(ThermoFisher Scientific, Waltham, Massachusetts) was added to the cartridge and centrifuged for 15 seconds at 12,000g. The flow-through was discarded and placed back into the same collection tube. The Wash Buffer II, centrifuge and discard steps were repeated. The Spin Cartridge was centrifuged for 1 minute at 12,000g to dry the membrane and placed in a new collection tube. 30µl of RNase-Free Water (ThermoFisher Scientific, Waltham, Massachusetts) was added to the center of the Spin Cartridge and left to incubate for 1 minute. The Spin cartridge was then centrifuged for 2 minutes at 12,000g. This addition of 30µl of RNase-Free Water was repeated to produce a final isolated RNA product of 60µl. The RNA concentration was measured using a Qubit Fluorometer (ThermoFisher Scientific, Waltham, Massachusetts).

A TURBO DNA-Free™ kit (ThermoFisher Scientific, Waltham, Massachusetts) was used to rid RNA sample of contaminating genomic DNA. 1µl of TURBO DNase (ThermoFisher Scientific, Waltham, Massachusetts) and 5µl of 10x TURBO DNase Buffer (ThermoFisher Scientific, Waltham, Massachusetts) was added to the sample and incubated for 30 minutes at 37°C in a water bath. 5µl of DNase Inactivation Reagent (ThermoFisher Scientific, Waltham, Massachusetts) was added and incubated at room temperature for 5 minutes. The sample was then centrifuged for 1.5 minutes at 10,000g, the supernatant containing the RNA was removed and placed in a new tube.

3.13.2 cDNA Synthesis

cDNA was synthesised from RNA using the High Capacity cDNA Reverse Transcription Kit (ThermoFisher Scientific, Waltham, Massachusetts) using 100 ng RNA input. The cDNA reagent mix is listed in **Table 3.15**.

Table 3. 15: cDNA synthesis reagents

Reagent	Volume Per Sample (µl)
10x RT Buffer (ThermoFisher Scientific, Waltham, Massachusetts)	2
25x dNTP Mix (100mM, ThermoFisher Scientific, Waltham, Massachusetts)	0.8
10x RT Random Primers (ThermoFisher Scientific, Waltham, Massachusetts)	2
MultiScribe™ Reverse Transcriptase (ThermoFisher Scientific, Waltham, Massachusetts)	1
RNase Inhibitor (ThermoFisher Scientific, Waltham, Massachusetts)	1
Nuclease-Free Water (ThermoFisher Scientific, Waltham, Massachusetts)	3.2

The RNA template was diluted to 100ng, making up a total volume of 10µl with Nuclease-Free Water (ThermoFisher Scientific, Waltham, Massachusetts). The cDNA master mix was added to each sample and placed on the following thermocycler program, **Table 3.16**.

Table 3. 16: Thermocycler program for cDNA synthesis

	Temperature (°C)	Time (minutes)
Step 1	25	10
Step 2	37	120
Step 3	85	5
Step 4	4	∞

A negative control was assembled consisting of master mix with no template. An additional control was assembled for each sample (just for the first qPCR run using these samples) consisting of master mix with template but no RT Buffer, in order to monitor genomic DNA contamination. cDNA sample concentrations were read with a nanodrop spectrophotometer (ThermoFisher Scientific, Waltham, Massachusetts) using the ssDNA program option and Nuclease-Free Water (ThermoFisher Scientific, Waltham, Massachusetts) to calibrate the device.

3.14 Quantitative Polymerase Chain Reaction (qPCR)

The TaqMan™ Gene Expression Assay Kit (ThermoFisher Scientific, Waltham, Massachusetts) was used in the reverse transcription quantitative PCR (RT-qPCR) from the cDNA using 50ng of product. The cDNA was made up into 50ng/μl working stocks and added in the following qPCR reaction mixture, **Table 3.17**. The *foxc1b* and *pdgfra* Gene Expression Assay were used along with the housekeeping gene assay, *tbp* (ThermoFisher Scientific, Waltham, Massachusetts). A separate master mix was compiled for each gene assay.

Table 3. 17: Reagents used for qPCR analysis

Reagent	Volume Per Sample (μ l)
20x TaqMan Gene Expression Assay (ThermoFisher Scientific, Waltham, Massachusetts)	1
2x TaqMan Gene Expression Master Mix (ThermoFisher Scientific, Waltham, Massachusetts)	10
cDNA Template (50ng)	0.5
RNase Free Water (ThermoFisher Scientific, Waltham, Massachusetts)	8.5

19.5 μ l of qPCR master mix was added to each well of a qPCR plate (Applied Biosystems, Foster City, California) along with 0.5 μ l of cDNA (50ng). It was crucial to ensure exactly 0.5 μ l of cDNA was added to each well as anything over or under would divert the concentration away from 50ng and therefore the analysis of comparable gene expression would be inaccurate. A plate with four biological replicates from the wildtype and mutant groups were set up in a technical triplicate for each gene assay, along with a no template control for each sample set. The first run of qPCR used the no reverse transcriptase and no-template control assembled with the cDNA kit to ensure there was no DNA contamination. Two gene assays were used, measuring the gene expression of *foxc1b* and *pdgfra*, against the housekeeping gene *tbp*. Each qPCR run was repeated in duplicate to ensure replicable results. An example of a plate set up seen in **Figure 3.3**. A number of sample runs were performed to determine the optimal cDNA input concentration to produce quality cycle number peaks.

	1	2	3	4	5	6	7	8	9	10	11	12
A	AB12	1BPI 12	1BPI 25	AB25	AB7	1BPI 7	1BPI 13	AB13	NTC	AB12	1BPI 12	1BPI 25
B	↓	↓	↓	↓	↓	↓	↓	↓	↓	AB25	AB7	1BPI 7
C	↓	↓	↓	↓	↓	↓	↓	↓	↓	1BPI 13	AB13	NTC
D	↓	↓	↓	↓	↓	↓	↓	↓	↓	AB12 - No RT	1BPI12 - No RT	1BPI25 - No RT
E	↓	↓	↓	↓	↓	↓	↓	↓	↓	AB25 - No RT	AB7 - No RT	1BPI17 - No RT
F	↓	↓	↓	↓	↓	↓	↓	↓	↓	1BPI13 - No RT	AB13 - No RT	
G	↓	↓	↓	↓	↓	↓	↓	↓	↓			
H	↓	↓	↓	↓	↓	↓	↓	↓	↓			

Figure 3. 3 qPCR sample plate. An example of a qPCR plate containing 3 technical replicates and 8 biological replicates for each gene assay. Legend: Wildtype embryos (AB#), *gmds* mutant embryos (1BPI#), No template control (NTC) and No RT Buffer (No RT).

An optical cover (Applied Biosystems, Foster City, California, Life Technologies, Carlsbad, California) was used to seal the plate, which was then loaded on the Applied Biosystems 7900HT Fast Real-Time PCR System for qPCR analysis using the SDS RQ Manager program. The qPCR results were analyzed using the delta-delta Ct method in Microsoft Excel. The p-value was calculated using a Student's t-test and a statistical significance of 0.05, along with standard error.

4. Results

4.1 *gmds* mutant creation

To utilize a zebrafish model to understand the function of *gmds* and determine its contribution to vascular development, a CRISPR *gmds* mutant was created to first categorize the consequences of a GDP-fucose loss of function. The flow chart (**Fig 3.1**) in the material and methods section “Microinjections of CRISPR/Cas9” provides a visual overview of the mutant creation and screening process. The CRISPR construct targeting exon 6 of *gmds* was injected into the 1-cell stage of embryos along with nuclear localized Cas9 protein, resulting in random INDELS. A large pool of embryos were injected with the CRISPR/Cas9 construct with the majority reared to adulthood. A small random sample of eight embryos were sequenced to ensure the gRNA had targeted the right sequencing site and had introduced a mutation. Although the entire gene was not sequenced to look for off target effects, the mutants were outcrossed to limit the effect of any potential off target mutations. A F0 mutation frequency of ~50% was found (**Fig. 4.1**), with a variety of introduced INDELS. Adult F0 generation were outcrossed with wildtype fish to establish the F1 generation and had a small subset of embryos selected for genotype screening to ensure the presence of *gmds* INDELS.

Sanger sequencing of the embryos from adult F1 mosaic outcrosses identified three types of INDELS, a 1 bpi, a 2 base pair deletion (bpd), and 1 bpd induced by the CRISPR mechanism. The 1 bpi mutation was accompanied by a missense mutation (**Fig. 4.2**), which created a premature stop codon, truncating the protein at the CRISPR cut site (**Fig. 4.3**). Cerebral hemorrhaging incidence was similar between all mutant genotypes. All defects seen as a result of loss of *gmds* (cerebral hemorrhaging, curled tail and abnormal swimming phenotypes) were

phenocopied in morphants and mutants. Unless otherwise noted, all experiments were performed with the 1 bpi mutant line, as the sex ratios and total sample size were the most abundant for this line. In addition, this mutant gave the most deleterious protein altering product. This line is designated *gmds*ⁿ¹⁰⁰².

PAM1 PAM2

```

Reference GGGGTGGAAACCTTCG-GCTGCTGGATGCAGTGAAGACCTGCGGTTTAACTGACACCGTCCGCTTACACAGGCCTCCACCAGCGAGI
WT GGGGTGGAAACCTTCG-GCTGCTGGATGCAGTGAAGACCTGCGGTTTAACTGACACCGTCCGCTTACACAGGCCTCCACCAGCGAGI
WT GGGGTGGAAACCTTCG-GCTGCTGGATGCAGTGAAGACCTGCGGTTTAACTGACACCGTCCGCTTACACAGGCCTCCACCAGCGAGI
Del (1bp)(28bp) GGGGTGGAAACCTTCG-G-TGCTGGATGCAGTGAAGACCTGCGGTTTAACTGACACCGTCCGCTTACACAGGCCTCCACCAGCGAGI
Del (13bp) GGGGTGGAAACCTTCG-GATGCTGGATGCAGTGAAGACCTGCGGTTTAACTGACACCGTCCGCTTACACAGGCCTCCACCAGCGAGI
Del (2bp) GGGGTGGAAACCTTCG-GCTGCTGGATGCAGTGAAGACCTGCGGTTTAACTGACACCGTCCGCTTACACAGGCCTCCACCAGCGAGI
Ins (1bp) GGGGTGGAAACAAAAGCAGGGTGGATGCAGTGAAGACCTGCGGTTTAACTGACACCGTCCGCTTACACAGGCCTCCACCAGCGAGI
WT GGGGTGGAAACCTTCG-GCTGCTGGATGCAGTGAAGACCTGCGGTTTAACTGACACCGTCCGCTTACACAGGCCTCCACCAGCGAGI
WT GGGGTGGAAACCTTCG-GCCGCTGGATGCAGTGAAGACCTGCGGTTTAACTGACACCGTCCGCTTACACAGGCCTCCACCAGCGAGI

```

Figure 4. 1 F0 mutation rate. The mutations present in the wildtype embryos injected with CRISPR targeted to *gmds*, exhibiting a 50% mutation frequency.

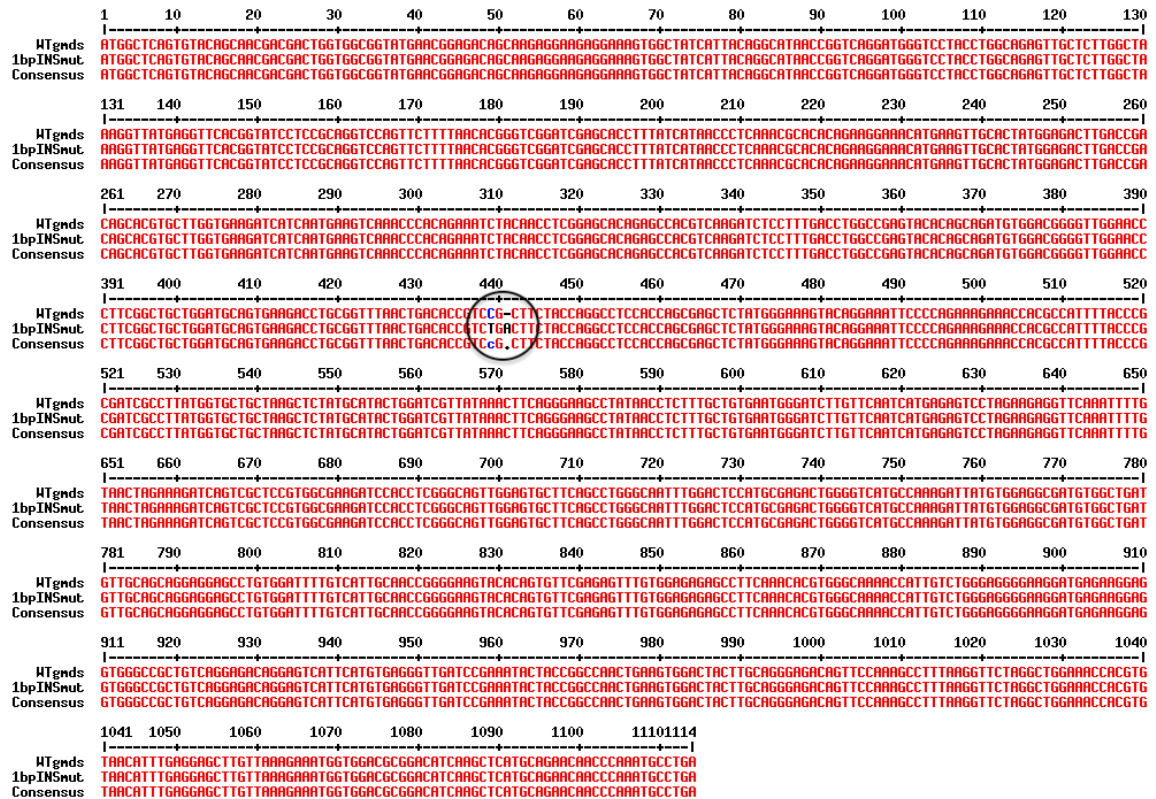


Figure 4. 2 Sequence alignment of wildtype and *gmds*ⁿ¹⁰⁰² mutant zebrafish. The sequence of a genotyped adult wildtype zebrafish (top row sequence) was aligned with a sequence from a *gmds* founder F1 mutant with a one missense and one base pair insertion mutation (middle row

sequence). A consensus sequence is created to exemplify the differences present between the two sequences (bottom row sequence).

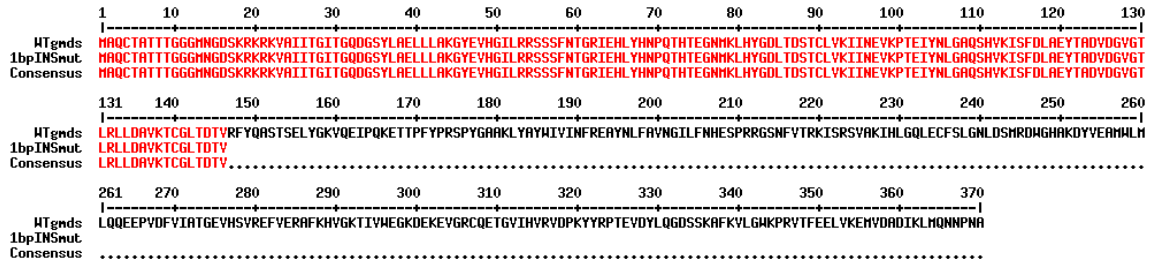


Figure 4. 3 Predicted protein sequence of *gmds*ⁿ¹⁰⁰² in wildtype and mutant zebrafish. The protein sequence of a genotyped adult wildtype zebrafish (top row sequence) was aligned with the protein sequence from a *gmds* mutant where the missense and insertion mutation (439th and 441st base pair respectively) created a premature stop codon at the 46th amino acid in exon 6 of the *gmds* gene, thereby truncating the protein coding sequence (middle row sequence). A consensus sequence is created to exemplify the differences present between the two sequences (bottom row sequence).

4.2 The loss of *gmds* results in cerebral hemorrhaging and curled tails

The loss of function induced by the introduction of an INDEL by CRISPR or morpholino injections resulted in cerebral hemorrhaging in the mid-hindbrain boundary (and occasionally other cerebral regions), accompanied by a curled tail (**Fig 4.5, B**) and circular swimming phenotype (Supplemental **Video 2**). The wildtype zebrafish injected with a *gmds* directed morpholino hemorrhaged at a rate of 23.4%, and 41.7% of morphants exhibiting a curly tail and circular swimming behaviour, respectively (**Fig. 4.4, B&C & Supplemental Video 2**). All *gmds* morphants and mutants experiencing cerebral hemorrhaging also had curled tails. The *gmds* homozygous mutants hemorrhaged at a rate of 55% and a 100% rate of bent tail and circular swimming behavior (**Fig. 4.5, B&C**). The wildtype siblings and heterozygous fish did not mirror this phenotype (**Fig. 4.5, C**). The curled tails and aberrant swimming behavior was previously reported in a mild hypomorphic *gmds* mutant strain, however a cerebral hemorrhage phenotype was not reported. The *gmds*ⁿ¹⁰⁰² mutants possess more severe swimming defects, appear to exhibit balance and touch response defects (Supplemental **Video 2**), not seen in videos provided of other *gmds* mutant strains.

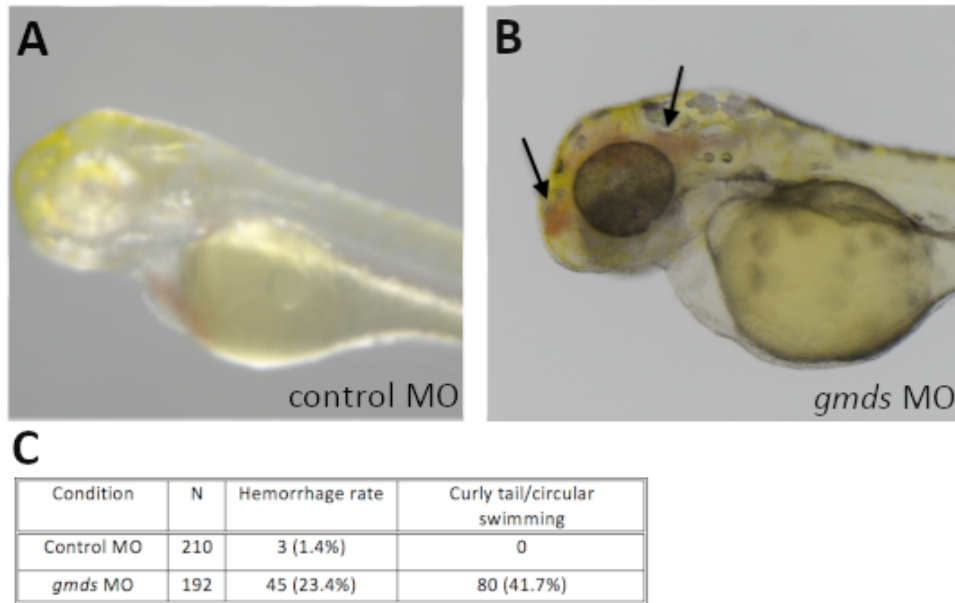


Figure 4. 4 Hemorrhaging and circular swimming rates of wildtype embryos injected with a control or *gmds* morpholino. (A) A wildtype embryo injected with a control morpholino (MO) reared to 3 dpf. (B) A wildtype embryo injected with *gmds* morpholino, reared to 3 dpf and exhibiting a curly tail and cerebral hemorrhage. (C) The rates of hemorrhage, curly tail and swimming behavior recorded at 3 dpf for wildtype embryos injected with a standard control or *gmds* morpholino.

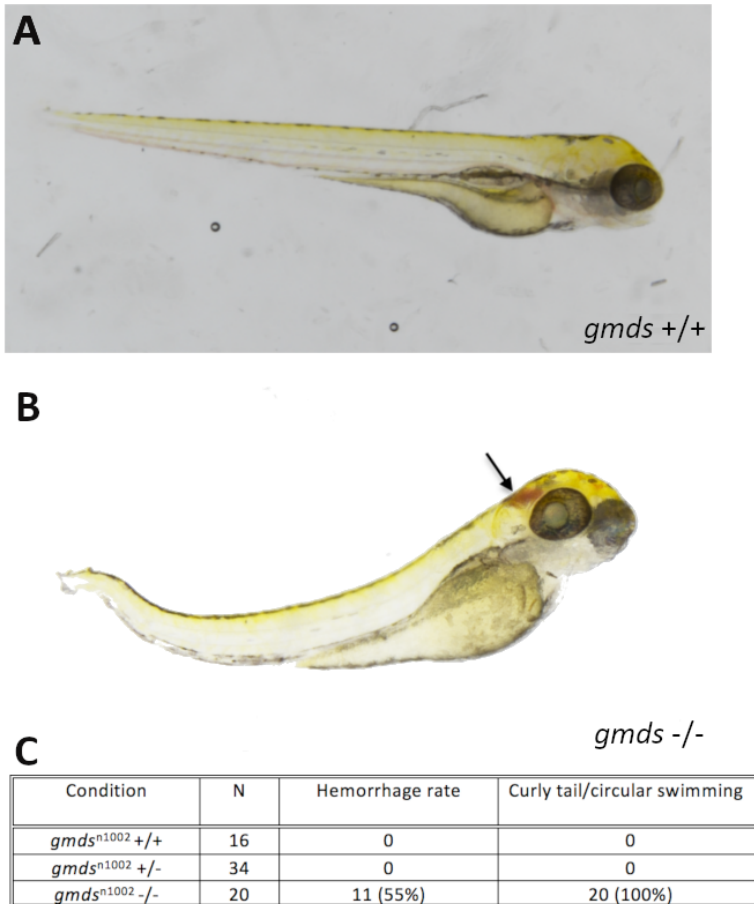


Figure 4. 5 Hemorrhaging and circular swimming rates of embryos positive or negative for *gmds* mutations. Embryos are deemed wildtype, heterozygous or homozygous based off of sequencing results. **(A)** A 3 dpf embryo with no *gmds* mutation. **(B)** A homozygous *gmds* 1BPI mutant embryo 3 dpf with a curly tail and cerebral hemorrhage. **(C)** The rates of hemorrhage, curly tail and swimming behavior recorded at 3 dpf for *gmds* negative, heterozygous, and homozygous mutants resulting from two pairwise incrosses of heterozygous carriers. Embryos were genotyped to ensure phenotypic characterization was an accurate form of genotypic identification.

4.3 *gmds* is expressed in the pharyngeal arches and lateral line neuromasts

To better understand the function of *gmds*, the expression profile was examined in wildtype embryos using *in situ* hybridization probes designed against *gmds*. At 2 hpf the *gmds* gene is maternally deposited and therefore appears throughout the embryo (**Fig. 4.6**). At 24 hpf *gmds* is expressed in the epidermis and mesenchyme. By 48 hpf *gmds* expression was localized to the brachial arches with staining intensity increasing by 72 hpf. Expression of *gmds* was also noted at 72 hpf in the lateral line neuromasts (**Fig. 4.6**). To demonstrate specificity of the antisense probe, at each time point, embryos were hybridized with a sense probe (a negative control), with any difference in staining pattern between sense and antisense probes being considered to demonstrate specific *gmds* localization.

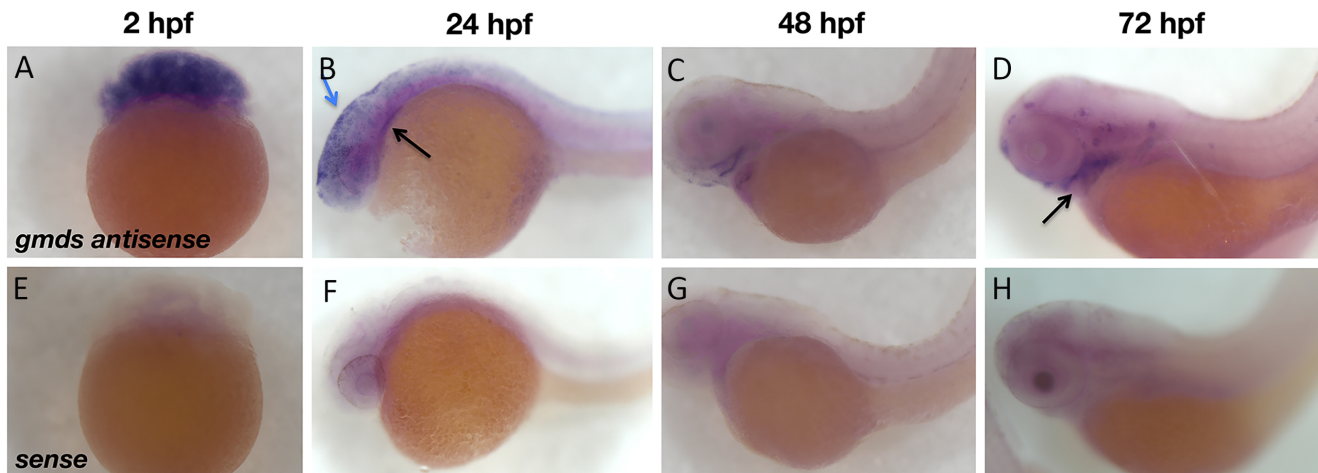


Figure 4. 6 Localized *gmds* gene expression. (A) The *gmds* gene is ubiquitously expressed at 2 hpf (A: n =11), typical of maternally deposited gene expression at this time point. (B) Expression of *gmds* was found in the epidermis and the developing mesenchyme at 24 hpf as indicated with arrows (B: n=22). (C) At 48 hpf, expression was noted in the pharyngeal (brachial) arches, an important blood vessel formation location that will eventually give rise to all blood vessels in the head (C: n=20). (D) By 72 hpf, the ventral head mesenchyme and sensory neuromasts have *gmds* expression staining (D: n=23). (E-H) Negative control staining of the embryos at all time points indicates nonspecific staining primarily in the dorsal yolk sac (24 hpf), brain (48 hpf), and eye (72hpf) (E: n=5, F: n=6, G: n=6 and H: n=23).

4.4 Salvage pathway genes contribute to hemorrhaging phenotypes

To assess the salvage pathways role in the hemorrhaging phenotype seen in *gmds* mutants and morphants, the expression profile was first assessed in wildtype embryos to determine if the genes were localized to important vascular areas. *In situ* hybridization probes directed against the *fcsk* gene found ubiquitous expression throughout the head at 24 hpf (**Fig. 4.7, A**). The same expression pattern was seen using the *fpgt* probes (**Fig. 4.7, C**). All expression patterns are compared to a wildtype embryo of the same point used with a sense probe, to act as a control probe (**Fig. 4.7, B & D**). The sense probe exhibits any background staining that the embryo may exhibit and is not indicative of gene specific staining. Therefore, any difference in staining in the embryos between the sense and antisense probe is considered gene specific expression. A Morpholino directed against *fcsk* was injected into wildtype embryos along with a P53 directed morpholino, to prevent off target cell death, finding a hemorrhaging rate of 9.4%. The rate of hemorrhage in *gmds* embryos from a heterozygous incross was 7.9%. When the *fcsk* morpholino was injected into *gmds* mutants, the rate of hemorrhage experienced an additive effect, reaching 18.4% (**Fig. 4.7, E**).

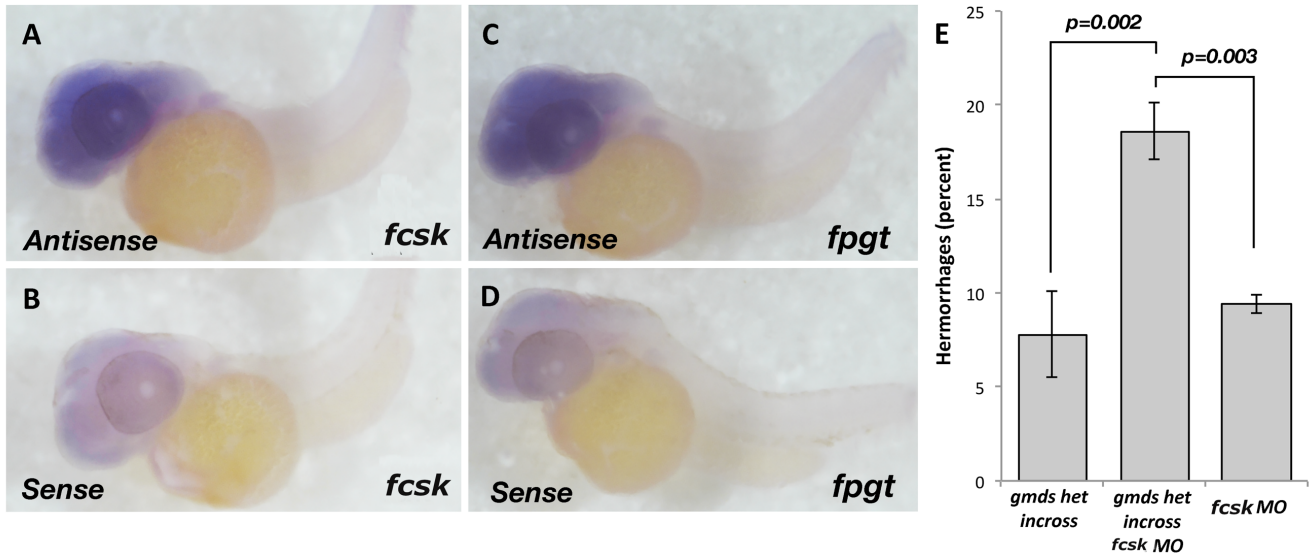


Figure 4. 7 Salvage pathway genes contribute to the hemorrhaging phenotype. (A) The *fcsk* gene is expressed ubiquitously in the head of wildtype 48 hpf embryos compared to the mild background staining (n=24) (B) in the wildtype control embryos using a sense probe (n=20). (C) The *fpgt* gene is expressed ubiquitously in the head of wildtype 48 hpf embryos compared to the mild background staining (n=28) (D) in the wildtype control embryos using a sense probe (n=22). (E) The recorded cerebral hemorrhaging rates of *gmds* mutant incrossed embryos, *gmds* incrossed mutants injected with *fcsk* and p53 morpholino, and wildtype embryos injected with *fcsk* and p53 morpholino. The loss of the salvage pathway genes increases hemorrhaging rates. Grey bars represent the mean hemorrhaging rate, while error bars are the standard error of the mean. Statistical analysis generated using a Chi-Squared test.

4.5 Hemorrhaging phenotype can be rescued with GDP-fucose and fucose injections.

Injections of GDP-Fucose and fucose were completed to determine if the curled tails and cerebral hemorrhage phenotypes present in *gmds* mutants could be rescued. Embryos from a *gmds* heterozygous cross were used in this experiment, thus we expect ~25% of the clutch to be *gmds* homozygous mutants. The results showed a dose dependent rescue from the fucose injections (reflective of a dietary fucose input), in that the 10mM injections rescued the cerebral hemorrhaging phenotype slightly less than the 50mM injection dosage. The GDP-fucose injections exhibited a similar pattern, rescuing the cerebral hemorrhage phenotype predominantly at the 50mM concentration (**Fig. 4.8, A**). This GDP-fucose rescue rate result met the statistical significance of $p < 0.05$ using a Chi-squared test. Neither the fucose or GDP-fucose injections rescued the curled tail or abnormal swimming phenotype (**Fig. 4.8, B**). It is important to note that the 50mM injection of GDP-fucose resulted in a more severe curly tail phenotype, potentially due to cell toxicity at this dose.

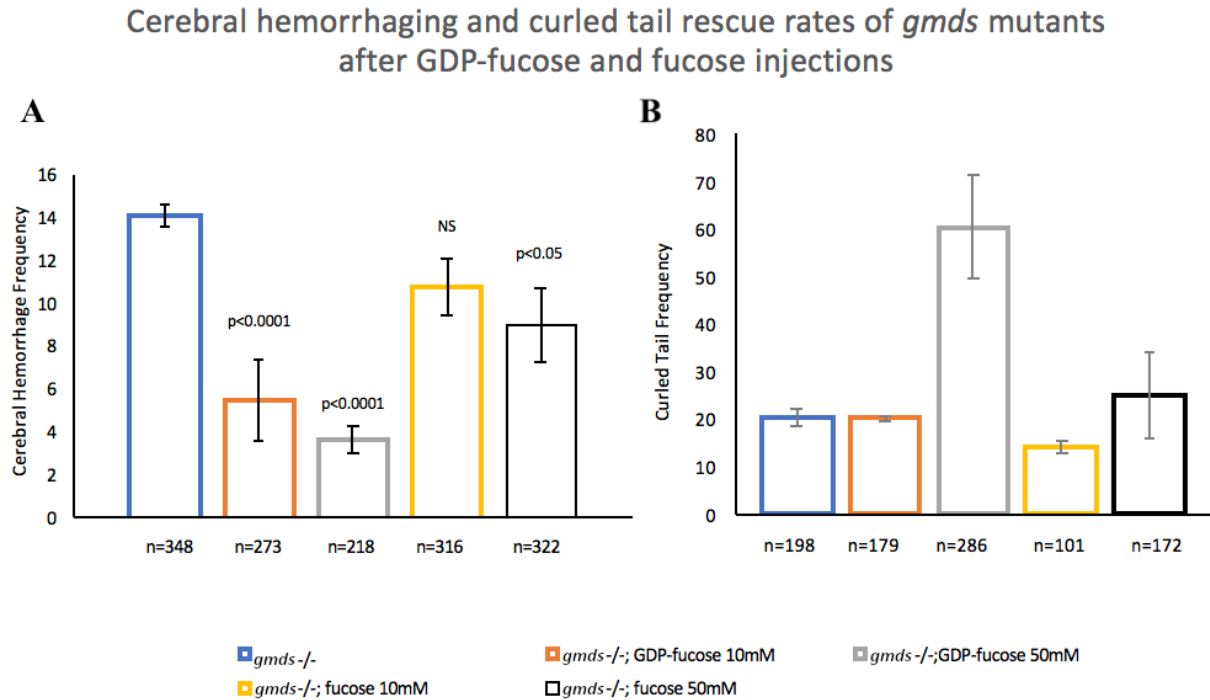


Figure 4. 8 Cerebral hemorrhage and curled tail rates after GDP-Fucose and fucose

injections. Embryos from *gmds* heterozygous crosses (ungenotyped clutch) were injected for

this experiment. *gmds* mutants experiencing no injections (control) experienced a cerebral

hemorrhaging rate of 14.0% and a curled tail rate of 20.2%. *gmds* mutants injected with 10mM

of GDP-fucose experienced a cerebral hemorrhaging rate of 5.5% and curled tail rate of 20.1%.

gmds mutants injected with 50mM of GDP-fucose experienced a cerebral hemorrhaging rate of

3.7% and curled tail rate of 60.4%. *gmds* mutants injected with 10mM of fucose experienced a

cerebral hemorrhaging rate of 10.8% and curled tail rate of 14%. *gmds* mutants injected with

50mM of fucose experienced a cerebral hemorrhaging rate of 9.0% and curled tail rate of 25%.

Colored bars represent the mean hemorrhaging rate, while error bars are the standard error of the

mean. Statistical analysis completed using a Chi-Squared test with a significance level of $p < 0.05$.

4.6 *foxc1a* and *foxc1b* expression was reduced in *gmds* mutants

To determine whether mural cell markers were affected by a mutation in *gmds* a number of probes directed against these markers were designed. *Foxc1b* was expressed in the pharyngeal arches, pectoral fins and the sprouting vessels that can be seen along the perimeter of the eye (**Fig. 4.9, A**) in wildtype embryos. The mutants showed the same expression pattern in the pharyngeal arches and pectoral fins. However, they show a decrease in *foxc1b* in the sprouting vessels in the midbrain region (**Fig. 4.9, B**). qPCR analysis also revealed a reduction of *foxc1b* expression in *gmds* mutants that was statistically significant (**Fig. 4.10**). The *foxc1a* gene was expressed in the pharyngeal arches and along the mid-hindbrain boundary (**Fig. 4.9, C**). The mutants experience a reduction in expression in the mid-hindbrain boundary region (**Fig. 4.9, D**). The *pdgfra* gene was also expressed in the pharyngeal arches and along the midbrain-hindbrain boundary, as well as the pectoral fins and mid-hindbrain boundary, with a subtle reduction in the midbrain-hindbrain boundary (**Fig. 4.9, E&F**). The *pdgfrb* gene was expressed in the pharyngeal arches and midbrain-hindbrain boundary, showing no difference in expression between wildtype or mutant embryos (**Fig. 4.9, G&H**).

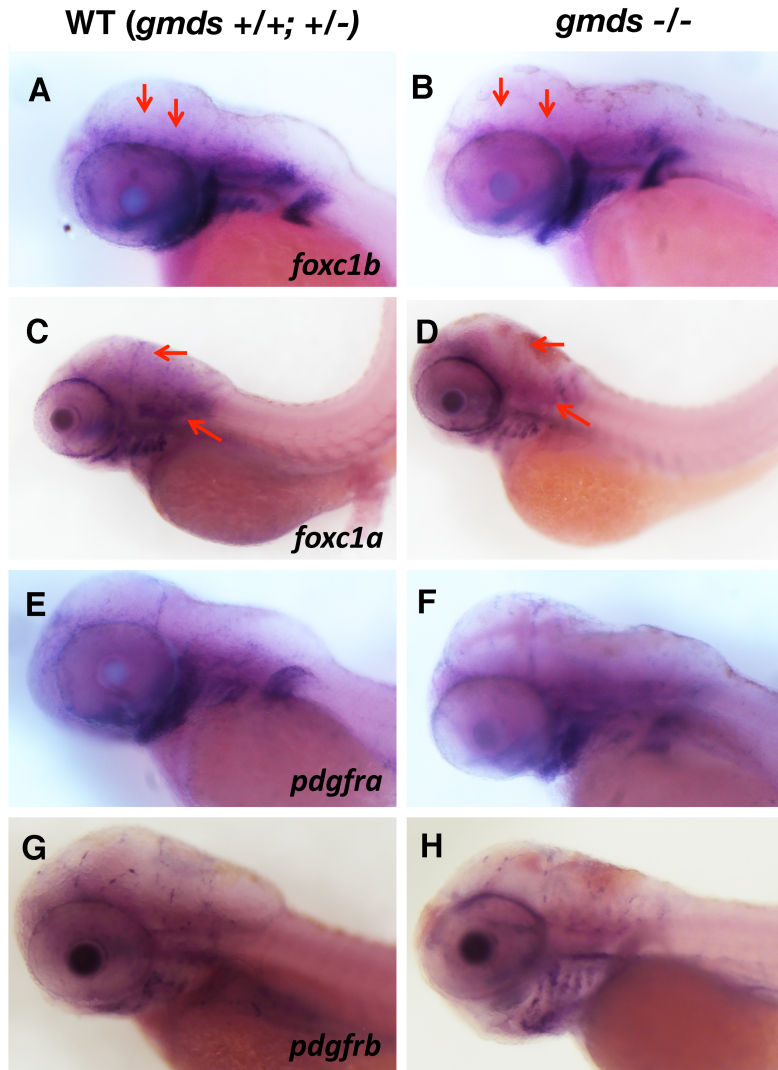


Figure 4. 9 Expression patterns of notch dependent mural cell markers: *foxc1b*, *foxc1a*, *pdgfra*, *pdgfrb*. Embryos are deemed wildtype or heterozygous based on a lack of hemorrhage and circular swimming (annotated as *gmds* +/+ and *gmds* +/- = WT). (A) At 48 hpf *foxc1b* was expressed in mural cell markers and vessels sprouting above the eye region, not present in the (B) *gmds* mutant embryos (WT n= 51, mut n= 67). (C) *foxc1a* (at 72 hpf) shows the same expression in the midbrain-hindbrain boundary and ear, not present in the (D) *gmds* mutant embryos (WT n= 19, mut n= 22). (E) Expression of *pdgfra*, at 72 hpf, in mural cell markers show distinctive staining in the sprouting vessel in the midbrain-hindbrain boundary region and

pharyngeal arches, with a subtle decrease in expression in the midbrain-hindbrain boundary of (F) *gmds* mutant embryos (WT n= 40, mut n= 46). (G) The same expression pattern is observed in the *pdgfrb* embryos at 48 hpf, without an observable change in expression in the (H) mutant embryos (WT n= 41, mut n= 46).

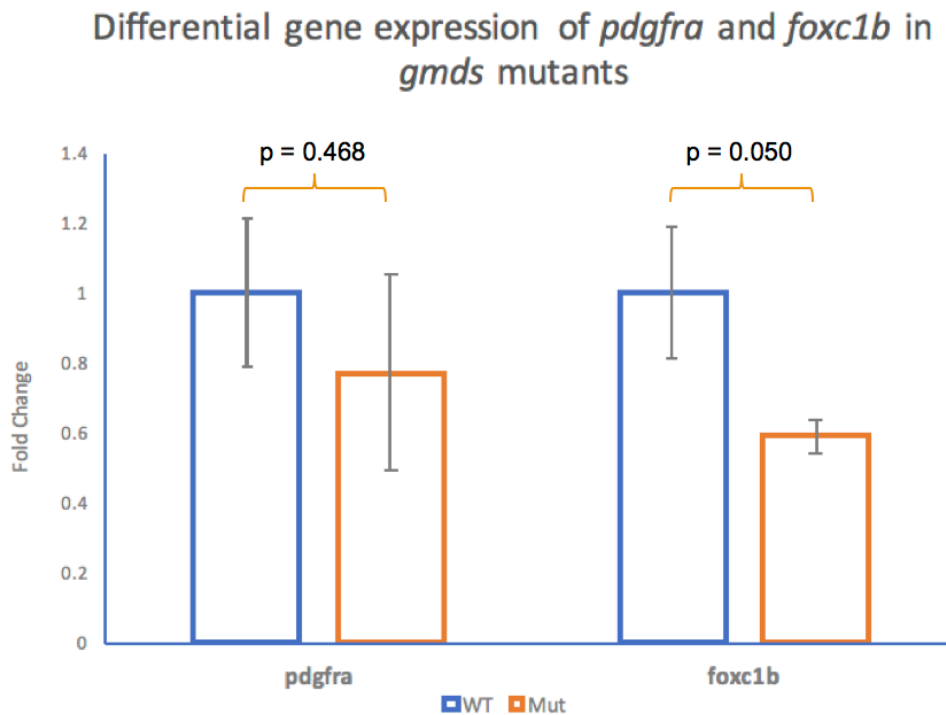


Figure 4. 10 qPCR expression profiles of *gmds* mutants and wildtype embryos. The expression profile of *pdgfra* showed a slight decrease, however not statistically significant. The expression of *foxc1b* was slightly reduced in *gmds* mutants and was statistically significant, using a significance level of <0.05 using a Student's t-test. qPCR was not completed to analyze the expression of *foxc1a*. The graph represents the fold change of the RQ values, while the error bars represent the standard deviation.

4.7 General mural cell markers show localized gene expression changes.

To determine whether general mural cell markers were affected by a mutation in *gmds* a number of probes directed against these markers were designed. The *tagln* gene was expressed in the hyaloid vasculature of the eye, which supplies the lens as it grows, is one of the first vessels to be coated with smooth muscle cells and will later regress to ensure a clear lens in adults. *tagln* is also expressed in the dorsal aorta, ear, swim bladder and gut in wildtype embryos (**Fig. 4.11, A**). There was a decrease in *tagln* expression only in the dorsal aorta and swim bladder in *gmds* mutants (**Fig. 4.11, B**). The *gmds* mutants showed no expressional changes in *myocd* between wildtype (**Fig. 4.11, C**) and mutants (**Fig. 4.11, D**). The wildtype expression of *fbln5* (**Fig. 4.11, E**) in the bulbus arteriosus was reduced in only a small subset of *gmds* mutants (5/34) (**Fig. 4.11, F**).

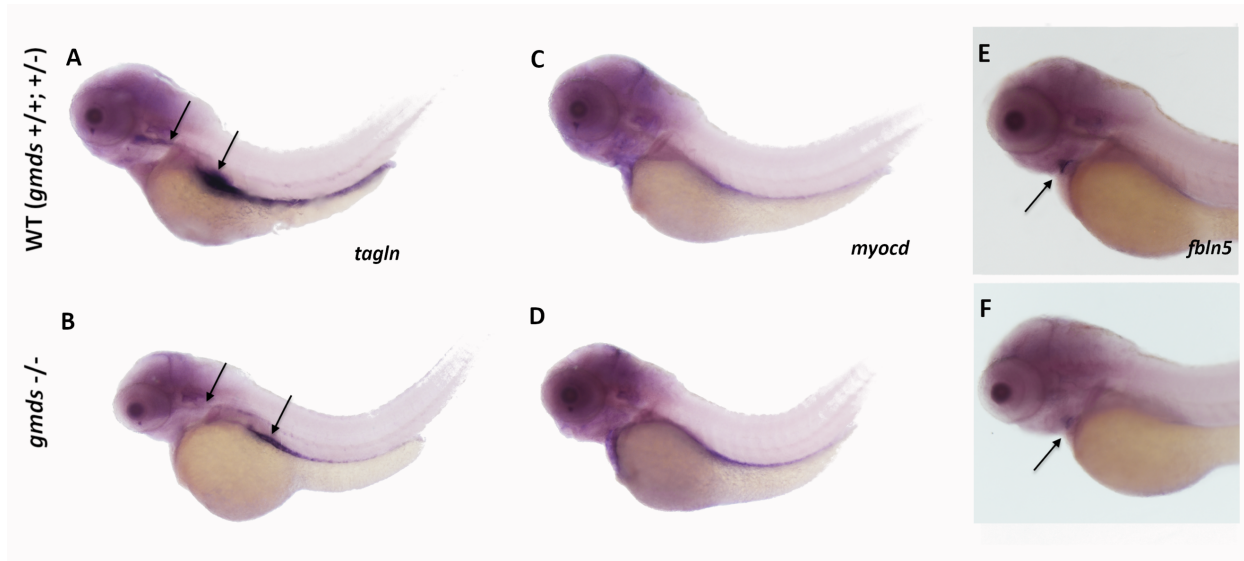


Figure 4.11 Expression patterns of general mural cell markers: *tagln*, *myocd* and *fbln5*.

Embryos are deemed wildtype or heterozygous based on a lack of hemorrhage and circular swimming (annotated as *gmds* +/+ and *gmds* +/- = WT). All embryos are 3 days old. The *tagln* gene was expressed in the smooth muscle cells of the eye, dorsal aorta, ear, swim bladder and gut in wildtype (A) embryos. A slight decrease in expression can be seen in the swim bladder and dorsal aorta in *gmds* mutants (B) (WT n= 10, mut n= 5). Ubiquitous expression throughout the head, that seems to be decreased in *gmds* mutants, is likely non-significant background staining. No difference in *myocd* expression in the gut, ear, heart, pharyngeal arches, eye or midbrain-hindbrain boundary are present between wildtype (C) and mutant embryos (D) (WT n= 8, mut n= 18). The *fbln5* gene is normally expressed in the bulbus arteriosus (E). A small subset (5/34) of *gmds* mutant embryos exhibit a distinct lack of expression in the bulbus arteriosus (F) (WT n= 12, mut n= 34).

4.8 Endothelial cell markers exhibited no expression changes.

To determine whether endothelial cell markers were affected by a mutation in *gmds*, probes directed against these featured markers were designed. No observable differences in expression in the pharyngeal arches, midbrain-hindbrain boundary or the dorsal head were observed in the *cldn5b*, *kdrl* or *pecam* gene in *gmds* mutants compared to controls (**Fig.4.12, A-F**).

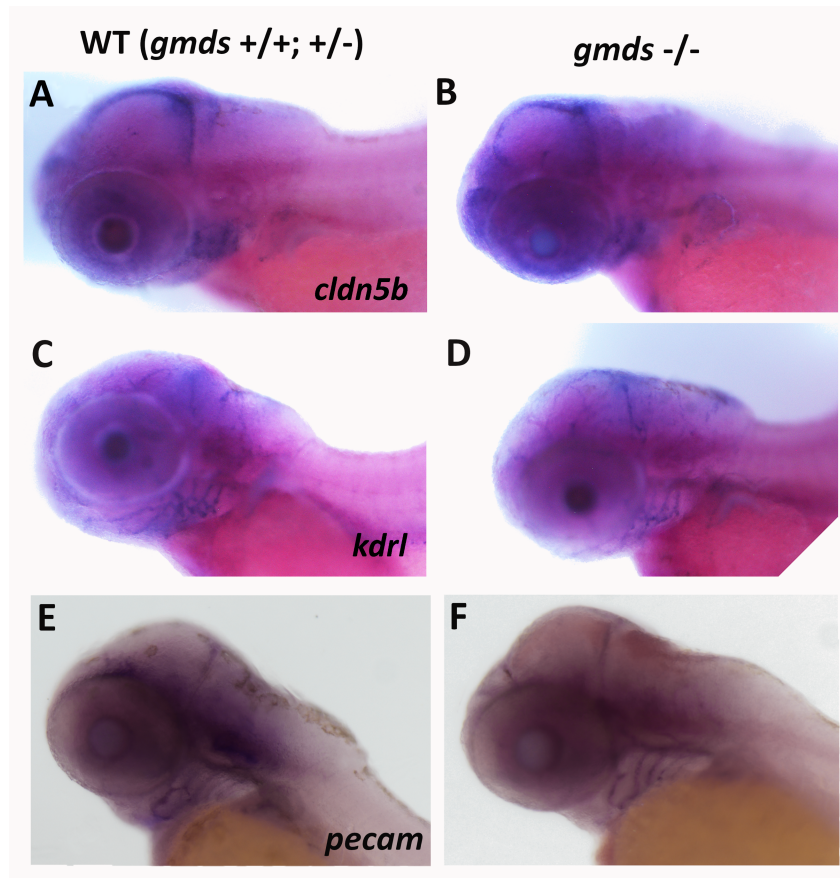


Figure 4. 12 Expression patterns of endothelial cell markers: *cldn5b*, *kdrl* and *pecam1*.

Embryos are deemed wildtype or heterozygous based on a lack of hemorrhage and circular swimming (annotated as *gmds* +/+ and *gmds* +/- = WT). No difference in *cldn5b* expression is present in the pharyngeal arches, midbrain-hindbrain boundary or dorsal head between 72 hpf wildtype (A) and mutant (B) embryos (WT n= 35, mut n= 14). The expression pattern of *kdrl* in the pharyngeal arches and midbrain-hindbrain boundary did not exhibit any differences between 48 hpf wildtype (C) and mutant (D) embryos (WT n= 6, mut n= 5). There was also no observable difference in *pecam* expression between 48 hpf wildtype (E) and mutant (F) embryos in the pharyngeal arches or midbrain-hindbrain boundary (WT n= 10, mut n= 13).

4.9 *gmds* mutants have less cerebral smooth muscle cell coverage

gmds mutants crossed onto an *acta2:gfp* line classified based on the presence or absence of cerebral hemorrhages and were imaged using confocal microscopy. The *gfp* attached to the *acta2* gene fluoresced smooth muscle cells in the cerebral vasculature, predominantly in the pharyngeal arches. Wildtype 6 dpf embryos exhibited robust *acta2* expression throughout the pharyngeal arches, dorsal aorta and dorsal head vasculature (**Fig. 4.13**, top row), while *gmds* mutants exhibited observably less *acta2:gfp* expression in these regions (**Fig. 4.13**, bottom row). Whole embryo examination also shows a distinct lack of *acta2* expression in the swim bladder of *gmds* mutants and the dorsal aorta throughout the tail of mutants (**Fig. 4.14, D**).

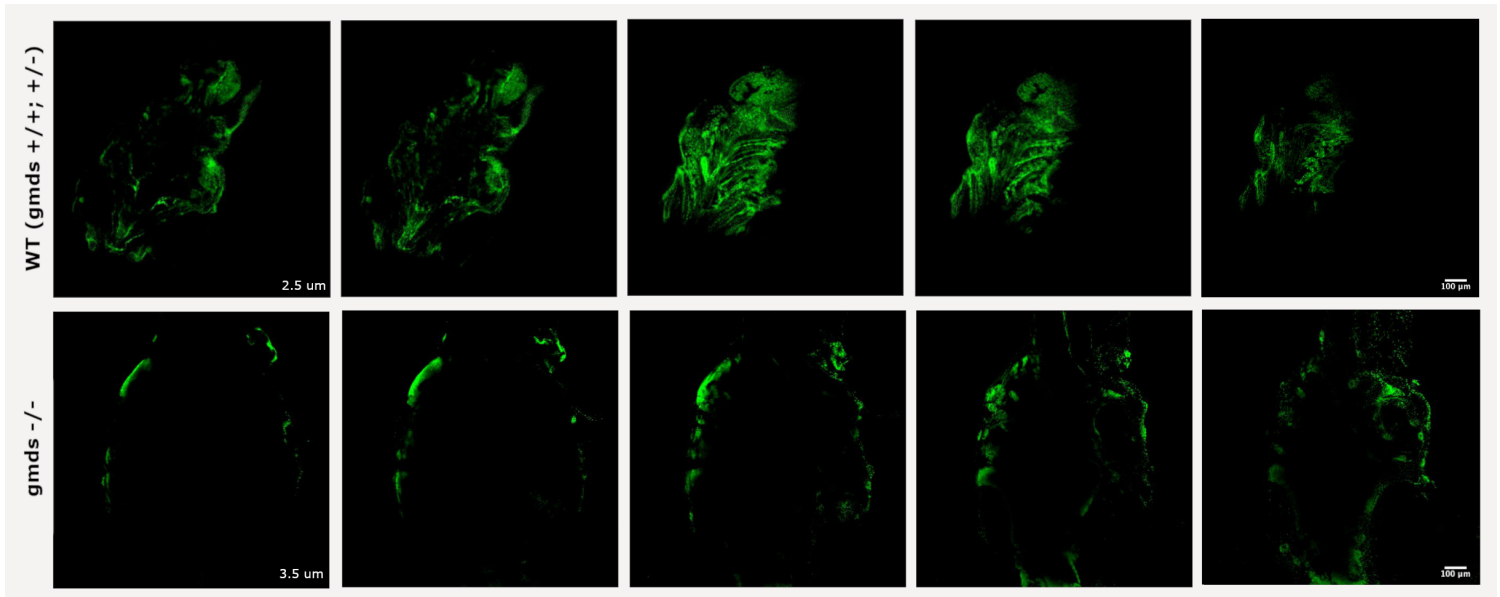


Figure 4. 13 Smooth muscle actin coverage in zebrafish cerebral vasculature. Embryos are deemed wildtype or heterozygous based on a lack of hemorrhage and circular swimming (annotated as *gmds* +/+ and *gmds* +/- = WT). The embryos were imaged from a ventral view with their nose pointing to the bottom of the figure. *gmds* mutant embryos show a significant decrease in cerebral smooth muscle actin coverage. Sequencing to genotypes these embryos was not possible as they were permanently mounted on slides for confocal microscopy (WT n= 10, mut n= 12). The top row displays a series of 2.5 μ m z-stack confocal ventral view images of one 6 dpf wildtype embryo, exhibiting *acta2:gfp* coverage of smooth muscle cells in the cerebral vasculature and predominantly in the pharyngeal arches and surrounding blood vessels. The bottom row is a series of 3.5 μ m z-stack ventral view images of one 6 dpf *gmds* mutant embryo with a significant, almost complete, reduction of *acta2:gfp* coverage of all cerebral vasculature.

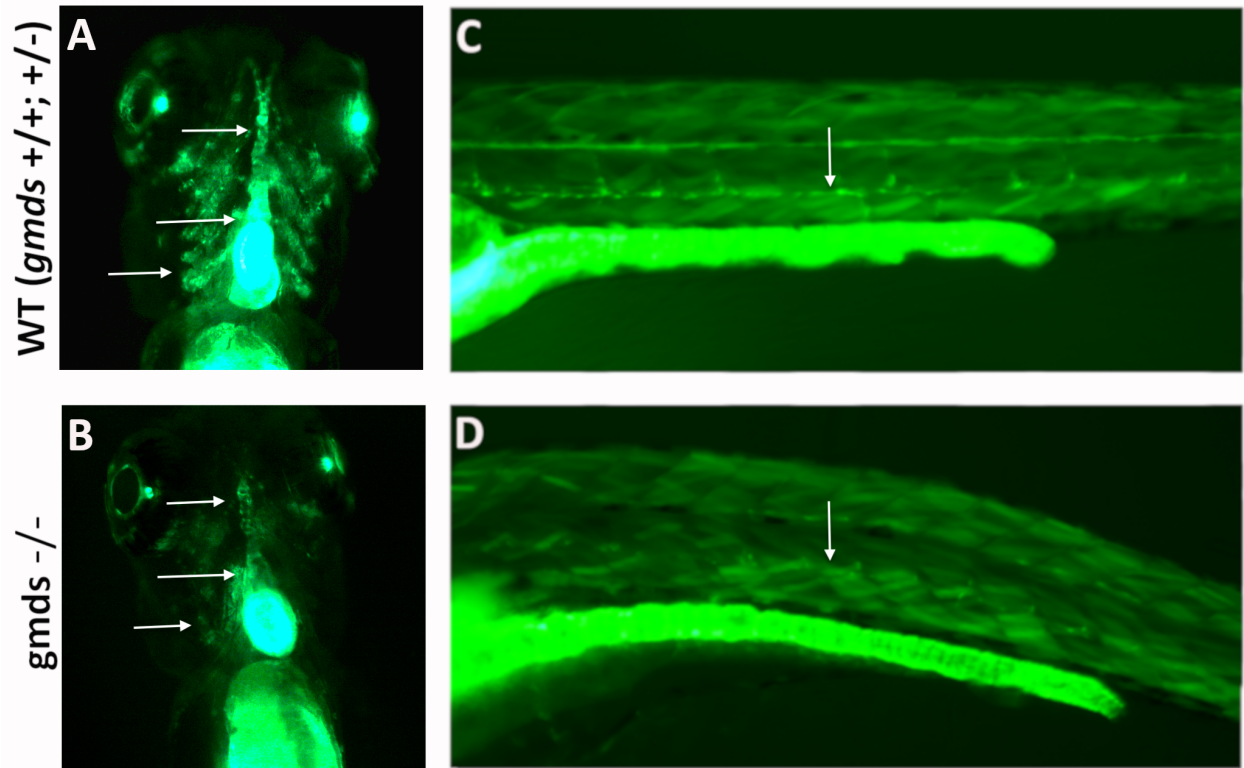


Figure 4. 14 Smooth muscle actin coverage in zebrafish. Embryos deemed mutants based on the presence of cerebral hemorrhages, curled tails and abnormal swimming and annotated as *gmds* *-/-* (WT n= 14, mut n= 9). *gmds* mutant embryos show an observable decrease in cerebral and swim bladder smooth muscle actin expression. Whole embryo ventral view photos of 6 dpf wildtype embryos show distinct expression of smooth muscle actin (*acta2:gfp*) cells in the aorta, pharyngeal arches and heart (**A, arrows**). The *gmds* mutant embryos show a dramatic reduction in expression throughout the aorta and pharyngeal arches, with the smooth muscle actin coverage remaining at normal levels (**B, arrows**). Lateral view images of the tail show *acta2:gfp* expression in the dorsal aorta (**C, arrow**) while the expression in mutants was almost completely eliminated (**D, arrow**).

4.10 Lateral line neuromasts lack fucosylation and subset of mutants lack *slc17a8* expression

To determine whether a mutation in *gmds* led to the complete reduction in fucosylation *AAL* staining was employed, finding a complete depletion of fucosylation in the *gmds* mutants, specifically along the lateral line neuromasts (**Fig. 4.15, A& B**). To determine if hair cells were damaged or malformed, lateral line neuromasts were imaged using SEM (**Fig. 4.15, C&D**) and measured using ImageJ, finding no statistical difference in length or width between wildtype and *gmds* mutant fish (**Fig. 4.16**). To determine if a defect in outer ear morphology was present that could result in a balance defect and contribute to irregular swimming, the outer ears of wildtype and *gmds* mutant fish were observed with no obvious morphological differences observed (**Fig. 4.15, E&F**). To assess whether irregular swimming behavior seen in *gmds* mutants was due to neuromast or ear defects *in situ* hybridization probes were designed against genes responsible for neuromast hair, support and mantle cell regeneration. The *sox2* and *fut9b* gene were expressed in the lateral line neuromasts and pharyngeal arches in wildtype fish (**Fig. 4.17, A&C**), showing no difference in expression in *gmds* mutants (**Fig. 4.17, B&D**). The *slc17a8* gene showed expression in the lateral line neuromasts and the ear in wildtype fish (**Fig. 4.17, E**), with an observable decrease in *gmds* mutants in the lateral line neuromasts of a subset of mutants (**Fig. 4.17, F**). The *pho* gene was expressed in the ear of wildtype fish (**Fig. 4.17, G**) and *gmds* mutants (**Fig. 4.17, H**) and showed no observable change in expression between the two groups.

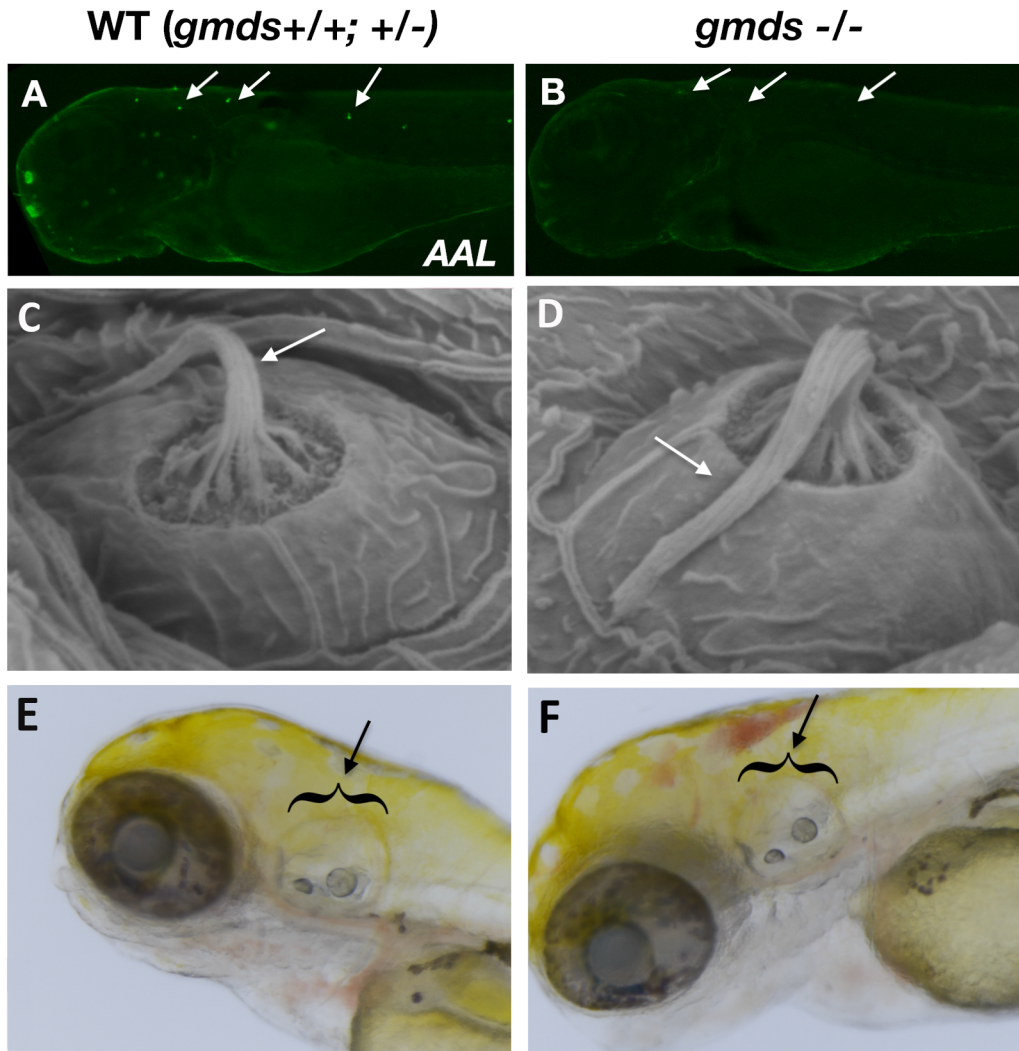


Figure 4. 15 Investigation of neuromast and ear morphology. Embryos are deemed wildtype or heterozygous based on a lack of hemorrhage and circular swimming (annotated as *gmds* *+/+* and *gmds* *+/-* = WT). (A) Staining of fucosylated glycans reveals an observable decrease in fucosylation in (B) *gmds* mutant embryos (WT n= 20, mut n= 14). (C-D) The lateral line neuromasts of five-day wildtype and *gmds* mutant embryos were observed using SEM and measured using ImageJ, finding no differences between the two groups (WT n= 27, mut n= 37). The outer ear of wildtype and (E-F) *gmds* mutants was examined and no morphological differences were observed (WT n= 34, mut n= 23).

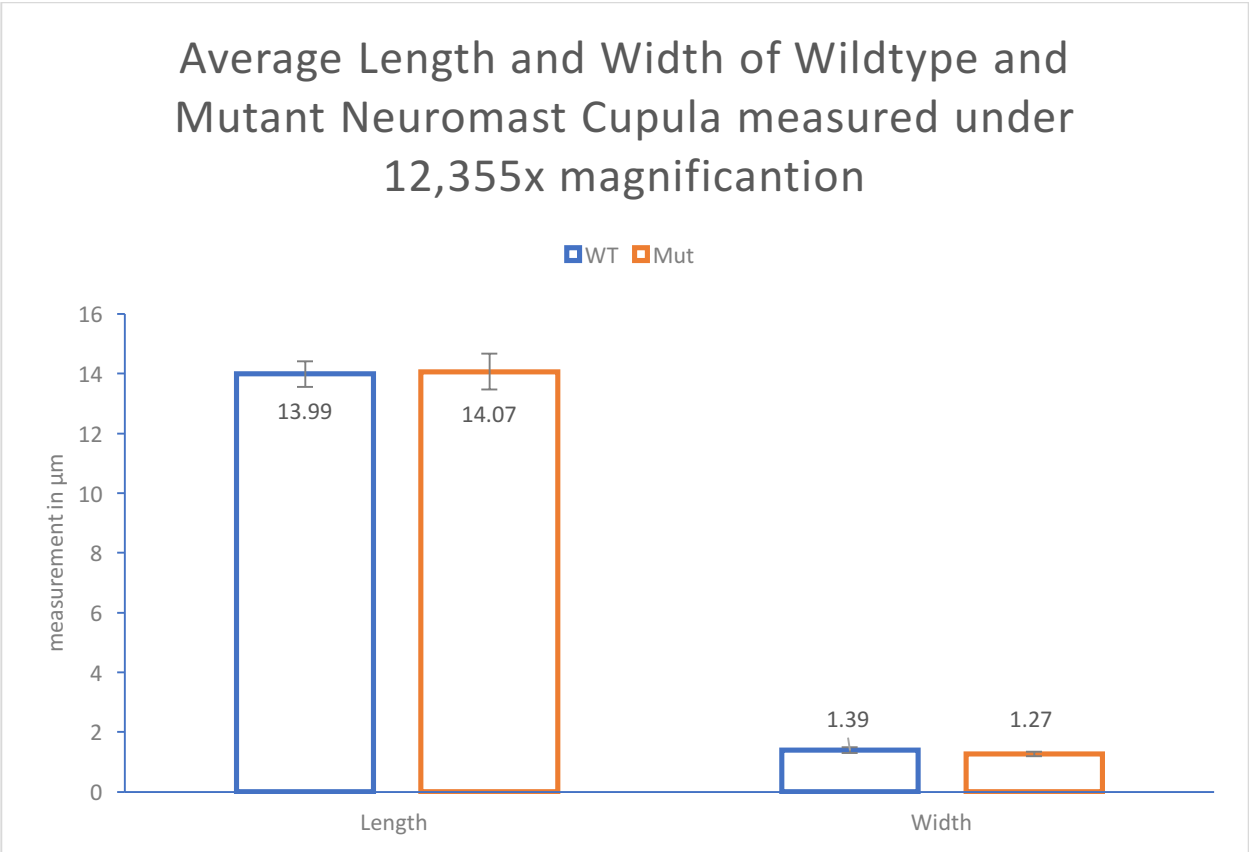


Figure 4. 16 Measurements of hair cell morphology. The lateral line neuromasts were measured using ImageJ to determine if a statistical difference was present in length and width of hair cells between wildtype and mutant zebrafish. There was no statistical difference in length and width between the two experimental groups, calculated using Chi-square test. The colored bars represent the mean length and width of hair cells, while the error bars represent the standard error.

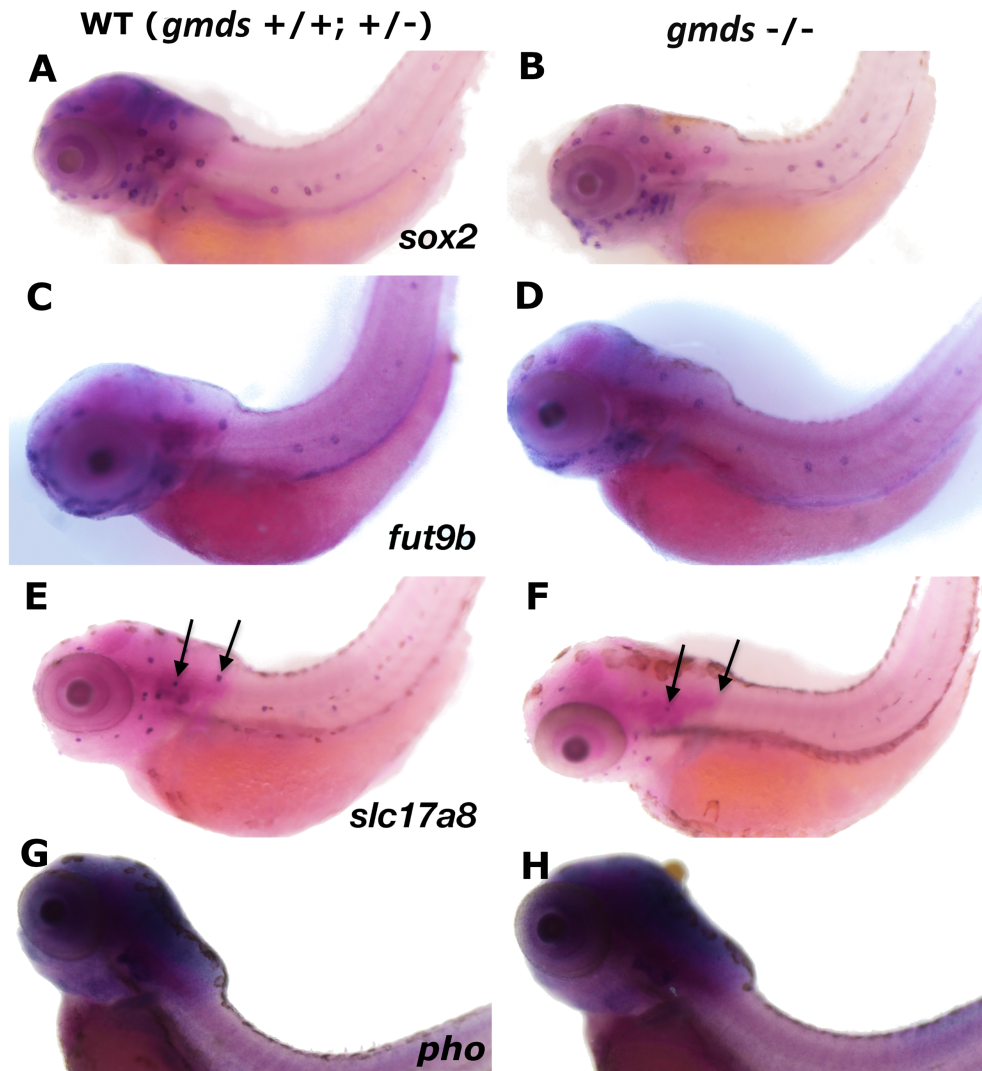


Figure 4.17 Expression markers of ear and lateral line neuromasts: *sox2*, *fut9b*, *slc17a8*, and *pho*. Embryos are deemed wildtype or heterozygous based on a lack of hemorrhage and circular swimming (annotated as *gmds* ^{+/+} and *gmds* ^{+/-} = WT). (A) The *sox2* gene is expressed in the support cells of the lateral line neuromasts and vessels in the mid hind boundary, which is also seen in (B) the *gmds* mutants (WT n= 21, mut n= 28). The gene expression for *fut9b* was localized to lateral line neuromasts, with no difference in expression between mutant (D) and wildtype embryos (C) (WT n= 5, mut n= 7). The *slc17a8* gene is expressed in lateral line

neuromasts and the inner ear (**E**), with this expression decreased in (**F**) a subset of *gmds* mutants (3/10) (WT n= 29, mut n= 10). The *pho* gene is expressed in the inner ear of the wildtype and (**G**) *gmds* mutants (**H**) with no difference between mutants and non-mutants (WT n= 19, mut n= 13).

5. Discussion

SNPs located within an intron of *GMDS* were shown to be associated with white matter hyperintensities, a stroke risk factor²⁵. The role *GMDS* played in vasculature development had not yet been investigated. This project set out to bridge the gap in how *gmds* and *foxc1* may be interacting to contribute to vascular anomalies. We employed antisense morpholinos to components of the GDP-fucose *de novo* and salvage pathways, and created a strong loss of function zebrafish *gmds* allele to test whether GDP-fucose synthesis is required for vascular stability. In addition, as *gmds* is expressed in neuromasts, we assessed neuromast morphology and function to determine if these structures contribute to defects in swimming behavior.

5.1 Disrupting *gmds* function results in cerebral hemorrhaging

The purpose of this study was to investigate the role of *gmds* in vascular phenotypes by investigating its potential downstream regulation of mural and endothelial cell markers. To do this we created a zebrafish *gmds* mutant model. The CRISPR-Cas9 mechanism introduced a missense mutation and a one base pair insertion (**Fig. 4.2**), creating a new in-frame stop codon in exon 6 of *gmds*, likely resulting in a truncated *gmds* protein (**Fig. 4.3**). To test the functionality of the CRISPR induced mutation to sufficiently abolish GDP-fucose production, an AAL stain was used to observe fucosylated proteins. Wildtype zebrafish exhibited fucosylation in the lateral line neuromasts, while we observed a reduction of general protein fucosylation in the *gmds* mutants (**Fig. 4.15, B**), indicating the efficacy of this mutation in producing a loss of

function mutant with severe phenotypes. The mutants demonstrated cerebral hemorrhaging in the forebrain and midbrain-hindbrain boundary starting at 2 dpf (**Fig. 4.5**). The homozygous *gmds* mutation caused a moderate penetrant hemorrhaging phenotype at a rate of 55% (**Fig. 4.5, C**). Additionally, 100% of homozygotes exhibited a curled tail and irregular swimming behavior. Homozygous mutants were not viable past 10 dpf. The stop codon introduced into *gmds* induced a severe phenotype, making it an optimal mutant line to study the vascular defects present from such a genetic anomaly, as this phenotype was present at an increased prevalence and severity compared to other *gmds* mutants (Appendix B). Cerebral hemorrhages were also observed using morpholino directed against *gmds* (**Fig. 4.4, B&C**)¹³, and in a previously generated hypomorphic *gmds* strain (*towhead*), albeit at lower frequencies (Appendix B). The replicated phenotypes seen between the morphants and mutants reinforce that *gmds* is required for vascular stability, and is consistent with GWA data demonstrating variants within *GMDS* associating with CSVD and increased stroke risk, albeit the human condition is due to a heterozygous mutation. Additionally, the ability of GDP-fucose injections to rescue the cerebral hemorrhage phenotype in *gmds* mutants supports the hypothesis that loss of GDP-fucose synthesis leads to cerebral hemorrhaging.

5.2 Hemorrhaging phenotype is caused by lack of GDP-fucose synthesis

Injections of fucose and GDP-fucose into *gmds* mutations were done to attempt to rescue the cerebral hemorrhage, curled tail and abnormal swimming phenotypes present as a result of a mutation in *gmds*. As fucose is the starting substrate of the salvage pathway, supplying embryos with injected fucose will provide further insight into the salvage pathways contribution to

cerebral hemorrhaging phenotypes observed in *gmds* mutants. Each treatment and dosage (with the exception of 10 mM fucose) resulted in a mild to significant rescue of the cerebral hemorrhaging phenotype. The *gmds* mutants injected with 10mM of GDP-fucose reduced the hemorrhage rate by 61% (**Fig. 4.9, A** orange bar). This rescue rate was dose dependent as the injection of 50mM of GDP-fucose (**Fig. 4.8, A** grey bar) further reduced the cerebral hemorrhaging rate from 61% to 74%, with both treatment dosages eliciting a statistically significant rescue response. The *gmds* mutants injected with 10mM of fucose, which is equivalent to dietary fucose, exhibited less cerebral hemorrhaging (with a decrease of 23.6%) but did not reach statistical significance (**Fig. 4.8, A** yellow bar). Increasing the dose of fucose to 50mM decreased the cerebral hemorrhaging rate by 36.1%, and reached a statistical significance level (**Fig. 4.8, A** black bar). Given, these results it can be concluded that a reduction of GDP-fucose production causing cerebral hemorrhaging phenotypes in *gmds* mutants. Considering it has been thought that the salvage pathway contributes to significantly less GDP-fucose production compared to the *de novo* pathway, it is unsurprising that supplemented fucose would not be able to produce a sufficient level of GDP-fucose to rescue cerebral hemorrhaging phenotypes with a total loss of the *de novo* pathway. This combined with the lower rates of cerebral hemorrhaging in *fcsk* morphants (compared to *gmds* morphants/mutants) and the non-specific expression of both *fcsk* and *fpgt* gives evidence that while the salvage pathway is contributing to the production of GDP-fucose, the major source of production is the *de novo* pathway. The salvage pathway does not appear to be able to fully compensate for the loss of *de novo* GDP-fucose production, although the rescue rate may be dose dependent. The rescue of cerebral hemorrhages with the addition of GDP-fucose tells us that it is the loss of the catalytic enzyme *gmds* that is halting the *de novo* synthesis of GDP-fucose and causing the cerebral

hemorrhaging phenotype. However, considering the curled tail and abnormal swimming behavior phenotype was not rescued by either treatment injection, this points to the conclusion that a buildup of the reactant GDP-mannose may be the culprit of this phenotype rather than a loss of GDP-fucose production (**Fig. 4.8, B**). The high rate of curled tails observed in the *gmds* mutants injected with the 50mM GDP-fucose dose indicate non-specific toxicity, which also induced a high rate of embryonic death. Alternatively, it is possible that a specific and controlled concentration of GDP-fucose is needed to maintain normal tail phenotypes, although the rescue of cerebral hemorrhages at this treatment dose lends evidence that this is not the case. The fucose injections, particularly the 10mM dose had a slightly lower rate of curled tails, however more experimentation, using a variety of lower doses, would be required to come to a concrete conclusion whether supplementing with fucose could have therapeutic values. Together, the results of supplementation experiments, and antisense inhibition of the salvage pathway, support a hypothesis whereby non-fully penetrant cerebral hemorrhaging in *gmds* homozygous mutants is partly due to the compensation of the salvage pathway.

5.3 Fucosylation pathway genes are expressed in areas important for vascular development

The *gmds* gene is a catalytic enzyme in the fucosylation pathway with no known association to vascular phenotypes. Given our hypothesis that *gmds* contributes to hemorrhaging phenotypes through aberrant regulation of genes required for vascular development, we first investigated the localized expression of *gmds* using *in situ* hybridization in wildtype embryos. *In situ* hybridization using a probe designed to demonstrate localized *gmds* gene expression

highlighted maternally deposited gene expression at 2 hpf and epithelial expression by 24 hpf. The expression of *gmds* in epithelial cells could contribute to non-cell autonomous influence of vascular development and stability in cerebral blood vessels. Expression of the *gmds* gene was present in the pharyngeal arches at 48 hpf and 72 hpf (**Fig. 4.6**, top row), the site where the first major cranial arteries develop⁵. A sense *gmds* probe was designed to act as a negative control, which exhibits non-specific background staining (**Fig. 4.6**, bottom row); the staining difference between the sense and antisense is considered gene specific expression.

Previous work had shown that GDP-fucose can be produced using dietary fucose as a substrate through a salvage pathway⁸⁷, however it has yet to be associated with any phenotype. *In situ* hybridization of the *fcsk* and fucose-1-phosphate guanylyltransferase (*fpgt*) gene showed ubiquitous expression throughout the head (**Fig. 4.7, A-D**). Morpholinos designed against the fucose kinase (*fcsk*) salvage pathway gene were injected into *gmds* mutant embryos, which increased hemorrhage rates in an additive manner (**Fig. 4.7, E**). While it is thought that only 10% of GDP-fucose is produced through the salvage pathway¹³, we hypothesized that loss of GDP-fucose through both methods combined would result in increased penetrance of vascular phenotypes, which supported our hypothesis. In this study, the functional significance of disrupting this pathway is made clear by the increase in phenotype severity with both methods of GDP-fucose production disrupted. However, the results of the fucose rescue and *fcsk* morpholino experiments gives evidence that the salvage pathway is likely contributing to the cerebral hemorrhaging phenotype, albeit at a lower rate than the *de novo*.

5.4 The loss of *gmds* results in downregulation of mural cell markers: *foxc1a*, *foxc1b*, *tagln* and *fbln5*.

The *foxc1* gene contributes to vascular development²⁴, specifically angiogenesis regulation, endothelial cell sprouting, pericyte function in developing brains⁸⁸, basement membrane integrity⁸⁹ and patterning of the CNS²⁵. A 2014 study²⁵ discovered cerebral hemorrhages in *foxc1* morphants, which was attributed to a reduction in expression of *acta2* positive vSMCs, *pdgfra* and *pdgfrb*^{24,25}. The reduced expression of these critical vascular development genes impeded the migration of neural crest cells and mural cell coverage of the vasculature, of which mural cells prove essential to its stability²⁵. Therefore, *foxc1a* and *foxc1b* are markers of perivascular mural cells²⁴, which are made up of vSMCs and pericytes and play a vital role in the development and stabilization of vasculature²². A follow up study investigated the role of *foxc1* in finer detail by utilizing *foxc1a* and *foxc1b* mutants²⁴. Whitesell *et al.*²⁴ found *foxc1b* labelled smooth muscle precursor cells and differentiated vSMCs. The genetic ablation of *foxc1b* positive cells in *foxc1a/foxc1b* compound mutants discovered reduced coverage of *acta2* positive vSMCs on the ventral aorta that may be due in part to migration or differentiation defects of the vSMCs. Although this warrants further study²⁴.

The motivation for this thesis project stemmed from the findings of this 2014 study, which completed a meta-analysis of GWAS data that discovered a cluster of SNPs within the *GMDS* gene that was associated with cerebral small vessel disease (a stroke risk factor)²⁵. The SNPs within *GMDS* were in linkage disequilibrium with *FOXCI*, which from the two studies above, had been studied for its role in the makeup and development of vasculature, however the

role *GMDS* played in vasculature development had not yet been investigated. This project set out to bridge the gap in how these two genes may be interacting to contribute to vascular anomalies.

In situ hybridization showed a decrease in *foxc1b* expression in the *gmds* mutants, mainly in the smaller vessels in the head, sprouting out in the region surrounding the eye (**Fig. 4.9, B**). The *gmds* mutants also exhibited a decrease in *foxc1a* expression in the ear and midbrain-hindbrain boundary where the middle cerebral vein develops (**Fig. 4.9, D**). An analysis of *foxc1b* expression through qPCR also revealed a significant reduction in expression in the *gmds* mutants, compared to wildtype embryos, with a statistical significance value of 0.05 (**Fig. 4.10**). This result is consistent with the decreased expression pattern of *foxc1b in situ*. Probes were also developed for *tagln*, *myocd* and *fbln5*. These genes are expressed in mural cells and vascular smooth muscle and transcriptional regulators of SMC differentiation and are commonly used markers for vSMC²⁴. No differences in *myocd* expression was found between wildtype and *gmds* mutants (**Fig. 4.11, C&D**). However, *fbln5* was strongly expressed in the bulbus arteriosus that connects the heart to the dorsal aorta, with a subset (5/34) of mutants with reduced expression in this area (**Fig. 4.11, F**). The *tagln* gene, a marker of smooth muscle cells was expressed in the ear, dorsal aorta, swim bladder and gut (**Fig. 4.11, A**). Decreased *tagln* expression was observed in the swim bladder and dorsal aorta in *gmds* mutants, indicating that the mutation is only affecting mural cell expression in specific tissue types (**Fig. 4.11, B**). However, the lack of *tagln* in the swim bladder could lend evidence to the orientation difficulties *gmds* mutants experience in the water column due to the failure of their swim bladder to develop or inflate.

Pdgfr signaling is required for the recruitment of vSMCs and pericytes to the vasculature²². The observable expression of *pdgfra* was slightly reduced at the midbrain-hindbrain boundary and pharyngeal arches (**Fig. 4.9, F**), while no change in expression was observed for *pdgfrb* in *gmds* mutants (**Fig. 4.9, H**). Reduced expression of *pdgfra* has been observed due to loss of *foxc1* function^{24,25}, indicating a possible mechanism of the observed vascular instability as *pdgfra* is required for mural cell recruitment and vessel stability²². The downregulation of *foxc1a* and *foxc1b* in *gmds* mutants indicates a, likely indirect, regulatory relationship. A previous study investigating the contribution of *FOXCI* to CSVD found *foxc1* morphants showed a decreased expression in both *pdgfra* and *pdgfrb*, likely playing a role in the cerebral hemorrhaging phenotype²⁵. Given that *pdgfrb* showed no observable decrease in our *gmds* mutants, and *pdgfra* only exhibited a slight observable decrease, it is likely that another alternative pathway is in place downstream of *foxc1* influencing vascular development and/or recruitment. However, the slight decrease seen in *pdgfra*, and thereby its decrease in vSMC recruitment, may still contribute to vascular malformation in *gmds* mutants. qPCR results of *pdgfra* expression found no reduction in expression (**Fig. 4.10**), although this may be attributed to using whole embryos as a starting substrate for the qPCR experiments that may have masked any *pdgfr* signal changes present. The *gmds* mutation, which downregulates *foxc1b* and *foxc1a*, likely disrupting mural cell recruitment to the developing vasculature, or their subsequent differentiation, and represents at least one key facet of the hemorrhaging phenotypes in *gmds* mutants. The *foxc1* gene is co-expressed with both *pdgfrb* and *acta2*²⁴, however given the expression profile of *pdgfrb* was unaltered in *gmds* mutants lends evidence that an alternate pathway may be involved in affecting blood vessel stability (**Fig. 5.1**).

In order to assess vascular development in these mutants the endothelial cell markers *kdrl*, *pecam* and *cldn5* were tested by *in situ* hybridization. *In situ* results showed no change in *cldn5*, *pecam* and *kdrl* (**Fig. 4.12**) expression in the midbrain-hindbrain boundary, pharyngeal arch or ear regions between wildtype and *gmds* mutant embryos.

ISH and qPCR results have shown differential gene expression for select mural cell markers, but have not shown any evidence for modified expression of endothelial cell markers. Additionally, the alteration of expression caused by a *gmds* mutant is localized to specific organs or cell types.

5.5 *gmds* mutants exhibit decreased smooth muscle actin expression of cerebral vasculature

Structural investigations of vessel abnormalities can be highlighted with the use of transgenic zebrafish⁶, such as *acta2:gfp* that express green fluorescence protein in smooth muscle cells^{90,91}. From these transgenic lines, live imaging can allow real-time visualization of angiogenesis and vasculogenesis⁶. An *acta2:gfp* line was crossed on my *gmds*ⁿ¹⁰⁰² mutant line created for this project to investigate vascular abnormalities²⁴ as a result of a loss of *gmds*. Smooth muscle actin began expression in the ventral head by 4 dpf in wildtype embryos. Mutants showed a significant decrease in cerebral *acta2* coverage in the bulbus arteriosus, dorsal aorta and pharyngeal (brachial) arches vasculature compared to the wildtype embryos (**Fig. 4.13**, bottom row & **Fig 4.14, D**). *Acta2* encodes smooth muscle actin proteins and defects in the gene have been linked to a diversity of vascular diseases, including stroke⁴⁹. Considering *foxc1* is

located and expressed upstream of *acta2* and is essential for *acta2* expression in vSMCs²⁴, it is not surprising that a defect in *gmds*, which led to a reduction in *foxc1a* and *foxc1b*, would also reduce the presence of *acta2* in the vasculature. The subtle change in *in situ* hybridization and qPCR expression profiles for *foxc1a* and *foxc1b* compared to the dramatic loss of smooth muscle actin coverage of cerebral vasculature in the *acta2:gfp* line indicates that an alternate pathway (**Fig. 5.1**) is likely affected by the loss of *gmds* and therefore vascular smooth muscle development. This gives strong evidence that a disruption of *gmds* results in a loss of vSMCs coverage of cerebral vasculature, particularly the dorsal aorta and pharyngeal arches that will feed into the mid-hindbrain boundary, possibly contributing to cerebral bleeding phenotypes.

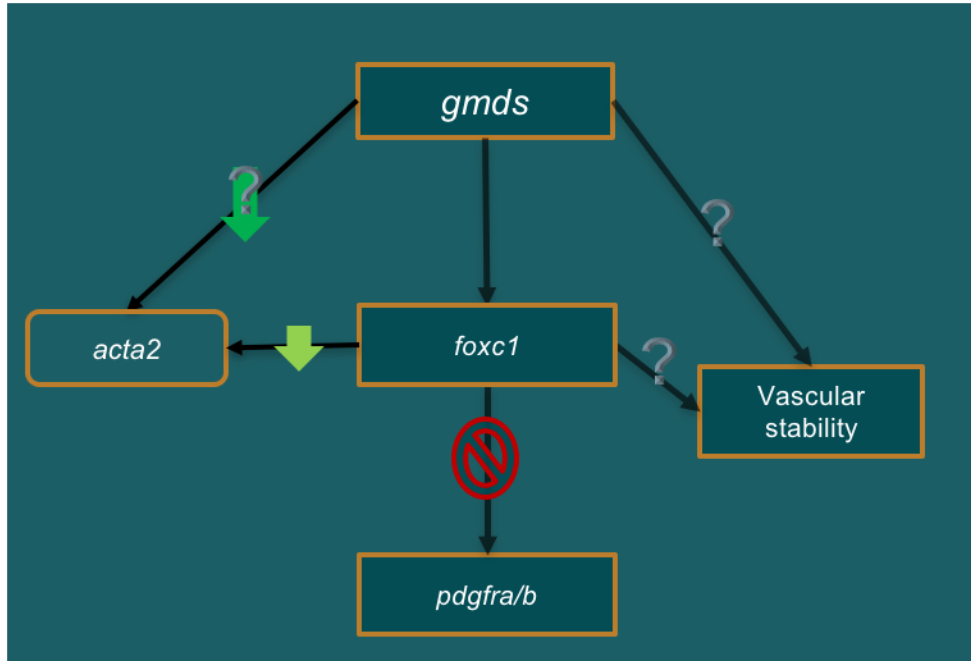


Figure 5. 1 Theoretical pathway interaction. While an interaction is evident between *gmds*, *foxc1a*, *foxc1b* and *acta2* it is not yet clear exactly what this pathway looks like or if there are other genes affecting the gene expression of *foxc1* and *acta2*. An alternate pathway is likely contributing to the dramatic downregulation of *acta2*, in combination with *foxc1*. A downregulation of *foxc1* is usually accompanied by a downregulation of *pdgfra* and *pdgfrb* in hemorrhaging *foxc1* mutants, however that trend is not present in *gmds* mutants. The green arrows propose a differential expression of the gene caused by a mutation in *gmds*. The red slash indicates that no expression change was seen in *pdgfra* or *pdgfrb* as a result of a decrease in *foxc1* expression. The grey question marks are alternative pathways that may be present which contribute to vascular instability, but have not yet been studied in this thesis.

Oscillations of the walls of the swim bladder are transmitted to the inner ear to aid in pressure, sound and movement sensitivities⁹². *Acta2:gfp* coverage was also observably reduced in the swim bladder of mutants (**Fig. 4.14, B**), potentially representing a source of the balance defects observed. Along with a lack of *acta2* coverage in the swim bladder, we observed the incomplete inflation of the swim bladder in *gmds* mutants, which is also likely impacting swimming behavior and difficulty maintaining vertical orientation in the water column. Measurement and quantification of swim bladder inflation rate and size would be beneficial to uncover the relationship between *gmds* and swim bladder function.

5.6 Comparison to previous *gmds* mutants

Previously, two zebrafish *gmds* mutants were used to model leukocyte adhesion deficiency in order to understand the molecular mechanisms of the disease¹³, and to study motor neuron progenitor migration and axon pathfinding⁵⁷. Leukocyte adhesion deficiency is caused by a mutation within the *FUCT1* gene, a gene responsible for the transport of GDP-fucose from the cytosol to the Golgi¹³. The *slytherin* (*gmds*) mutant, identified through a forward genetic screen for its swimming defects, was used to study the link between decreased fucosylation and its effects on neuron development, function and synapse formation to provide more insight into molecular mechanisms causative of neurodevelopmental symptoms seen in patients¹³. These mutants were identified based on their phenotype through forward genetic screens, discovering the causative mutation with *gmds*. They reported bent tails and abnormal swimming phenotypes also seen within our *gmds* allele^{13,57}. The *towhead* mutant was utilized to investigate vagus motor neuron migration in the hindbrain, finding that fucosylated glycans expressed in

neuroepithelial cells were required to guide motor neuron migration. This mutant also possessed a curled tail. These mutants had an introduced missense mutation within the *gmds* gene, and while giving an apparent phenotype, both mutants retained a level of *gmds* function, apparent by the low levels of fucosylation measured using AAL staining^{13,57}. This retention of *gmds* function likely resulted in milder phenotypes compared to our *gmds* mutant, which truncated approximately half of the protein. Our *gmds* mutant exhibit swimming and balance defects different from the *slytherin* and *towhead* reported phenotypes, potentially due to the stronger introduced mutation. Specifically, our *gmds* mutants failed to right themselves in the water column, slowly falling and resting on their sides, the majority of the time. When startled, the embryos swim in erratic circles; an extremely irregular behavior compared to the upright straight swimming behavior normally seen in wildtype embryos (Supplemental **video 1 & 2**). Supplemental videos of the *slytherin* mutants¹³, do not show the same behavior, potentially due to decreased phenotype severity of the missense mutation in their mutant line.

5.7 Notch signaling contributions to phenotypes seen in the *gmds*ⁿ¹⁰⁰², *slytherin* and *towhead* mutants

These two studies^{13,57} investigated the relationship between Notch signalling and their observed phenotypes, as Notch receptors require fucosylation to facilitate ligand binding. Notch signaling has important roles in a wide array of functions including: endothelial cell fate⁹³, epithelial cell fate⁵⁹, neurogenesis⁹⁴, gliogenesis, migration of facial motor neurons, segregation of the rhombomere boundary^{13,57}, and is a very common pathway in cancer progression⁹⁵. Song *et al.*¹³ and Ohata *et al.*⁵⁷ investigated the relationship between Notch signalling and their observed

phenotypes as a decrease in fucosylation was present in both mutants. The *towhead* mutant showed no alteration in notch activity⁵⁷, while the *slytherin* mutant showed reduced notch transcriptional activity which they attributed as the culprit of the neural defects seen within this mutant¹³.

Studies have found the *foxc1* and *foxc2* genes induce the transcription of Notch ligand receptor genes, such as Delta-like 4, to regulate arterial specification^{96,97}. Notch signalling also plays a key role in regulating vascular development by targeting and dysregulating the mural cell marker *pdgfr*^{98,99}. In *notch3* deficient zebrafish and mice, *pdgfr* expression was reduced in vSMCs, resulting in hemorrhaging phenotypes due to disrupted mural cell differentiation and decreased pericyte proliferation⁹⁸⁻¹⁰⁰. Past literature has shown an association of *pdgfr* as a Notch target gene and Notch mutants hemorrhage as pericyte proliferation requires *pdgfr* expression^{98,99}. Therefore, we assessed the expression of *pdgfra* and *pdgfrb* using *in situ* hybridization and *pdgfrb* using qPCR as an indirect measure of Notch signaling function. *In situ* hybridization and qPCR analysis of *pdgfra* exhibit no significant reduction in expression, consistent with no defects in Notch signalling in our *gmds* mutants.

These results imply that other signaling mechanisms are in play downstream of *foxc1* that may be important for vascular stability that are independent of Notch, although testing of other Notch target genes besides *pdgfra* and *pdgfrb* would be informative. More experimental procedures, such as Notch inhibitor experiments, are necessary to make a definitive conclusion regarding notch signaling involvement in this intricate pathway.

5.8 Irregularity of inner ear and neuromast hair cells markers may contribute to abnormal balance and swimming behavior in *gmds* mutants.

Neuromasts along the lateral line of fish contain hair cells that act as sensory receptors that detect water movement and pressure. Damage to the hair cells along the neuromasts through genetic defects or chemical exposure can result in abnormal swimming behavior, specifically circular swimming in zebrafish⁷⁴. A high level of genetic and morphological conservation exists between human inner ear hair cells and, zebrafish hair cells within the ear and lateral line. Genetic defects and ototoxic chemicals that damage hair cells in humans, also target zebrafish hair cells causing circular swimming, indicative of deafness in the zebrafish¹⁰¹. The *slytherin* mutants were responsive to touch at 48 hpf and moved in what was described as “a large C-bend and a smaller counter bend followed by alternating tail flips” by Panzer *et al.*¹⁰². The *towhead* mutants exhibited a bent tail, however the authors did not report information regarding swimming phenotypes⁵⁷. In contrast, our *gmds* mutant embryos swim in erratic circles and normally rest on their sides in the water column; an extremely irregular behavior compared to the straight swimming behavior normally seen in wildtype embryos. The *gmds*ⁿ¹⁰⁰² mutants also lacked a touch response, in that when touched they did not show a dramatic avoidance response by swimming away. A behavior not described by the authors of the *towhead* or *slytherin* mutants. Abnormal swimming could be attributed to defects in the neuromast morphology or function. To investigate the molecular mechanisms contributing to the observed swimming phenotypes seen within the *gmds* mutants, marker analysis for genes responsible for lateral line neuromast and ear hair cell function were tested.

The lateral line neuromasts exhibit *gmds* expression by 72 hpf (**Fig. 4.6**). Lateral line neuromasts that run along a fish's length have protruding hair cells that aid in balance and detection of water movement⁶⁹. The specific expression of *gmds* in the neuromasts gives evidence to the fact that loss of *gmds* in the neuromast may be leading to its dysfunction and resulting in abnormal swimming behaviors, although this warrants further investigation. Abnormal swimming can be attributed, but not limited to: neuromuscular and muscle defects, sensory reception and motor neuron firing defects¹⁰³, defects or dysfunction of neuromast hair cells of the ear or lateral line⁷⁴, and defects in the Weberian ossicles, which connects a fluid filled sac to the swim bladder and is essential for sound transduction⁶⁶.

An AAL stain was used to localize fucosylated proteins throughout the body of *gmds* mutants and wildtype embryos. Wildtype zebrafish exhibited fucosylation on the mechanosensory cilia of the lateral line neuromasts and nasal pits, which contain hair cells that also possess mechanosensory cilia. The *gmds* mutants exhibit a observable reduction in protein fucosylation (**Fig. 4.15, B**). Comparatively, the *towhead* and *slytherin* hypomorphs retained low levels of fucosylation, potentially contributing to the lower rates of hemorrhage in the *towhead* mutants (unpublished data, Appendix B) and less severe swimming phenotypes characterized as c-shaped tail whips^{13,57} compared to the *gmds*ⁿ¹⁰⁰² mutants. This swimming phenotype remains distinctively different from our mutant swimming behavior in that the inability to remain vertical in the water column is an indication of balance defects that predominantly arise from inner hair cell defects. Our *gmds* mutants exhibit a circular swimming behavior, a lack of touch response to stimuli and balance defects, evident by their difficulty to right themselves in the water column

and resting on their sides (Supplemental **Video, 1 & 2**). More experimentation is needed to conclude how a mutation in *gmds* is effecting swimming behaviors in this mutant line.

The retinoic acid signaling pathway mediates hair cell regeneration in neuromasts by regulating the transcription of *p27^{kip}* and transcription factor SOX-2 (*sox2*) in the support cells of the inner ear and lateral line⁷¹. The *sox2* gene is expressed sensory progenitors, predominantly in support cells, and is essential for sensory development. *Sox2* is a transcription factor for tissue development, epithelial-mesenchymal and endothelial-mesenchymal transitions and acts as a cell-fate regulator^{104,105}. Two recent studies have discovered that an excess of *sox2* signaling resulted in endothelial-mesenchymal transitions in endothelial cells of cerebral arteriovenous malformations^{104,105}. One group found bone morphogenetic protein induced Notch1 receptors, which in turn altered the transcriptional regulatory complex in *sox2* promoter regions, resulting in the expression of *sox2* in cerebral endothelial cells¹⁰⁴. This bone morphogenetic protein and notch signaling are important in vascular development and specifically endothelial cell differentiation¹⁰⁴. The *sox2* and *fut9b* gene markers showed no observable difference in expression in lateral line neuromasts between wildtype and *gmds* mutants (**Fig. 4.17, A-D**). However, a reduction in *sox2* the midbrain-hindbrain boundary (**Fig. 4.17, B**) is evident in the *gmds* mutants, indicating its possible contribution to vascular development.

The *slc17a8* gene is involved in L-glutamate transmembrane transporter activity and equilibrioception. The *slc17a8* is essential for synaptic transmission in zebrafish hair cells⁶⁶ and known to cause deafness in humans when mutated¹⁰⁶. *In situ* hybridization of *slc17a8* results reveal neuromast and ear specific expression patterning, which is reduced in a subset of *gmds*

mutants (**Fig. 4.17, F**). Therefore, it is likely the loss of GDP-fucose causes a downstream downregulation of *slc17a8*, thereby disrupting the synaptic activity in the lateral line and ear hair cells. Measurement and quantification of the intensity of staining between the experimental and control groups would add confidence to this conclusion. The dysfunction of inner hair cells results in loss of balance in the water column, conversely the lack of synaptic function in the hair cells along the lateral line neuromasts result in the circular swimming phenotype observed. The *pho* gene is expressed in neuromast support cells and inner ear, and is responsible for hair cell regeneration⁶⁷. This gene is ubiquitously expressed in the head, with some expression in the ear in wildtype zebrafish and in *gmds* mutants (**Fig. 4.17, G&H**). Zebrafish with mutations affecting ear development have shown abnormal swimming such as circular or balance defects^{107,108}, our mutants showed no abnormal ear morphology (**Fig. 4.15, E&F**). Damage to the lateral line and ear hair cells can cause balance defects in zebrafish. However, neuromast hair cell morphology (**Fig. 4.1, C&D, & Fig. 4.16**) appeared normal in *gmds* mutants.

The reduction in *slc17a8* expression in a subset of mutants is likely reducing hair cell function through transduction dysfunction. The lack of *acta2:gfp* presence in the swim bladder may also be contributing to the failure to remain upright in the water column and likely contributes to the mutant's high mortality rate. Once the embryo has depleted the contents of their yolk they cannot sustain their selves without the ability to maintain an upright stature in the water column, which also corresponds to the same time point at which most homozygous *gmds* mutants begin to die. The reduction in *slc17a8* and smooth muscle actin expression represent a potential mechanism, in addition to motor neuron axon pathfinding defects described previously⁵⁷, for swimming and balance defects observed in our *gmds* mutants. These

conclusions potentially explain the source of abnormal swimming behaviors, however more experimentation is needed to investigate the cause of curled tails in *gmds* mutants. It is likely the bent tails are contributing, at least in part, to the abnormal swimming, and probably accentuating the phenotype in conjunction with a defect of *slc17a8* and swim bladder inflation.

5.9 Strengths and limitations

The utilization of zebrafish as a model was a significant strength of this study as their fecundity and abundance of embryos produced from a single pairing, resulted in ample sample sizes for each experiment conducted. Additionally, their optical transparency allowed us to view cerebral hemorrhages and vasculature over time without sacrificing the animal. The link between *foxc1* and cerebral hemorrhaging seen in fish and mice mutants as well as its contribution to cerebral small vessel disease, has established its role in mural cell development and its critical importance in vascular stability. The decreased expression of *foxc1* in *gmds* mutants, discovered through *in situ* hybridization and qPCR, provides support of an association between the two using quantitative and qualitative methods.

Ideally, the injection rescue experiments would have included the use of an alternative sugar injection in the *gmds* mutants to ensure hemorrhaging and curled tail phenotypes of *gmds* mutants injected with fucose or GDP-fucose were reliably comparable to the control group. It also would have added more confidence to the comparative differences seen between experimental and control embryos in the *in situ* hybridization experiments if we could have sequenced the embryos to ensure the genotype. While heterozygous embryos exhibit no curled tails or cerebral hemorrhages, it is possible that a heterozygous mutation could affect gene

expression, however sequencing of embryos that had gone through the *in situ* process were unsuccessful. Given the qualitative nature of *in situ* hybridization coloration, it would have ensured unbiased results had we blinded the photographs of staining in embryos to ensure accurate observation of staining differences in addition to conducting quantitative analyses. Additionally, it would be advantageous to separate vascular tissue, or at least cerebral tissue, from the rest of the body for qPCR experiments to ensure that the expression pattern of tested genes were only coming from the region of interest and not being skewed to appear unchanged due to an accumulation of global expression levels. More experimentation is needed to bridge the gap pertaining to the role that *gmds* plays in vascular phenotypes. However, the results described in this thesis have provided a solid foundation for the role of *gmds* in vascular development, and is likely an important step in the discovery of mechanisms contributing to cerebral small vessel disease.

6. Conclusion

The results support our hypothesis that *gmds* has a role in vascular development by downregulating essential smooth muscle cell genes such as *foxc1b* and *acta2*. Mutations in *FOXC1* and *ACTA2* have been linked to various forms of stroke in disease cohorts, pointing us to the conclusion that a mutation in *gmds* may act as a cascade to disrupting these other known stroke inducing pathways. Considering mutations within *FOXC1* causes increased stroke risk and hearing loss in humans^{25,109,110}, it is possible that the decreased expression of *foxc1a* (which was expressed in the ear) and *foxc1b* disrupts key regulators of hair cell function, such as *slc17a8*. In addition, the lack of *acta2* positive cell coverage in the swim bladder, although not directly tested, is likely contributing culprit of the high homozygous mortality due to failure to maintain balance and direction in the water column. Further experimentation is needed to make conclusions about the relationship between a *gmds* mutation and the swimming behavior observed, namely the role of the neuromast related genes discussed in this contributing to this phenotype. The cerebral hemorrhaging phenotype is a result of deficient GDP-fucose production that primarily stems from *de novo* production, although the salvage pathway likely makes a small contribution. While the abnormal swimming behavior is likely caused by the buildup of GDP-mannose as supplemented end products of the fucosylation pathway did not rescue this phenotype. The link between *gmds* and vascular development, as well as balance defects attributed to inner ear malfunction are key novel findings of this study.

Supplemental Videos

Video 1. Three-day old wildtype embryos in a petri dish are stimulated to initiate swimming, which is straight-lined and rapid.

https://youtu.be/KfpG_4hrfWc

Video 2. Three-day old *gmds* mutant embryos in a petri dish are stimulated to initiate swimming, which is circular, unbalanced and erratic.

https://youtu.be/ndWL_G5J2UU

References

1. Streisinger, G., Walker, C., Dower, N., Knauber, D. & Singer, F. Production of clones of homozygous diploid zebra fish (*Brachydanio rerio*). *Nature* **291**, 293 (1981).
2. Lawrence, C. The husbandry of zebrafish (*Danio rerio*): A review. *Aquaculture* **269**, 1–20 (2007).
3. ZFIN: Zebrafish Book: Contents. https://zfin.org/zf_info/zfbook/cont.html#cont1.
4. Gore, A. V., Monzo, K., Cha, Y. R., Pan, W. & Weinstein, B. M. Vascular Development in the Zebrafish. *Cold Spring Harb. Perspect. Med.* **2**, a006684–a006684 (2012).
5. Isogai, S., Horiguchi, M. & Weinstein, B. M. The Vascular Anatomy of the Developing Zebrafish: An Atlas of Embryonic and Early Larval Development. *Dev. Biol.* **230**, 278–301 (2001).
6. Walcott, B. P. & Peterson, R. T. Zebrafish Models of Cerebrovascular Disease. *J. Cereb. Blood Flow Metab.* **34**, 571–577 (2014).
7. Howe, K. *et al.* The zebrafish reference genome sequence and its relationship to the human genome. *Nature* **496**, 498–503 (2013).
8. Vilella, A. J. *et al.* EnsemblCompara GeneTrees: Complete, duplication-aware phylogenetic trees in vertebrates. *Genome Res.* **19**, 327–335 (2009).
9. Daga, R., Thode, G. & Amores, A. Chromosome complement, C-banding, Ag-NOR and replication banding in the zebrafish *Danio rerio*. *Chromosome Res.* **4**, 29–32 (1996).
10. Postlethwait, J., Amores, A., Force, A. & Yan, Y.-L. Chapter 8 The Zebrafish Genome. in *Methods in Cell Biology* (eds. Detrich, H. W., Westerfield, M. & Zon, L. I.) vol. 60 149–163 (Academic Press, 1998).

11. Postlethwait, J. H. *et al.* Zebrafish Comparative Genomics and the Origins of Vertebrate Chromosomes. *Genome Res.* **10**, 1890–1902 (2000).
12. ZFIN Lab: Postlethwait Zebrafish Genetics Laboratory. <https://zfin.org/ZDB-LAB-970408-67>.
13. Song, Y. *et al.* Neural and Synaptic Defects in slytherin, a Zebrafish Model for Human Congenital Disorders of Glycosylation. *PLoS ONE* **5**, e13743 (2010).
14. BLAST/BLAT search - Homo sapiens - Ensembl genome browser 95.
https://useast.ensembl.org/Homo_sapiens/Tools/Blast?db=core;g=ENSG00000112699;r=6:1623806-2245692;t=ENST00000380815;tl=ySchuO93JgwrW7Wz-4956957.
15. Belanger, A. C. *Vascular anatomy and physiology: an introductory text.* (Davies Pub., 1999).
16. Adair, T. H. & Montani, J.-P. *Angiogenesis.* (Morgan & Claypool Life Sciences, 2010).
17. Alberts, B. *et al.* Blood Vessels and Endothelial Cells. *Mol. Biol. Cell 4th Ed.* (2002).
18. Torres-Vázquez, J., Kamei, M. & Weinstein, B. M. Molecular distinction between arteries and veins. *Cell Tissue Res.* **314**, 43–59 (2003).
19. Blanco, R. & Gerhardt, H. VEGF and Notch in Tip and Stalk Cell Selection. *Cold Spring Harb. Perspect. Med.* **3**, a006569–a006569 (2013).
20. Chen, J.-N., Haffter, P., Odenthal, J., Vogelsang, E. & Brand, M. Mutations affecting the cardiovascular system and other internal organs in zebrafish. **10**.
21. Schilling, T. F. *et al.* Jaw and branchial arch mutants in zebrafish I: branchial arches. *Dev. Camb. Engl.* **123**, 329–344 (1996).

22. Stratman, A. N. *et al.* Interactions between mural cells and endothelial cells stabilize the developing zebrafish dorsal aorta. *Development* **144**, 115–127 (2017).
23. Corrigendum to: New models to study vascular mural cell embryonic origin: implications in vascular diseases. *Cardiovasc. Res.* **114**, 1908–1908 (2018).
24. Whitesell, T. R. *et al.* *foxc1* is required for embryonic head vascular smooth muscle differentiation in zebrafish. *Dev. Biol.* **453**, 34–47 (2019).
25. French, C. R. *et al.* Mutation of FOXC1 and PITX2 induces cerebral small-vessel disease. *J. Clin. Invest.* **124**, 4877–4881 (2014).
26. Morpholino Antisense Oligos | Gene Tools, LLC. http://www.genetools.com/morpholino_antisense_oligos.
27. Eisen, J. S. & Smith, J. C. Controlling morpholino experiments: don't stop making antisense. *Development* **135**, 1735–1743 (2008).
28. Bill, B. R., Petzold, A. M., Clark, K. J., Schimmenti, L. A. & Ekker, S. C. A Primer for Morpholino Use in Zebrafish. *Zebrafish* **6**, 69–77 (2009).
29. Corey, D. R. & Abrams, J. M. Morpholino antisense oligonucleotides: tools for investigating vertebrate development. *Genome Biol.* **2**, reviews1015.1-reviews1015.3 (2001).
30. Timme-Laragy, A. R., Karchner, S. I. & Hahn, M. E. Gene Knockdown by Morpholino-Modified Oligonucleotides in the Zebrafish (*Danio rerio*) Model: Applications for Developmental Toxicology. in *Developmental Toxicology* (eds. Harris, C. & Hansen, J. M.) vol. 889 51–71 (Humana Press, 2012).

31. Czopka, T. & Lyons, D. A. Chapter 2 - Dissecting Mechanisms of Myelinated Axon Formation Using Zebrafish. in *Methods in Cell Biology* (eds. Detrich, H. W., Westerfield, M. & Zon, L. I.) vol. 105 25–62 (Academic Press, 2011).
32. Drummond, I. Chapter 11 - Studying Cilia in Zebrafish. in *Methods in Cell Biology* (eds. King, S. M. & Pazour, G. J.) vol. 93 197–217 (Academic Press, 2009).
33. Renninger, S. L., Schonhaler, H. B., Neuhauss, S. C. F. & Dahm, R. Investigating the genetics of visual processing, function and behaviour in zebrafish. *neurogenetics* **12**, 97–116 (2011).
34. Jeon, H.-Y. & Lee, H. Depletion of Aurora-A in zebrafish causes growth retardation due to mitotic delay and p53-dependent cell death. *FEBS J.* **280**, 1518–1530 (2013).
35. Stainier, D. Y. R. *et al.* Guidelines for morpholino use in zebrafish. *PLOS Genet.* **13**, e1007000 (2017).
36. Barrangou, R. & Marraffini, L. A. CRISPR-Cas systems: prokaryotes upgrade to adaptive immunity. *Mol. Cell* **54**, 234–244 (2014).
37. Sander, J. D. & Joung, J. K. CRISPR-Cas systems for genome editing, regulation and targeting. *Nat. Biotechnol.* **32**, 347–355 (2014).
38. Jinek, M. *et al.* A programmable dual-RNA-guided DNA endonuclease in adaptive bacterial immunity. *Science* **337**, 816–821 (2012).
39. Doudna, J. A. & Sternberg, S. H. *A Crack in Creation: Gene Editing and the Unthinkable Power to Control Evolution.* (Mariner Books, 2018).
40. Luo, M. L., Leenay, R. T. & Beisel, C. L. Current and future prospects for CRISPR-based tools in bacteria. *Biotechnol. Bioeng.* **113**, 930–943 (2016).

41. Malzahn, A., Lowder, L. & Qi, Y. Plant genome editing with TALEN and CRISPR. *Cell Biosci.* **7**, 21 (2017).
42. Davis, A. J. & Chen, D. J. DNA double strand break repair via non-homologous end-joining. *Transl. Cancer Res.* **2**, 130–143 (2013).
43. Gharahkhani, P. *et al.* Analysis combining correlated glaucoma traits identifies five new risk loci for open-angle glaucoma. *Sci. Rep.* **8**, 1–12 (2018).
44. Stroke Statistics | Internet Stroke Center. <http://www.strokecenter.org/patients/about-stroke/stroke-statistics/>.
45. Rost, N. S. Clinical Neurogenetics. *Neurol. Clin.* **31**, 915–928 (2013).
46. Yamada, Y. *Molecular genetics of stroke.* (Morgan & Claypool, 2013).
47. Guo, J., Liu, A. & Su, D. Genetics of stroke. *Acta Pharmacol. Sin.* **31**, 1055–1064 (2010).
48. Liu, L., Xu, X., Li, J., Li, X. & Sheng, W. Lentiviral-Mediated shRNA Silencing of PDE4D Gene Inhibits Platelet-Derived Growth Factor-Induced Proliferation and Migration of Rat Aortic Smooth Muscle Cells. *Stroke Res. Treat.* **2011**, 1–7 (2011).
49. Guo, D.-C. *et al.* Mutations in Smooth Muscle Alpha-Actin (ACTA2) Cause Coronary Artery Disease, Stroke, and Moyamoya Disease, Along with Thoracic Aortic Disease. *Am. J. Hum. Genet.* **84**, 617–627 (2009).
50. Igarashi, P. Genetics and Pathogenesis of Polycystic Kidney Disease. *J. Am. Soc. Nephrol.* **13**, 2384–2398 (2002).
51. Rivera, M. *et al.* Stroke in adult polycystic kidney disease. *Postgrad. Med. J.* **68**, 735–738 (1992).
52. Li, Q. *et al.* Cerebral Small Vessel Disease. *Cell Transplant.* **27**, 1711–1722 (2018).

53. van Norden, A. G. *et al.* Causes and consequences of cerebral small vessel disease. The RUN DMC study: a prospective cohort study. Study rationale and protocol. *BMC Neurol.* **11**, (2011).
54. Moriwaki, K. Fucosylation and gastrointestinal cancer. *World J. Hepatol.* **2**, 151 (2010).
55. Ma, B., Simala-Grant, J. L. & Taylor, D. E. Fucosylation in prokaryotes and eukaryotes. *Glycobiology* **16**, 158R-184R (2006).
56. Ginsburg, V. Formation of Guanosine Diphosphate I-Fucose from Guanosine Diphosphate d-Mannose. *J. Biol. Chem.* **235**, 2196–2201 (1960).
57. Ohata, S. *et al.* Neuroepithelial cells require fucosylated glycans to guide the migration of vagus motor neuron progenitors in the developing zebrafish hindbrain. *Development* **136**, 1653–1663 (2009).
58. Sturla, L. *et al.* Defective intracellular activity of GDP-D-mannose-4,6-dehydratase in leukocyte adhesion deficiency type II syndrome. *FEBS Lett.* **429**, 274–278 (1998).
59. Waterhouse, C. C. M. *et al.* Secretory Cell Hyperplasia and Defects in Notch Activity in a Mouse Model of Leukocyte Adhesion Deficiency Type II. *Gastroenterology* **138**, 1079-1090.e5 (2010).
60. Miyoshi, E. *et al.* Fucosylation Is a Promising Target for Cancer Diagnosis and Therapy. *Biomolecules* **2**, 34–45 (2012).
61. Moriwaki, K., Shinzaki, S. & Miyoshi, E. GDP-mannose-4,6-dehydratase (GMDS) Deficiency Renders Colon Cancer Cells Resistant to Tumor Necrosis Factor-related Apoptosis-inducing Ligand (TRAIL) Receptor- and CD95-mediated Apoptosis by Inhibiting Complex II Formation. *J. Biol. Chem.* **286**, 43123–43133 (2011).

62. Gharahkhani, P. *et al.* Common variants near ABCA1, AFAP1 and GMDS confer risk of primary open-angle glaucoma. *Nat. Genet.* **46**, 1120–1125 (2014).
63. Wiggs, J. L. & Pasquale, L. R. Genetics of glaucoma. *Hum. Mol. Genet.* **26**, R21–R27 (2017).
64. Souzeau, E. *et al.* Glaucoma spectrum and age-related prevalence of individuals with FOXC1 and PITX2 variants. *Eur. J. Hum. Genet. EJHG* **25**, 839–847 (2017).
65. Umali, J., Hawkey-Noble, A. & French, C. R. Loss of foxc1 in zebrafish reduces optic nerve size and cell number in the retinal ganglion cell layer. *Vision Res.* **156**, 66–72 (2019).
66. Nicolson, T. The genetics of hair-cell function in zebrafish. *J. Neurogenet.* **31**, 102–112 (2017).
67. Behra, M. *et al.* Phoenix Is Required for Mechanosensory Hair Cell Regeneration in the Zebrafish Lateral Line. *PLoS Genet.* **5**, e1000455 (2009).
68. Lush, M. E. & Piotrowski, T. Sensory hair cell regeneration in the zebrafish lateral line: Zebrafish Sensory Hair Cell Regeneration. *Dev. Dyn.* **243**, 1187–1202 (2014).
69. Ghysen, A. & Dambly-Chaudière, C. Development of the zebrafish lateral line. *Curr. Opin. Neurobiol.* **14**, 67–73 (2004).
70. Trump, W. J. V. & McHenry, M. J. The morphology and mechanical sensitivity of lateral line receptors in zebrafish larvae (*Danio rerio*). *J. Exp. Biol.* **211**, 2105–2115 (2008).
71. Rubbini, D., Robert-Moreno, À., Hoijman, E. & Alsina, B. Retinoic Acid Signaling Mediates Hair Cell Regeneration by Repressing *p27 kip* and *sox2* in Supporting Cells. *J. Neurosci.* **35**, 15752–15766 (2015).

72. Obholzer, N. *et al.* Vesicular glutamate transporter 3 is required for synaptic transmission in zebrafish hair cells. *J. Neurosci. Off. J. Soc. Neurosci.* **28**, 2110–2118 (2008).
73. Nicolson, T. *et al.* Genetic Analysis of Vertebrate Sensory Hair Cell Mechanosensation: the Zebrafish Circler Mutants. *Neuron* **20**, 271–283 (1998).
74. Jiang, L., Romero-Carvajal, A., Haug, J. S., Seidel, C. W. & Piotrowski, T. Gene-expression analysis of hair cell regeneration in the zebrafish lateral line. *Proc. Natl. Acad. Sci.* **111**, E1383–E1392 (2014).
75. Media, M. Premium Grade Brine Shrimp Eggs, 16 oz. *BrineShrimpDirect*
<https://www.brineshrimpdirect.com/premium-grade-brine-shrimp-eggs-16-ounces>.
76. GEMMA Micro 300. *SKRETTING ZEBRAFISH*
<https://zebrafish.skrettingusa.com/products/gemma-micro-300>.
77. Kimmel, C. B., Ballard, W. W., Kimmel, S. R., Ullmann, B. & Schilling, T. F. Stages of embryonic development of the zebrafish. *Dev. Dyn. Off. Publ. Am. Assoc. Anat.* **203**, 253–310 (1995).
78. Aranda, P. S., LaJoie, D. M. & Jorcyk, C. L. Bleach gel: A simple agarose gel for analyzing RNA quality. *ELECTROPHORESIS* **33**, 366–369 (2012).
79. Thisse, C. & Thisse, B. High-resolution in situ hybridization to whole-mount zebrafish embryos. *Nat. Protoc. Lond.* **3**, 59–69 (2008).
80. SuperScript III One-Step RT-PCR System with Platinum Taq DNA Polymerase.
<https://www.thermofisher.com/order/catalog/product/12574018?SID=srch-srp-12574018>.

81. Kohli, V. & Elezzabi, A. Y. Laser surgery of zebrafish (*Danio rerio*) embryos using femtosecond laser pulses: Optimal parameters for exogenous material delivery, and the laser's effect on short- and long-term development. *BMC Biotechnol.* **8**, 7 (2008).
82. PureLink™ RNA Mini Kit.
<https://www.thermofisher.com/order/catalog/product/12183018A>.
83. The Qubit® 2.0 Fluorometer: The Next Generation in Nucleic Acid and Protein Quantitation - CA. <https://www.thermofisher.com/ca/en/home/references/newsletters-and-journals/bioprobess-journal-of-cell-biology-applications/bioprobess-issues-2011/bioprobess-64-april-2011/the-qubit-2-0-fluorometer-april-2011.html>.
84. TURBO DNA-free™ Kit.
<https://www.thermofisher.com/order/catalog/product/AM1907>.
85. High-Capacity cDNA Reverse Transcription Kit.
<https://www.thermofisher.com/order/catalog/product/4368813>.
86. TaqMan™ Gene Expression Assay (FAM).
<https://www.thermofisher.com/order/catalog/product/4331182?SID=srch-srp-4331182>.
87. Dehnert, K. W. *et al.* Metabolic labeling of fucosylated glycans in developing zebrafish. *ACS Chem. Biol.* **6**, 547–552 (2011).
88. Siegenthaler, J. A. *et al.* Foxc1 is required by pericytes during fetal brain angiogenesis. *Biol. Open* **2**, 647–659 (2013).
89. Prasitsak, T. *et al.* Foxc1 is required for early stage telencephalic vascular development: FOXC1 In Early Telencephalic Vasculature. *Dev. Dyn.* **244**, 703–711 (2015).

90. Reference, G. H. ACTA2 gene. *Genetics Home Reference*
<https://ghr.nlm.nih.gov/gene/ACTA2>.
91. ACTA2 Gene - GeneCards | ACTA Protein | ACTA Antibody.
<https://www.genecards.org/cgi-bin/carddisp.pl?gene=ACTA2>.
92. Alexander, R. McN. PHYSICAL ASPECTS OF SWIMBLADDER FUNCTION. *Biol. Rev.* **41**, 141–176 (1966).
93. Siekmann, A. F. & Lawson, N. D. Notch signalling limits angiogenic cell behaviour in developing zebrafish arteries. *Nature* **445**, 781–784 (2007).
94. Thomas, J.-L. *et al.* Interactions between VEGFR and Notch signaling pathways in endothelial and neural cells. *Cell. Mol. Life Sci.* **70**, 1779–1792 (2013).
95. Yuan, X. *et al.* Notch signaling: An emerging therapeutic target for cancer treatment. *Cancer Lett.* **369**, 20–27 (2015).
96. Seo, S. *et al.* The forkhead transcription factors, Foxc1 and Foxc2, are required for arterial specification and lymphatic sprouting during vascular development. *Dev. Biol.* **294**, 458–470 (2006).
97. Hayashi, H. & Kume, T. Foxc Transcription Factors Directly Regulate Dll4 and Hey2 Expression by Interacting with the VEGF-Notch Signaling Pathways in Endothelial Cells. *PLoS ONE* **3**, e2401 (2008).
98. Jin, S. *et al.* Notch signaling regulates platelet-derived growth factor receptor-beta expression in vascular smooth muscle cells. *Circ. Res.* **102**, 1483–1491 (2008).
99. Wang, Y., Pan, L., Moens, C. B. & Appel, B. Notch3 establishes brain vascular integrity by regulating pericyte number. *Dev. Camb. Engl.* **141**, 307–317 (2014).

100. Mašek, J. & Andersson, E. R. The developmental biology of genetic Notch disorders. *Development* **144**, 1743–1763 (2017).
101. Monroe, J. D., Rajadinakaran, G. & Smith, M. E. Sensory hair cell death and regeneration in fishes. *Front. Cell. Neurosci.* **9**, (2015).
102. Panzer, J. A. *et al.* Neuromuscular synaptogenesis in wild-type and mutant zebrafish. *Dev. Biol.* **285**, 340–357 (2005).
103. Burgess, H. A. & Granato, M. The neurogenetic frontier--lessons from misbehaving zebrafish. *Brief. Funct. Genomic. Proteomic.* **7**, 474–482 (2008).
104. Wu, X. *et al.* Crosstalk between BMP and Notch Induces Sox2 in Cerebral Endothelial Cells. *Cells* **8**, 549 (2019).
105. Yao, J. *et al.* Elevated endothelial Sox2 causes lumen disruption and cerebral arteriovenous malformations. *J. Clin. Invest.* **129**, 3121–3133 (2019).
106. Ruel, J. *et al.* Impairment of SLC17A8 encoding vesicular glutamate transporter-3, VGLUT3, underlies nonsyndromic deafness DFNA25 and inner hair cell dysfunction in null mice. *Am. J. Hum. Genet.* **83**, 278–292 (2008).
107. Malicki, J. *et al.* Mutations affecting development of the zebrafish ear. *Development* **123**, 275–283 (1996).
108. Whitfield, T. T. *et al.* Mutations affecting development of the zebrafish inner ear and lateral line. *Development* **123**, 241–254 (1996).
109. Reis, L. M. *et al.* PITX2 and FOXC1 spectrum of mutations in ocular syndromes. *Eur. J. Hum. Genet.* **20**, 1224–1233 (2012).

110. Linkroum, K., DelBono, E., McKenna, M. & Wiggs, J. L. A Novel FOXC1 Nonsense Mutation Is Associated With Sensorineural Hearing Loss, Primary Empty Sella Syndrome and Anterior Segment Dysgenesis. *Invest. Ophthalmol. Vis. Sci.* **48**, 5599–5599 (2007).

Appendix A

0.25M EDTA pH 8.0

Per Litre:

93.05g disodium EDTA-2H₂O (Brand)

800ml DEPC water

Stir and pH to 8.0 with NaOH pellets (ACP Chemicals Inc.)

Fill to 1L and autoclave

1x TAE

Per 10L:

200ml 50x TAE

9800ml RO water

4% Paraformaldehyde fixative

Per 100ml:

4g paraformaldehyde (Sigma-Aldrich, St. Louis, Missouri - Aldrich)

10mls 10x PBS

90mls RO water

Stir and add one 1M NaOH pellet (ACP Chemicals Inc.) to dissolve

Vacuum filter

10x PBS

Per Liter:

80g NaCl (ThermoFisher Scientific, Waltham, Massachusetts)

2g KCl (Sigma-Aldrich, St. Louis, Missouri)

14.4g Na₂HPO₄ (Sigma-Aldrich, St. Louis, Missouri)

2.4g KH_2PO_4 (Sigma-Aldrich, St. Louis, Missouri)

800mls RO water

pH to 7.4 and autoclave

20x Embryo Media

Per Litre:

17.5g NaCl (ThermoFisher Scientific, Waltham, Massachusetts)

0.75g KCl (Sigma-Aldrich, St. Louis, Missouri)

2.9g $\text{CaCl}_2 \cdot 2\text{H}_2\text{O}$ (Sigma-Aldrich, St. Louis, Missouri)

Add RO water 800ml

0.41g KH_2PO_4 (Sigma-Aldrich, St. Louis, Missouri)

0.142g Na_2HPO_4 anhydrous (Sigma-Aldrich, St. Louis, Missouri)

4.9g $\text{MgSO}_4 \cdot 7\text{H}_2\text{O}$ (Sigma-Aldrich, St. Louis, Missouri)

Add RO water to 1L

Vacuum filter

20x SSC

per 500ml:

350ml RO water

87.65g NaCl (ThermoFisher Scientific, Waltham, Massachusetts)

44.1 Sodium Citrate (ThermoFisher Scientific, Waltham, Massachusetts)

Stir and then add remaining volume to 500mls

50x TAE

Per liter:

242g Trizma® Base (Sigma-Aldrich, St. Louis, Missouri)

200ml 0.25M EDTA

57.1 acetic acid (ThermoFisher Scientific, Waltham, Massachusetts Scientific)

Fill to 1L with RO water

500x Sodium Bicarbonate

Per 10ml:

0.3g NaHCO₃ (Sigma-Aldrich, St. Louis, Missouri)

10ml RO water

Agar plates

~20 plates:

15g Agar Broth (Bio Basic Canada Inc., Toronto, Canada)

400ml RO water

Autoclave

100µl Kanamycin

Agarose Gel (1%)

Per 50ml (Small gel):

50ml of 1X TAE Buffer

0.5g of Agarose (FroggaBio, Toronto, Ontario)

Microwaved until clear

0.5µl of RedSafe™ (iNtRON)

Pour into gel electrophoresis chamber when lukewarm and let set

Coloration Buffer

Per 50ml:

5ml 1M Tris-HCl pH 9.5

2.5ml 1M MgCl₂

1ml 5M NaCl (ThermoFisher Scientific, Waltham, Massachusetts)

250µl 20% Tween-20 (ThermoFisher Scientific, Waltham, Massachusetts)

41.25ml RO water

Embryo Media

Per Liter:

50ml 20x embryo media

2ml 500x NaHCO₃ (Sigma-Aldrich, St. Louis, Missouri)

Fill to 1L

Heparin

250mg Heparin (Sigma-Aldrich, St. Louis, Missouri)

5ml DEPC water

Aliquot to 250µl

Hybridization Solution

Per 50ml:

25ml 50% Formamide (Ambion Inc, ThermoFisher Scientific, Waltham, Massachusetts)

12.5ml 20x SSC

50µl 50mg/ml Heparin

500µl 50mg/ml tRNA (Roche, Basel, Switzerland)

250µl 20% Tween-20 (Sigma-Aldrich, St. Louis, Missouri)

460µl 1M citric acid

Fill to 50ml with RO water

In situ stop solution

Per 500ml

50ml 10X PBS

450ml RO water

2ml 0.25M EDTA

2.5ml 20% Tween-20 (Sigma-Aldrich, St. Louis, Missouri)

pH to 5.5 with HCl

LB Broth

Per Litre:

10g Bacto-tryptone

5g Bacto-yeast extract

10g NaCl (ThermoFisher Scientific, Waltham, Massachusetts)

pH to 7.0 with 100µl 10N NaOH (ACP Chemicals Inc.)

Autoclave

Antibiotic 1ml/1L LB

Mesab

Per 500 ml (stock):

400 mg Tricaine powder (Sigma-Aldrich, St. Louis, Missouri)

97.9 ml deionized water

2.1 ml 1M Tris, pH 9 (Trizma® Base, Sigma-Aldrich, St. Louis, Missouri)

Per 300 ml (working stock):

12.6 ml tricaine solution

300 ml zebrafish tank water

PBST

Per 500ml:

50ml 10x PBS

2.5ml 20% Tween-20 (Sigma-Aldrich, St. Louis, Missouri)

447.5ml RO water

Proteinase K

0.5ml 1M Tris pH 8.5

9.5ml DEPC water

10mg Proteinase K (Sigma-Aldrich, St. Louis, Missouri)

Make 200 μ l aliquots

Appendix B

Hemorrhaging rate data was personally communicated by Ohata *et al.*, who created a *gmds* mutant for studying migration of motor neuron progenitors. This data has not been published.

